GENERATION, STORAGE AND DELIVERY OF SINGLET OXYGEN BY A MULTIFUNCTIONAL AGENT

A THESIS SUBMITTED TO
THE GRADUATE SCHOOL OF ENGINEERING AND SCIENCE
OF BILKENT UNIVERSITY
IN PARTIAL FULFILLMENT OF THE REQUIREMENTS FOR
THE DEGREE OF
MASTER OF SCIENCE
IN
CHEMISTRY

By
Abdurrahman TÜRKSOY
April 2017

GENERATION, STORAGE AND DELIVERY OF SINGLET OXYGEN BY A MULTIFUNCTIONAL AGENT
By Abdurrahman TÜRKSOY
April 2017

We certify that we have read this thesis and that in our opinion it is fully adequate, in scope and in quality, as a thesis for the degree of Master of Science.

Engin Umut AKKAYA(Advisor)

Bilge BAYTEKİN

Salih ÖZÇUBUKÇU

Approved for the Graduate School of Engineering and Science:

Ezhan KARAŞAN
Director of the Graduate School

ABSTRACT

GENERATION, STORAGE AND DELIVERY OF SINGLET OXYGEN BY A MULTIFUNCTIONAL AGENT

Abdurrahman TÜRKSOY
MSc. in Chemistry
Advisor: Engin Umut AKKAYA
April 2017

Photodynamic therapy (PDT) relies on the photosensitized generation of singlet oxygen (by consuming dissolved oxygen) within tumor tissues whose oxygen level is already low enough to make this treatment self-limiting. In certain applications, hypoxia induced by photosensitizer is minimized by introducing light intermittently (fractional PDT) in order to allow time for the replenishment of cellular oxygen, resulting in more effective treatment. In this particular study, we demonstrated that a photosensitizer with an attached 2-pyridone module to halogenated di-styryl BODIPY would be useful in fractional PDT. Upon illumination of photosensitizer (PYR) with a light at specific wavelength in therapeutic window the endoperoxide of 2-pyridone is generated along with singlet oxygen. During the time required for replenishment of cellular oxygen the endoperoxide undergoes cycloreversion to produce singlet oxygen, regenerating the 2-pyridone moiety. Such mechanism enables continuation of photodynamic process in the dark, resulting improved fractional photodynamic therapy drug validated by cell-culture studies in vitro.

Keywords: BODIPY, peroxide, photochemistry, photodynamic therapy, singlet oxygen.

ÖZET

ÇOK ÖZELLİKLİ ETMEN ARACIĞILI İLE SİNGLET OKSİJEN ÜRETİMİ, SAKLANMASI VE İLETİLMESİ

Abdurrahman TÜRKSOY
Kimya, Yüksek Lisans
Tez Danışmanı: Engin Umut AKKAYA
Nisan 2017

Hipoksik tümör hücreleri içerisinde çözünmüş oksijeni fotosentetik metot ile kullanarak, singlet oksijen üretme prensibine dayanan fotodinamik tedavi, bu özelliğinden dolayı kendini kısıtlamaktadır. Bazı uygulamalarda ışığın parçalı olarak gönderilmesi, tedavi sırasında hücrenin oksijen seviyesini artırmasına izin vermesinden dolayı daha etkili sonuçlar gözlemlenmiştir. Bu çalışmada, 2-piridon modülü ile zenginleştirilmiş, halojen ve iki sitiren grubu ile fonksiyonlanmış organik BODIPY tipi boyanın, parçalı fotodinamik tedavide daha etkili olacağı öngörülmüştür. Tedavi için uygun dalga boyunda ışık ile uyarılma sonucu endoperoksit yapısı oluşumu ve singlet oksijen üretimi gözlemlenmiştir. Tasarlanan bu boya ile parçalı fotodinamik tedavide hücrenin oksijen seviyesini artırması için gereken karanlık evre süresince endoperoksit yapısı siklik evirtim ile singlet oksijen üretebilmektedir. Bu tasarım tedavinin karanlık evrede de devam etmesine olanak sağlamasından ötürü hücre kültürü deneylerinde de gözlemlendiği üzere parçalı fotodinamik tedavi için daha gelişmiş bir ilaç olduğu kanıtlanmıştır.

Anahtar sözcükler: BODIPY, peroksit, fotokimya, fotodinamik tedavi, singlet oksijen.

Acknowledgement

I owe my supervisor and mentor Prof. Dr. Engin Umut Akkaya a debt of gratitude. Throughout the course of my MSc. study, not only he was the guiding spirit but also he was the quintessential representative of a scientist. I will never forget what he has taught me, and I will always follow his lead.

I would like to thank to TUBITAK (The Scientific and Technological Research Council of Turkey) for funding me with Graduate Student Scholarship (2210-E/2211) throughout my study.

I would like to express my deepest and sincere thanks to Dr. İlke Şimşek Turan and Dr. Serdal Kaya. Without their guidance, wisdom and help, I would not be standing where I am today.

I would like to express my sincere thanks to Dr. Gürcan Günaydın for his collaborative work to test designed drug on cell culture experiments.

I would like to thank to Dr. Özlem Seven, Dr. Tuna Subaş, Dr. Safacan Kölemen, Dr. Taha Bilal Uyar, Simay Aydonat, Pınar Erdil, Merve Canyurt, Yahya Fikry, Seylan Ayan, Cansu Kaya for their support and help.

I specifically want to thank Simay Aydonat, Pınar Erdil and Merve Canyurt for making countless hours of laboratory work enjoyable and unforgettable.

I would like to thank to Zeynep Erdoğan for helping me to obtain MS data and also for her lovely attitude.

I also want to thank Fatih Yergöz and Nurcan Haştar for their companionship. I will miss every single minute we spent together.

I dont know how to express my gratitude to my shining star, Deniz Yıldız. Her indispensable companionship means world to me. The days I spent in Bilkent University would be as dull as ditchwater without her. Spending countless hours

of lab work with her was the dearest part of my life. I hope you nothing but the very best and very best only from bottom of my heart.

I would like to thank to my father, mother and siblings for their understanding, help and support throughout my MSc. study as well as my life. I fall short in words to describe what they mean to me. I am jubilant for having them and I would not imagine my life without them.

List of Abbreviations

PDT: Photodynamic Therapy

HPD: Haematoporphyrin

ROS: Reactive Oxygen Species

LED: Light Emitting Diode

HEL: Heli-anthracene

NMR: Nuclear Magnetic Resonance

TMS: Tetramethylsilane

DPBF: 1.3-dipheylisobenzofuran

BODIPY: Boron-dipyrromethane, 4,4-difluoro-4-bora-3a,4a-diaza-s-indacene

ISC: Intersystem crossing

Contents

Introduction 1

1.1 Photodynamic Therapy 1

1.2 Keystones of Effective Photodynamic Therapy 2

1.2.1 Photosensitizers 2

1.2.1.1 Photophysics of Photosensitizers 2

1.2.1.2 Types of Photosensitizers 4

1.2.1.3 Subcellular Uptake of Photosensitizers 6

1.2.1.4 Cell Death and Tumor Destruction Imposed by PDT 8

1.2.1.5 Properties of Ideal Photosensitizer 9

1.2.2 Light in PDT 11

1.2.3 Oxygen in PDT 14

1.2.4 Fractional Photodynamic Therapy 17

1.3 BODIPY Dyes 19

1.3.1 BODIPY as Photosensitizer 19

1.3.2 Heavy Atom Effect 20

1.3.3 Halogen Free BODIPY Dyes 20

1.3.4 Longer Wavelength Absorbing and Emitting BODIPY Dyes 22

1.4 Alternative Singlet Oxygen Delivery System 23

1.4.1 Endoperoxide Formation Mechanism 24

1.4.2 Dissociation of EPOs 25

1.4.3 Singlet Oxygen Carriers 26

Experimental Procedures 28

2.1 General Procedures 28

2.2 Synthesis Scheme 29

2.2.1 Synthesis of Compound **12** 29

2.2.2 Synthesis of Compound **13** 30

2.2.3 Synthesis of Compound **14** 30

2.2.4 Synthesis of Compound **15** 31

2.2.5 Synthesis of Compound **16** 32

2.2.6 Synthesis of Compound **17** 32

2.2.7 Synthesis of Compound **18** 33

2.2.8 Preparation of Micelle of **17** (**m-PYR**) 33

2.2.9 Preparation of Micelle of **18** (**m-EPO**) 34

2.3 Singlet Oxygen Trap Experiments 34

2.4 Singlet Oxygen Quantum Yield Calculations 35

2.5 Emission and Fluorescence Measurements 35

2.6 Cell Studies 36

2.6.1 Cell Culture and MTT Assay 36

Results and Discussion 38

3.1 Insight into the Structure 39

3.2 Initial Characterization of Structures 41

3.3 Emission and Fluorescence Measurements 42

3.4 Reversibility of the Transformations 44

3.5 Power of the Dark Side in Action 46

3.6 Cell Study 48

Conclusion 50

References 51

Appendix-A NMR Spectra 61

Appendix-B MS Data 82

Appendix-C Zeta Potential 84

List of Figures

Figure 1. Electronic transitions of photosensitizer and production of singlet oxygen mechanism..... 2

Figure 2. Possible reaction pathways of photosensitizer after excitation with light.3

Figure 3 Simplified reaction pathways of photosensitizer at triplet state. 5

Figure 4. Graphical representation of types of tumor reduction mechanisms by singlet oxygen and ROS..... 8

Figure 5. List of examples of photosensitizers with trade name, potential indications and activation wavelength. 10

Figure 6. Absorbance of water, hemoglobin and melanin depending on wavelength and optical window for PDT..... 12

Figure 7. Illustration of light penetration depending on wavelength and scattering, reflection and absorption of light. 13

Figure 8. Potential energy curves of ground and first two excited states of oxygen depending on internuclear distance..... 14

Figure 9. Lifetime of singlet oxygen in different solvents 16

Figure 10. BODIPY type dye (**1**) obtained from 2,4-dimethylpyrrole..... 19

Figure 11. Iodine functionalized BODIPY (**2**) at 2 and 6 positions 20

Figure 12. Orthogonal designed BODIPY (**3**) being capable of producing singlet oxygen 21

Figure 13. C_{60}-dyads containing, halogen free BODIPY design (**4**) 21

Figure 14. Relatively longer wavelength absorbing, aromatic group substituted BODIPY designs 22

Figure 15. Mono (**9**) and di-styryl (**10**) substituted BODIPY designs 23

Figure 16. Heli-anthracene (HEL) (**11**) 24

Figure 17. Endoperoxide formation mechanism through exciplex.. 25

Figure 18. Two major dissociation mechanisms of endoperoxide structures..... 25

Figure 19. Mechanisms of singlet oxygen release from endoperoxides 26

Figure 20. Synthesis scheme of 2-pyridone containing di-halogenated, di-styryl BODIPY PYR (**17**) and its endoperoxide version EPO (**18**) 29

Figure 21. Operation principle of multifunctional agent which produces, stores and releases singlet oxygen 39

Figure 22. ^{1}H NMR spectra of PYR (**17**) and EPO (**18**) with highlighted structure specific peaks..... 40

Figure 23. Excitation and emission spectra of PYR (**17**) and EPO (**18**) 41

Figure 24. Relative singlet oxygen quantum yield experiment.. 43

Figure 25. ^{1}H NMR study showing reversibility of transformation between PYR (**17**) and EPO (**18**). Table contains percentages of each structure in corresponding NMR spectrum..... 45

Figure 26. Singlet oxygen mediated bleaching of trap molecule (1,3-diphenylisobenzofuran) in the presence of EPO (**18**) (5 µM) in DMSO..... 46

Figure 27. Comparison of singlet oxygen mediated bleaching of trap molecule (1,3-diphenylisobenzofuran) in the presence of EPO (**18**) (5 µM) in DMSO and trap molecule as control group 47

Figure 28. Cell viabilities as determined by MTT assays..... 48

Figure 29. ^{1}H NMR Spectrum A of Cycloreversion Experiment..... 61

Figure 30. ^{1}H NMR Spectrum B of Cycloreversion Experiment..... 62

Figure 31. ^{1}H NMR Spectrum C of Cycloreversion Experiment..... 63

Figure 32. ^{1}H NMR Spectrum D of Cycloreversion Experiment..... 64

Figure 33. ^{1}H NMR Spectrum E of Cycloreversion Experiment..... 65

Figure 34. ^{1}H NMR Spectrum F of Cycloreversion Experiment..... 66

Figure 35. ^{1}H NMR Spectrum G of Cycloreversion Experiment..... 67

Figure 36. ^{1}H NMR Spectrum of Compound **12** 68

Figure 37. ^{13}C NMR Spectrum of Compound **12** 69

Figure 38. ^{1}H NMR Spectrum of Compound **13** 70

Figure 39. ^{13}C NMR Spectrum of Compound **13** 71

Figure 40. ^{1}H NMR Spectrum of Compound **14** 72

Figure 41. ^{13}C NMR Spectrum of Compound **14** 73

Figure 42. ^{1}H NMR Spectrum of Compound **15** 74

Figure 43. ^{13}C NMR Spectrum of Compound **15** 75

Figure 44. ^{1}H NMR Spectrum of Compound **16** 76

Figure 45. ^{13}C NMR Spectrum of Compound **16** 77

Figure 46. ^{1}H NMR Spectrum of Compound **17** 78

Figure 47. ^{13}C NMR Spectrum of Compound **17** 79

Figure 48. ^{1}H NMR Spectrum of Compound **18** 80

Figure 49. ^{13}C NMR Spectrum of Compound **18** 81

Figure 50. HRMS Spectrum of **12** 82

Figure 51. HRMS Spectrum of **14** 82

Figure 52. HRMS Spectrum of **15** 83

Figure 53. HRMS Spectrum of **16** 83

Figure 54. HRMS Spectrum of **17** 83

Figure 55. Size distribution of compound micellar compound **17** 84

CHAPTER I

Introduction

1.1 Photodynamic Therapy

Starting from the beginning of 20th century photodynamic therapy (PDT) has been recognized as an alternative treatment for various types of cancer [1-4]. Even though the first experiments to cure cancer date back to 1903, modern treatment of cancer cells with photodynamic therapy started in mid-20th century with the synthesis and application of compound called 'haematoporphyrin' known as HPD [3]. In 1975, Thomas Dougherty and co-workers reported the elimination of mammary tumor growth with HPD and red light in mice [5]. Following this initial demonstration of PDT in mice, patients of bladder cancer became first subjects of human trials in 1976 [6]. Afterwards, lung tumors [7], oesophageal cancer [8] and gastric carcinoma [9] patients were treated with PDT and promising responses were obtained from early-stage patients [3]. In subsequent studies PDT was utilized as a treatment for following tumors and cancer types: brain tumors [10-13], intraocular cancer [14-16], breast cancer [17-19], head and neck tumors [20,21], pancreatic cancer [22], gynaecological tumors [23,24]. In these studies PDT was partially successful due to intrinsic limitations [3]. In addition to intrinsic limitations, it was reported that PDT is applied on advanced stage patients such that local effect of PDT was unable to change the outcome of a disease [25]. However, in order to achieve a better PDT treatment, it is of crucial importance to understand the limitations of photodynamic therapy since properties of systematic disease cannot be changed. Therefore, each element of photodynamic therapy should be analyzed to gain better insight.

1.2 Keystones of Effective Photodynamic Therapy

Photodynamic therapy requires three elements: photosensitizer, light and oxygen. That is, lack of any of the elements results in unsuccessful treatment. Therefore, for a better treatment proper photosensitizer, delivery of light and existence of oxygen should be considered carefully.

1.2.1 Photosensitizers

1.2.1.1 Photophysics of Photosensitizers

Photosensitizers are responsible for production of main cytotoxic reagent in photodynamic therapy; singlet oxygen [26-28]. Formation of singlet oxygen requires excitation of photosensitizer with proper wavelength of light. That is, upon illumination of light, photosensitizer which is in the ground state (singlet ground state) can be transformed to higher energy states, to singlet excited state,

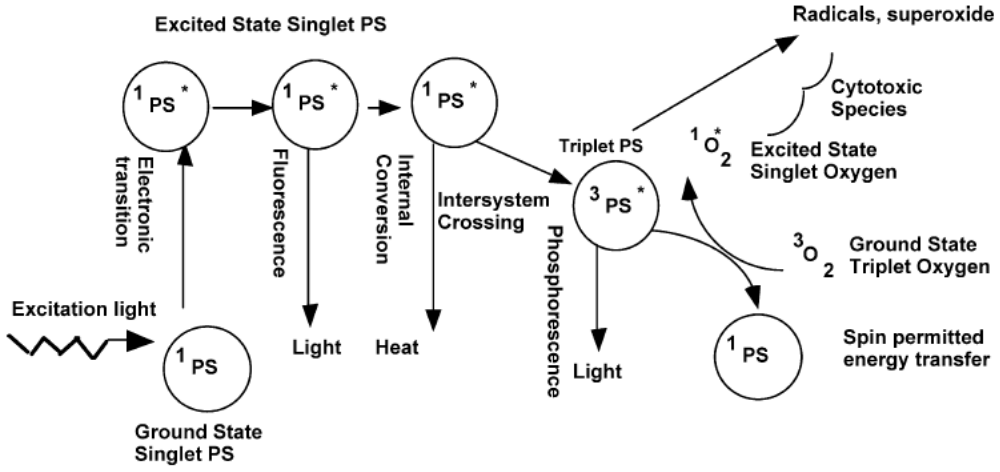

Figure 1. Electronic transitions of photosensitizer and production of singlet oxygen mechanism. Copyright © 2005, Elsevier B.V. Reprinted with permission from ref (26)

by one photon excitation [26]. Formed short lived excited state can undergo different relaxation pathways as seen in Figure 1. Upon emission of light, relaxation of photosensitizer to the ground state is known as fluorescence [26]. Instead of emission of light, during relaxation of photosensitizer heat can be generated and this process is known as internal conversion [26]. However, these processes do not contribute to the formation of main cytotoxic agent in PDT. Main electronic transition that leads to the formation of singlet oxygen is transition of singlet excited state of photosensitizer to triplet excited state; intersystem crossing [26,27]. Photosensitizer at triplet excited state can undergo various pathways as well. One of them is returning back to high energy singlet excited state and then following relaxation to the ground state; delayed fluorescence [29]. Another pathway is relaxation from triplet excited state to the ground state; phosphorescence [26]. However, key transition resulting in formation of singlet oxygen is energy transfer from photosensitizer at triplet excited to molecular oxygen at triplet ground state [26,27].

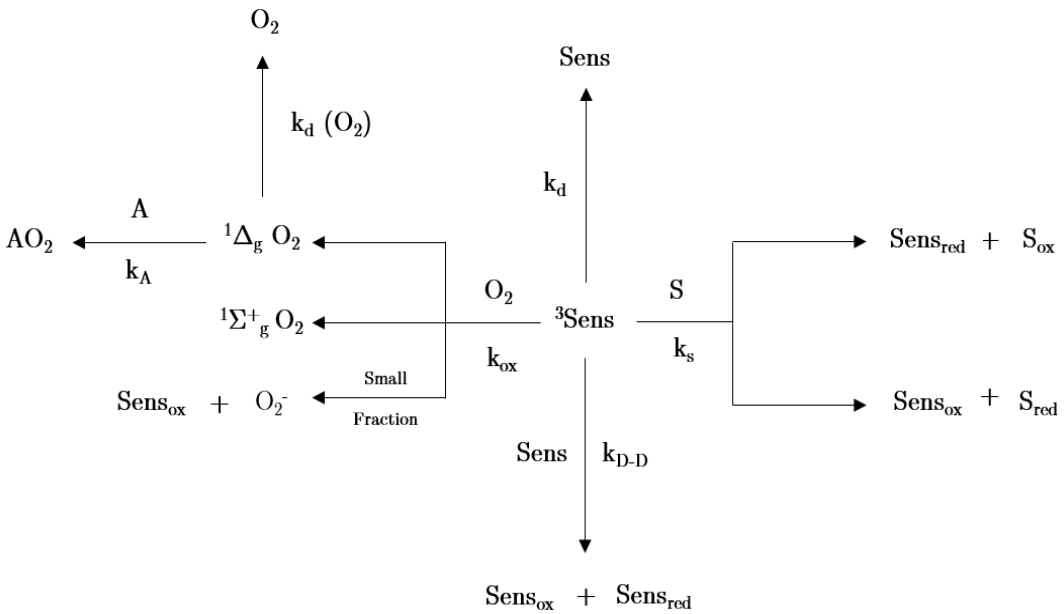

Figure 2. Possible reaction pathways of photosensitizer after excitation with light. Copyright © 1968, The American Association for Advancement of Science. Adapted with permission from ref (31)

These electronic transitions and formation of singlet oxygen give a general idea of how a photosensitizer behaves. However, for photodynamic action relatively long-lived triplet excited [30] state of photosensitizer compared to singlet excited state deserves more attention and detailed analysis.

Figure 2 depicts possible reaction pathways that a photosensitizer at triplet state can undergo. Triplet state photosensitizer may not only interact with molecular oxygen to form singlet oxygen but also react with any substrate by electron or proton transfer mechanisms or with itself by simply going through disproportionation to form oxidized and reduced form of the sensitizer [31].

1.2.1.2 Types of Photosensitizers

Photosensitizer at triplet excited state can react with substrate such as cell membrane or organic molecules in cell environment by simply electron or proton transfer to yield radical species [26]. These formed radicals are capable of forming superoxide anion which is in fact not harmful to cell [26]. In addition, superoxide anion can be formed with electron transfer from photosensitizer at triplet state to molecular oxygen [32,33]. Formed superoxide anion can react by itself to produce hydrogen peroxide in a reaction known as dismutation which is catalyzed by superoxide dismutase enzyme [26]. Formed hydrogen peroxide can yield hydroxyl radical in existence of superoxide anion and metal ions that naturally exist in biological systems [26]. Metal ions act as a catalyst and transfer electron from superoxide to hydrogen peroxide to form hydroxyl radical and hydroxyl anion [26]. Formed hydroxyl radical interacts with superoxide to form singlet oxygen, yet this is not the only reaction pathway that it pursues. Hydroxyl radical easily penetrates through cell membrane and reacts with organic molecules within cell [26]. For instance, fatty acids are capable of forming radical adduct with hydroxyl radicals and produced radical keeps reacting with either oxygen or other organic molecules in a chain reaction manner [26]. That

is, cell can be damaged with formation of reactive oxygen species in this particular way; Type I.

In Type II, photosensitizers at triplet state transfer energy to the molecular oxygen to produce singlet oxygen which is in fact capable of forming other reactive oxygen species and dealing damage to organic molecules within a cell [28]. For example, reactive oxygen species may react with cysteine, methionine, tyrosine, histidine and tryptophan, even direct interaction of singlet oxygen is capable of destruction of amino acids including histidine and methionine [26,31].

Formation of reactive oxygen species (ROS) is mechanistically easy via Type II process compared to Type I process [28]. This can be realized in a general reaction scheme depicted in Figure 3. Unless photosensitizer relaxes, it can either react with molecular oxygen or a substrate. Reported k value of the interaction

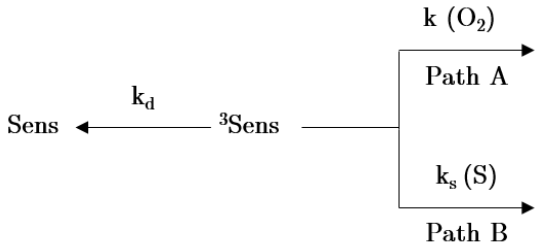

Figure 3 Simplified reaction pathways of photosensitizer at triplet state. Copyright © 1968, The American Association for Advancement of Science. Reprinted with permission from ref (31)

of photosensitizer with molecular oxygen is in the order of 10^9 M^{-1} sec^{-1} [31]. If k value of the reaction of substrate with photosensitizer is small or the concentration of the substrate is low, even trace amount of molecular oxygen is capable of inhibiting reaction path B [31]. Therefore, oxygen containing medium is expected to favor mostly reaction path A, meaning that Type II process is expected to overwhelm path B. Therefore, main pathway that photosensitizer operates is considered to be Type II process [28].

1.2.1.3 Subcellular Uptake of Photosensitizers

Singlet oxygen has half-life lower than 0.04 µs in biological systems, and, therefore its effective area of action is no larger than 0.02 µm [3]. Cytotoxicity of photosensitizer is not only dependent on oxygen level, light exposure, light penetration, amount of the photosensitizer and type of a sensitizer but also highly related with interaction of the photosensitizer with cells of tumor or target tissue [27]. By considering the effective radius of singlet oxygen, localization of photosensitizer is of crucial importance for an effective photodynamic effect.

Studies have shown that photosensitizers can localize in different organelles such as mitochondria, lysosome, endoplasmic reticulum, golgi apparatus and plasma membranes [34]. Intracellular uptake and localization of photosensitizers vary depending on several structural features. The net ionic charge has been reported to be between -4 and +4 in order to penetrate cell membrane [26,27]. Hydrophobicity (reported with a scale of octanol/water partition coefficient) of the photosensitizer in another constraint for cellular uptake and intracellular localization [26,27]. Asymmetry of photosensitizer plays a role in intracellular localization of photosensitizer as well [26,27]. Hydrophobic photosensitizer whose net ionic charge is lower than negative four can penetrate through cell membrane and localize in a cell [26,27]. Less hydrophobic photosensitizers whose net ionic charge is higher than negative two are taken into cell by endocytosis [26,27].

Lysosome was considered to be a critical target in PDT; however, subsequent studies proved that mitochondria or other organelle localized photosensitizers have shown significant cytotoxicity upon illumination compared to lysosome localized photosensitizers [35-37]. This was explained by aggregation of photosensitizer localized in lysosome greatly [26]. Yet, efficacy of lysosome localize photosensitizer can be increased by lower light exposure which leads to

enhancement in permeability of lysosome membrane and redistribution of photosensitizers in cytoplasm and nucleus [38,39].

Net negative ionic charge bearing photosensitizers localize in lysosome; in contrast, positively charged photosensitizers preferentially locate in mitochondria [26]. Localization of positively charged photosensitizers in mitochondria is attributed to the membrane potential of mitochondria and lipid bilayer structure of the organelle membrane [40]. Mitochondria localized photosensitizers are capable of destroying energy power plant of a cell and releasing Ca^{+2} ions associated with cell death [27].

Photosensitizers have been shown to locate in plasma membrane although this is uncommon in cultured cells. Plasma membrane localized photosensitizers caused disruption of plasma membrane and swelling of cell immediately after photodynamic therapy [26]. That is, localization of photosensitizers varies and their effect on the cell viability is highly dependent on the where they locate during photodynamic therapy.

1.2.1.4 Cell Death and Tumor Destruction Imposed by PDT

There are three possible mechanisms of tumor disappearance or reduction in photodynamic therapy as seen in Figure 4. Reactive oxygen species formed in PDT can damage the vasculature of tumor tissue [27,28]. This yields the dissipation of blood vessels that carry oxygen and nutrition to tumor tissue via thrombosis and hemorrhage [41-43]. Consequently, tumor death is observed due to lack of oxygen and essential nutrients [27].

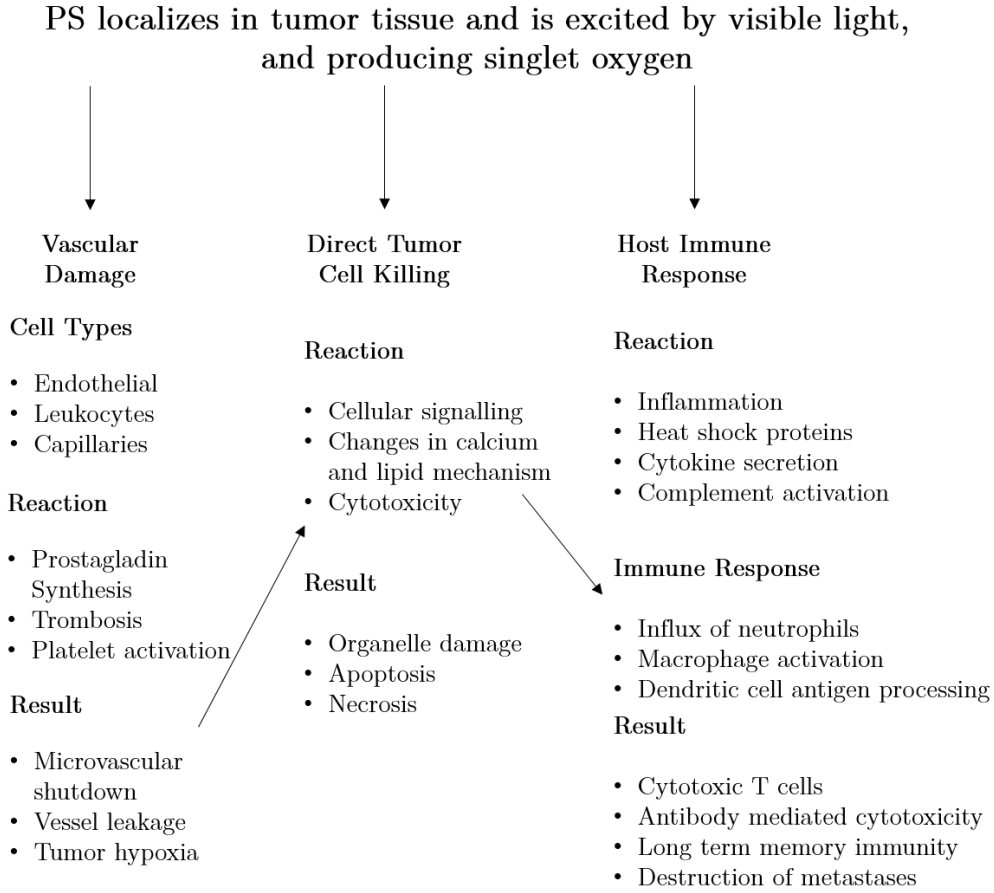

Figure 4. Graphical representation of types of tumor reduction mechanisms by singlet oxygen and ROS. Copyright © 2009, Elsevier B.V. Adapted with permission from ref (27)

Photodynamic therapy can induce release of cytokines, inflammation and synthesis of proteins as a response in tumor [44,45]. These changes in tumor result in invasion of white blood cells which facilitate the destruction of tumor and trigger immune system [46].

Lastly, photodynamic therapy directly kills tumor cells (if photosensitizer locates inside of the tumor cells) by forming reactive oxygen species. Cell death takes place in different mechanisms [26]. These mechanisms are dependent on cell type, localization of photosensitizer and amount of exposure to light [27,47]. Generally, mild doses of photodynamic therapy leads to mainly apoptotic cell death which is controlled destruction of cell without causing inflammation [48]. In apoptotic cell death, cell shrinkage is observed along with retaining of cell unity and remaining of cell is wiped away by phagocytes [27]. However, exhaustive doses of photodynamic therapy yield necrotic cell death which is unprogrammed, abrupt destruction of cell with causing inflammation and destruction of cell unity [27]. Apoptosis and necrosis have similar initiation pathways but an active caspase (protease enzymes causing programmed cell death) determines the type of death. In addition, inhibition of apoptosis doesn't decrease of efficiency of photodynamic therapy, and main cell death pathways follow necrosis [43].

1.2.1.5 Properties of Ideal Photosensitizer

First approved photosensitizer for treatment of different cancer types throughout the world is semi-purified haematoporphyrin known as Photofrin® (PF) [49]. In time, PDT treatments with this particular drug has showed that drug is not selective for tumor, light that it absorbs (around 630 nm) has poor penetration, its structure is uncertain and it causes skin sensitivity leading patients to avoid sunlight for a few weeks [50]. Therefore, there has been many attempts to produce new photosensitizer as a drug to overcome these problems.

In many reviews ideal photosensitizer is discussed and followings are the properties of an ideal photosensitizer [51,52],

- Low dark toxicity
- Red or Near-IR absorption

Sensitizer	Trade name	Potential indications	Activation wavelength
HPD (partially purified), porfimer sodium	Photofrin	Cervical*, endobronchial*, oesophageal*, bladder* and gastric cancers*, and brain tumours	630 nm
BPD-MA	Verteporfin	Basal-cell carcinoma	689 nm
m-THPC	Foscan	Head and neck tumours*, prostate and pancreatic tumours	652 nm
5-ALA	Levulan	Basal-cell carcinoma, head and neck, and gynaecological tumours Diagnosis of brain, head and neck, and bladder tumours	635 nm 375–400 nm
5-ALA-methylesther	Metvix	Basal-cell carcinoma*	635 nm
5-ALA benzylesther	Benzvix	Gastrointestinal cancer	635 nm
5-ALA hexylesther	Hexvix	Diagnosis of bladder tumours	375–400 nm
SnET2	Purlytin	Cutaneous metastatic breast cancer, basal-cell carcinoma, Kaposi's sarcoma, prostate cancer	664 nm
Boronated protoporphyrin	BOPP	Brain tumours	630 nm
HPPH	Photochlor	Basal-cell carcinoma	665 nm
Lutetium texaphyrin	Lutex	Cervical, prostate and brain tumours	732 nm
Phthalocyanine-4	Pc 4	Cutaneous/subcutaneous lesions from diverse solid tumour origins	670 nm
Taporfin sodium	Talaporfin	Solid tumours from diverse origins	664 nm

*Indications that are registered in one or more countries (all other indications are in development). 5-ALA, 5-aminolevulinic acid; BPD-MA, benzoporphyrin derivative-monoacid ring A; HPD, haematoporphyrin derivative; HPPH, 2-(1-hexyloxyethyl)-2-devinyl pyropheophorbide-alpha; mTHPC, meta-tetrahydroxyphenylchlorin; SnET2, tin ethyl etiopurpurin.

Figure 5. List of examples of photosensitizers with trade name, potential indications and activation wavelength. Copyright © 2003, Rights Managed by Nature Publishing Group. Reprinted with permission from ref (3)

- High absorption coefficient (>20 000 M^{-1} cm^{-1})
- Easy synthesis of photosensitizer
- Known composition and long shelf-life
- Easy elimination from patient
- High singlet oxygen quantum yield

As a consequence of such expectations from a drug, there has been various types of photosensitizers designed and under clinical investigation as given examples in Figure 5.

1.2.2 Light in PDT

Light is not only necessary for production of singlet oxygen via excitation of photosensitizer but also it plays a crucial role for selectivity. That is, by simply illumination of light to certain tissue, photodynamic action can be selectively directed. Also, independent of dose of the photosensitizer, change in light exposure can be utilized to regulate photodynamic therapy [3]. However, delivery and homogenous distribution of light in tissue is a challenging issue [26].

Assuming that delivery of light to tissue is accomplished, light is either absorbed or scattered. Inhomogeneity stemming from cell organelles, macromolecules and cell structure causes turbidity in cell environment [26]. This turbid environment causes scattering of light which restricts light penetration by simply causing loss of directionality and is dependent on the type of a cell [26]. In addition, macromolecules such as cytochromes, myoglobin, and hemoglobin also absorb delivered light. In addition, water in cell environment absorbs light wavelengths higher than 1300 nm greatly [26].

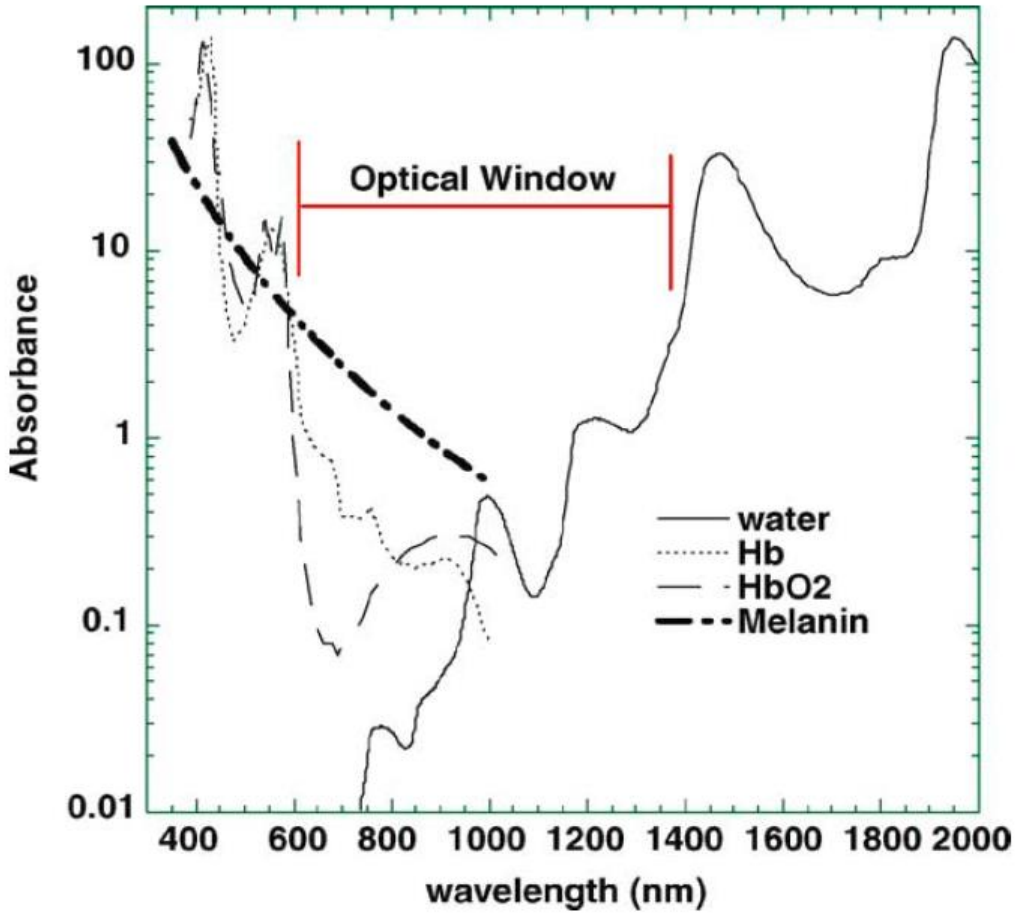

Figure 6. Absorbance of water, hemoglobin and melanin depending on wavelength and optical window for PDT. Copyright © 2005, Elsevier B.V. Reprinted with permission from ref (26)

All these conditions are taken into account, most penetrable light range lies between 600 and 1200 nm known as 'therapeutic window' or 'optical window' as seen in Figure 6 [53]. Therefore, delivered light needs to be red or infrared so that maximum penetration can be achieved. However, light having wavelength higher than 800 nm is not able to produce singlet oxygen effectively as reported by Golab et.al. [28].

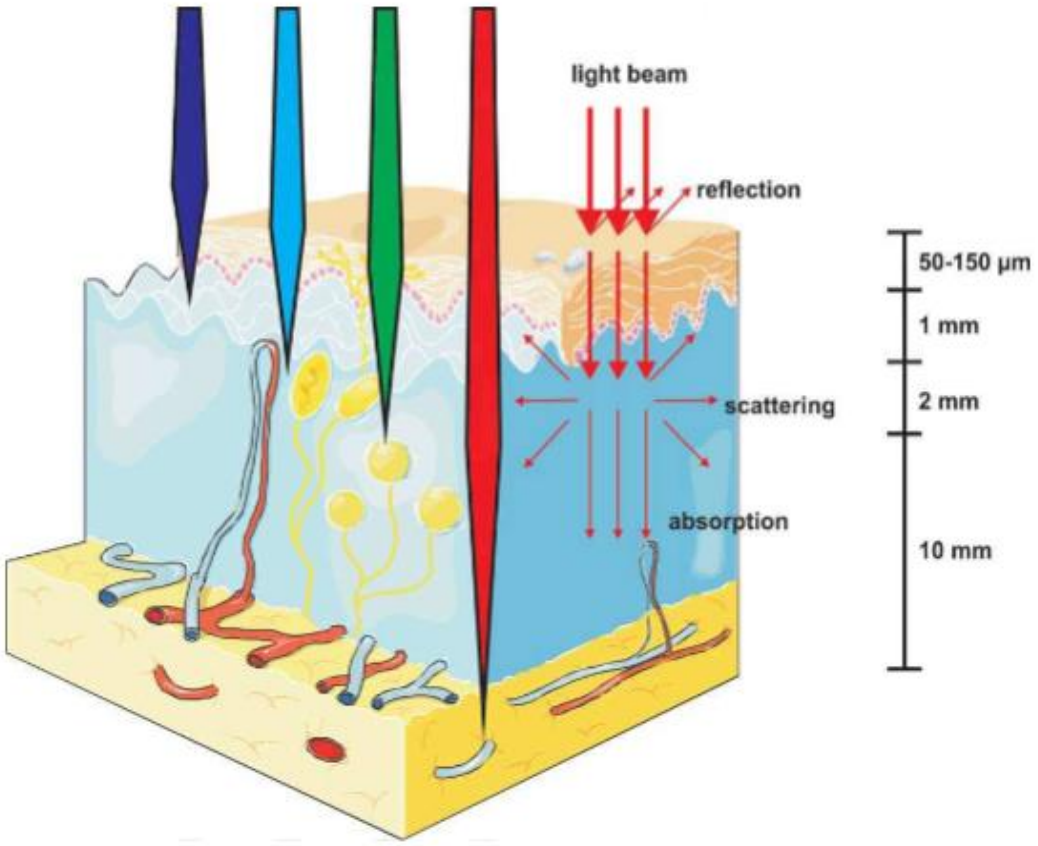

Figure 7. Illustration of light penetration depending on wavelength and scattering, reflection and absorption of light. Copyright © 2011 American Cancer Society, Inc. Reprinted with permission from ref (28)

600 nm wavelength light can penetrate 1 to 3 mm into tissue, but penetration can be doubled with usage of light between 700 and 800 nm as seen in Figure 7 [53]. Therefore, longer wavelength absorbing photosensitizers is required to increase the efficiency of the photodynamic therapy as stated in properties of ideal photosensitizer.

Light delivery is also an issue that needs an interest. Incandescent light sources are not suitable for photodynamic action due to thermal effect, lack of control on light dose and low light intensity, yet with engineering this type of light source can be utilized in PDT [28]. Therefore, more advanced light sources are highly required. Fiber optic delivery systems are capable of tuning the

wavelength of light between 350 and 800 nm with intensity for broad range of photosensitizers for clinical applications. Light emitting diodes (LEDs) can satisfy high intensity of light at desired wavelength, yet this is not its only superiority. LEDs can be arranged in different geometric shapes and sizes such that LEDs can be utilized in vide variety of ways ranging from light delivery to superficial lesions (by usage of array of LEDs) to tumor implanted light delivery (in catheter) [2]. Power of lasers and optical fibers can be utilized for better light delivery systems. Lasers can produce monochromatic light with high intensity such that focused laser light to optical fiber is capable of delivering light directly to tumor effectively [54,2]. That is, depending on type of tissue, cell and depth in body, there are several choices for delivery of light.

1.2.3 Oxygen in PDT

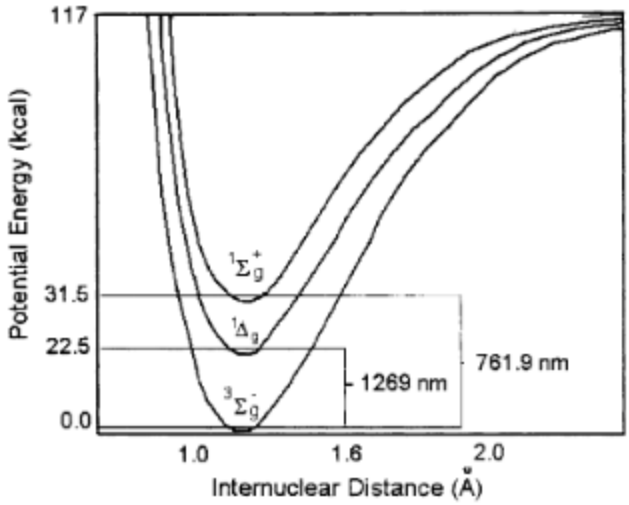

Figure 8. Potential energy curves of ground and first two excited states of oxygen depending on internuclear distance. Copyright © 2002 Elsevier Science B.V. Reprinted with permission from ref (55)

It is stated that singlet oxygen is the main cytotoxic agent in photodynamic therapy; therefore, electronic states of singlet oxygen deserve attention. Figure 8 contains two excited and ground electronic states of molecular oxygen.

First excited state of molecular oxygen is $^1\Delta_g$ lies 22.5 kcal/mol or 95 kj/mol above the ground state of molecular oxygen ($^3\Sigma^-_g$) [55]. Second excited state ($^1\Sigma^+_g$) of molecular oxygen is higher in energy than ground state of molecular oxygen by 31.5 kcal/mol or 158 kj/mol [55]. Comparing the two excited state of molecular oxygen, first excited state ($^1\Delta_g$) is more stable than second excited state ($^1\Sigma^+_g$) since transition from second excited state to first excited state is spin-allowed; therefore, $^1\Delta_g$ O_2 is considered to be long-lived compared to $^1\Sigma^+_g$ O_2 [55]. This is because transition from first excited state ($^1\Delta_g$) to ground state ($^3\Sigma^-_g$) is spin-forbidden. In gas phase lifetimes of first and second excited states were found as 45 minutes and 7-12 seconds, respectively [56].

Also, in solution range of lifetime of excited states are ranging from 10^{-6} to 10^{-3} s and 10^{-11} to 10^{-9} s, respectively [57]. Besides, emission and absorption spectra of transition between ground state and metastable first excited state of molecular oxygen at 1268.7 nm has been observed even though the transition is spin forbidden [55]. Therefore, singlet oxygen in photodynamic therapy can be considered as first excited state of molecular oxygen. However, its lifetime varies depending on the type of the solution as expected [58]. Figure 9 shows the dependence of lifetime of singlet oxygen on solvents at various temperatures. Singlet oxygen lifetime decreases drastically from gas phase to solution indicating that existence of solvent has a huge effect on the lifetime of singlet oxygen [59,60]. This observation is explained by dependence of electronic transitions of singlet oxygen on perturbations (such as electronic-vibrational coupling) induced by solvent molecules since 0-0 transition of singlet oxygen at 1268.7 nm coincides with overtones of C-H and O-H bonds [60]. Also, it is reported that there is state of charge transfer of oxygen with solvents [59]. Given situation above, singlet oxygen lifetime decreases in existence of solvent. Interaction of singlet oxygen with solvent is expected to change depending chemical structure of solvent. One trend is that increase in polarity of solvent decreases singlet oxygen lifetime. But, singlet oxygen lifetime drastically decreases in the existence of O-H bond and it was argued by Young et. al. that

such drastic decrease can be correlated with existence of hydrogen bonding [59]. Therefore, such interaction is expected to decrease in existence of deuterated

Solvent	τ_Δ/μs				
	5 °C	25 °C	50 °C	75 °C	90 °C
Benzene-h_6	—[b]	30.4	30.3	30.2	—[b]
Benzene-d_6	—[b]	731	592	453	—[b]
Toluene-h_8	31.6	30.3	28.7	27.1	26.1
Toluene-d_8	407	298	205	143	114
α,α,α-Trifluorotoluene	61.3	61.8	62.7	63.8	64.5
o-Xylene	25.6	23.0	19.9	17.0	15.2
Mesitylene	20.0	16.4	12.8	10.1	8.9
Chlorobenzene	43.7	43.5	43.3	43.1	42.9
Iodobenzene	39.2	38.8	38.2	37.6	37.2
1,2-Dichlorobenzene	57.1	57.0	56.6	55.9	55.2
1,2,4-Trichlorobenzene	—[b]	93.9	94.2	94.4	94.5
Cyclohexane-h_{12}	—[b]	23.9	23.5	23.2	—[b]
Cyclohexane-d_{12}	—[b]	485	494	501	—[b]
n-Pentane	34.9	34.8	—[b]	—[b]	—[b]
n-Hexane-h_{14}	32.6	32.1	31.5	—[b]	—[b]
n-Hexane-d_{14}	573	588	608	—[b]	—[b]
n-Heptane	30.3	30.0	29.6	28.9	28.5
n-Octane	29.1	28.5	27.8	26.9	26.4
n-Decane	27.0	26.4	25.6	25.0	24.6
Methanol-h_4	8.9	9.5	9.7	—[b]	—[b]
Methanol-OD	32.0	31.3	30.3	—[b]	—[b]
Methanol-d_4	282	275	257	—[b]	—[b]
1-Propanol	15.8	15.9	16.1	16.4	16.6
1-Octanol	17.8	17.7	17.7	17.6	17.4
Benzyl alcohol	15.0	14.3	13.1	11.8	10.9
Acetone-h_6	43.9	45.8	47.6	—[b]	—[b]
Acetone-d_6	989	1046	1083	—[b]	—[b]
Acetonitrile-h_3	81.6	80.9	79.9	78.8	—[b]
Acetonitrile-d_3	1604	1613	1662	1752	—[b]
Benzonitrile	40.0	40.1	40.1	40.1	40.1
H_2O[c]	3.57	3.45	3.27	3.07	2.93
D_2O[c]	77.8	67.9	58.3	51.9	49.5

Figure 9. Lifetime of singlet oxygen in different solvents at varying temperatures. Copyright © 2016, Royal Society of Chemistry. Reprinted with permission from ref (58).

solvents as seen in Figure 9 as well. Therefore, it can be argued that in the existence of deuterium in solvent molecules interaction of solvent molecules in terms of hydrogen bonding and electronic-vibrational coupling (since vibrational modes change) with singlet oxygen decreases greatly leading longer lifetime.

As already mentioned previously, photosensitizers operate in two different ways leading the separation of photosensitizer as Type I and Type II [26,28,31]. In Type II photosensitizers, transfer of energy from triplet excited state of photosensitizer to molecular oxygen yields singlet oxygen. Capability of

production of singlet oxygen by photosensitizer in this type is characterized by singlet oxygen quantum yield [61]. This indicates efficiency of singlet oxygen production compared to other chemical and physical quenching pathways including physical quenching with molecular oxygen as P(T1) + O2 →P(S0) + O2 [61].

In upcoming section increase of singlet oxygen quantum yield will be discussed. However, it is obvious that for better treatment and usage of lower drug concentration, high singlet oxygen quantum yield is expected from photosensitizers as listed in properties of ideal photosensitizers.

Along with physical quenching of singlet oxygen with solvents and quenchers, there is also chemical quenching which is at the core of photodynamic therapy. That is, formed singlet oxygen at target area is capable of reacting with macromolecules and structural elements of cell to induce cell death [26,31]. However, to be able to employ such a treatment method, dissolved oxygen is necessary, yet for application of treatment to cancer tissue which imposes hypoxic condition lack of oxygen renders the treatment ineffective [62,63]. Besides, hypoxia induced by photodynamic action by usage of dissolved oxygen in cell and causing vascular closure leads treatment to be self-limiting [62,63]. Therefore, for better treatment issue of lack of oxygen needs to be solved.

1.2.4 Fractional Photodynamic Therapy

Photodynamic therapy is employed to destroy tumor which imposes hypoxia. However, for PDT oxygen is one of the key elements. In photodynamic therapy, photosensitizer produces singlet oxygen by consuming dissolved oxygen in cell within minutes [64]. Also, it is mentioned that PDT mediated tumor reduction stems from different pathways including destruction of blood vessels feeding tumor [62,63]. During PDT such damage on blood vessels may lead to drastic oxygen level decrease. Therefore, lack of oxygen decreases the efficiency of

photodynamic action during treatment. However, such damage should not be considered as an obstacle to overcome since it is one of the major ways of destruction of tumor [26]. That is, during treatment it is imperative to keep the oxygen level as high as possible. Moore et. al. reported that during treatment of prostate carcinoma in rats fractionated light delivery showed better performance compared to light delivery in continuous manner [62]. Chen et. al. reported that fractionation of light leads to increase in oxygen supplement to enhance the treatment. That is, allowing cells to replenish dissolved oxygen increases the efficiency of the treatment during dark cycle of photodynamic therapy [63]. However, this type of an approach increases treatment time while dark cycle is practically not utilized for treatment (off-time for replenishment of oxygen). That is, usage of this dark cycle for better treatment would be an ideal way for the design of a drug.

1.3 BODIPY Dyes

4,4-difluoro-4-bora-3a,4a-diaza-s-indacene known as BODIPY (Figure 10) is a fluorescent dye core ($\phi_f = 0.7$, $\varepsilon = 120000\ M^{-1}\ cm^{-1}$) found by Treibs and Kruzer in 1968 [65]. BODIPY has drawn attention greatly since its unique properties such as high extinction coefficient, chemical stability, large fluorescence quantum yield, and resistance to photobleaching and low dark toxicity along with ease of synthesis, purification and functionalization [49]. Therefore, BODIPY dyes have many application areas; solar cells [66,67], energy transfer cassettes [68], molecular logic gates [69], light harvesting systems [70], and photodynamic therapy [71,72].

1.3.1 BODIPY as Photosensitizer

BODIPY type dye (**1**) as seen in Figure 10 is not an optimal photosensitizer for photodynamic application since it has low singlet oxygen quantum yield and its absorption maxima ($\lambda_{max} = 508$ nm) is not in most penetrable light range [49]. However, BODIPY type dyes can be functionalized for photodynamic applications.

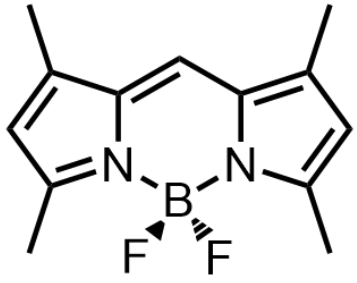

Figure 10. BODIPY type dye (**1**) obtained from 2,4-dimethylpyrrole

1.3.2 Heavy Atom Effect

BODIPY dye (**2**) shown in Figure 11 has low fluorescence quantum yield compared to BODIPY dye given in Figure 10 and singlet oxygen generation rate

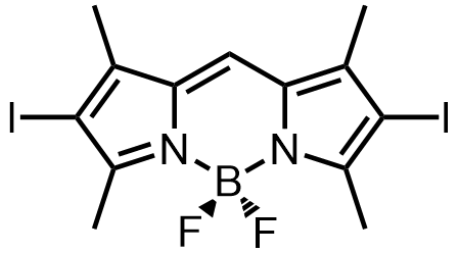

Figure 11. Iodine functionalized BODIPY (**2**) at 2 and 6 positions

is 24 times of methylene blue [73]. The major difference in between these dyes is functionalization of **1** with iodine atoms at 2 and 6 positions. This effect of iodine atoms is known as heavy atom effect. The reason behind the increase in singlet oxygen quantum yield is the increase in efficiency of intersystem crossing due to spin orbit coupling [73]. Therefore, in order to utilize BODIPY type dyes in photodynamic therapy functionalization at positions 2 and 6 with heavy atoms such as bromine and iodine can be employed to increase singlet oxygen quantum yield of a dye.

1.3.3 Halogen Free BODIPY Dyes

In previous section, one of the ways of increase in singlet oxygen quantum yield of BODIPY type dye is mentioned. Yet, functionalization of BODIPY type dyes with heavy atoms is not the only way of increasing singlet oxygen quantum yield. BODIPY dye **3** in Figure 12 has been reported by Akkaya et. al. as a halogen free orthogonal BODIPY dye with singlet oxygen quantum yield of 0.51 [74]. Another halogen free low fluorescent quantum yield BODIPY type dye **4** which is capable of producing singlet oxygen (singlet oxygen quantum yield is

0.85) is given in Figure 13. In this structure fluorescence of BODIPY dye is

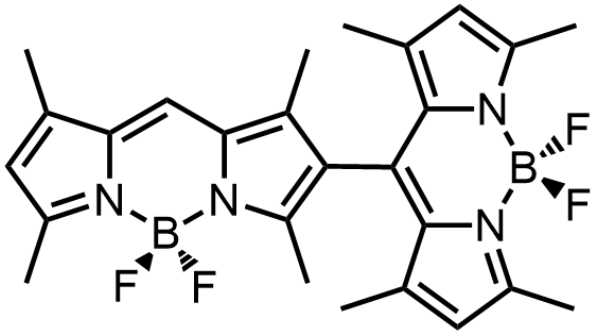

Figure 12. Orthogonal designed BODIPY (**3**) being capable of producing singlet oxygen

quenched through intramolecular energy transfer to C_{60}-dyads, leading formation of long-lived triplet excited states of this design [75].

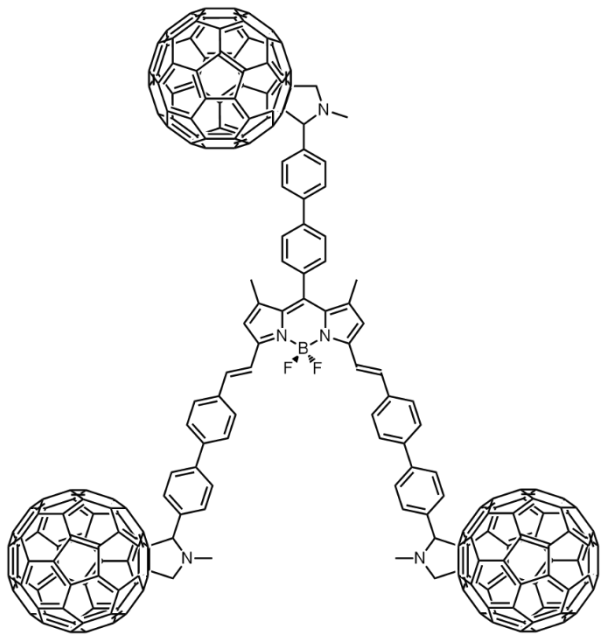

Figure 13. C_{60}-dyads containing, halogen free BODIPY design (**4**)

1.3.4 Longer Wavelength Absorbing and Emitting BODIPY Dyes

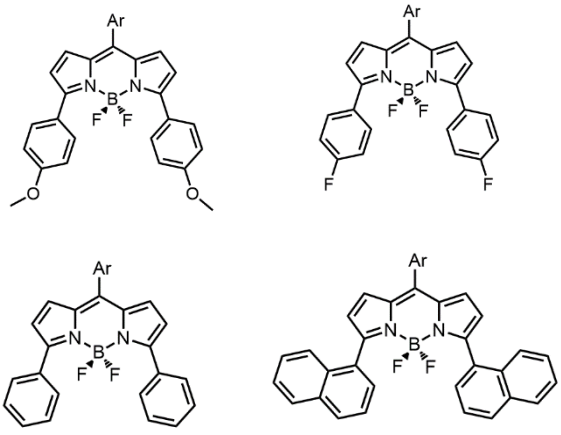

Figure 14. Relatively longer wavelength absorbing, aromatic group substituted (at 3 and 5 position) BODIPY designs (**5**, **6**, **7**, and **8** from top-left to bottom-right)

For photodynamic therapy application, a dye has to absorb in therapeutic window. However, BODIPY **1** has absorbance maximum at 508 nm which is not in the therapeutic window. Therefore, this core dye needs to be functionalized for PDT applications. One of the reported ways of preparing relatively longer wavelength absorbing BODIPY dye is using aryl-pyrroles to prepare dyes **5-8** given in Figure 14 [76,77]. However, these dyes are still not in the photodynamic therapeutic window. Functionalization of BODIPY from 3 and 5 positions is another approach to obtain longer wavelength absorbing photosensitizers. Hydrogen atoms at 3 and 5 positions are capable of participating in Knoevenagel condensation reaction which enables to form mono [78] and also di styryl-BODIPY dyes shown for the first time by Akkaya et. al.[79]. BODIPY type dyes **9**, **10** absorb and emit higher than 550 nm as seen in Figure 15 [78,79].

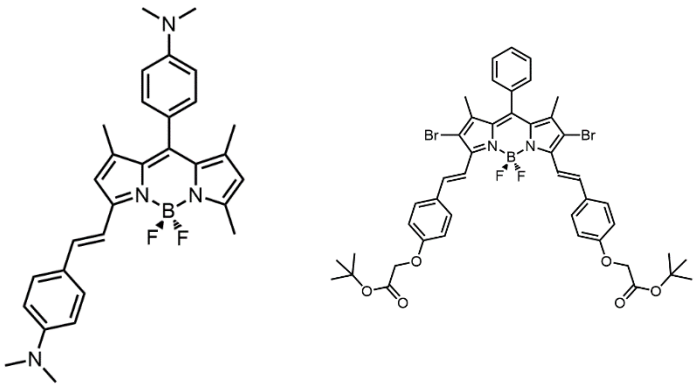

Figure 15. Mono (**9**) and di-styryl (**10**) substituted (at 3 and 5 positions) BODIPY designs

By using methods mentioned above desired BODIPY type dye can be prepared for photodynamic therapy applications.

1.4 Alternative Singlet Oxygen Delivery System

Singlet oxygen is not necessarily to be produced by photosensitizer in tumor. That is, produced and stored singlet oxygen can be released in desired tissue for treatment purposes [80]. This kind of singlet oxygen delivery and release system can be achieved by using electron-rich aromatic structures. Singlet oxygen can effectively form endoperoxides with vide variety of structures by following [4+2] cycloaddition mechanism [81].

Storage of singlet oxygen by means of endoperoxides is controlled by steric and electronic effects. That is, aromatic hydrocarbons with high electron densities tend to react faster with singlet oxygen, indicating the electrophilicity of singlet oxygen [81]. For example, methoxy group containing aromatic hydrocarbon reacts faster than methyl containing counterpart [82]. Steric effects may vary depending on the structure, so analysis of some cases would lead to better insight. Heli-anthracene known as HEL (**11**) can readily react even with triplet

oxygen and its reactivity toward singlet oxygen is at almost diffusion controlled rate [81]. Considering the structure of HEL, hydrogen of carbon 11 and 12 forces

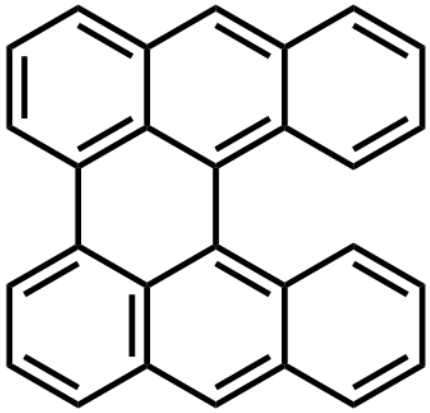

Figure 16. Heli-anthracene (HEL) (**11**)

to benzene rings to twist out so that benzene rings cannot be on the same plane. This causes severe strain on the structure, especially adjacent double bonds. Upon addition of singlet oxygen to form endoperoxides such strain can be released, indicating why this reaction occurs at almost diffusion controlled rate constant [81,83].

Another example is naphthalene derivative; 1,8-dimethylnaphthalene. This aromatic compound reacts faster compared to 1,5-isomer and this is explained by release of steric strain in the transition state while forming singlet oxygen [84].

1.4.1 Endoperoxide Formation Mechanism

[4+2] addition of singlet oxygen to aromatic rings occurs in a concerted mechanism as in the case of Diels-Alder reaction, yet it is not entirely the same. Figure 17 shows the mechanism of addition of singlet oxygen to the aromatic ring. At first singlet exciplex forms reversibly. Strong electrophilic character of singlet oxygen imposes charge-transfer character to exciplex. This exciplex either

forms endoperoxide in a concerted manner or goes through spin-forbidden ISC to yield complex at triplet state which further dissociates to form aromatic ring

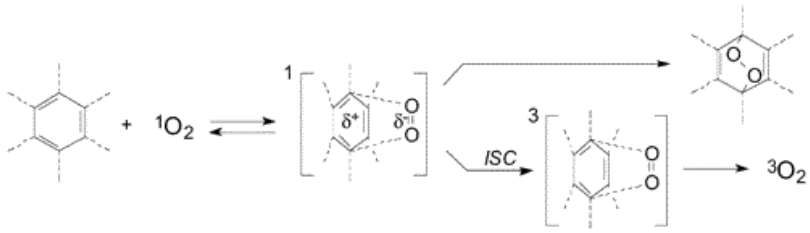

Figure 17. Endoperoxide formation mechanism through exciplex. Reprinted (adapted) with permission from (81). Copyright © 2003 American Chemical Society.

and ground state oxygen. Formation of singlet oxygen and ground state oxygen is considered as chemical quenching, and physical quenching, respectively [85].

1.4.2 Dissociation of EPOs

Endoperoxide structures can dissociate in two competing pathways: cycloreversion, yielding parent aromatic hydrocarbon and oxygen (either singlet or triplet oxygen); hemolytic cleavage followed by rearrangement or decomposition as seen in Figure 18 [81].

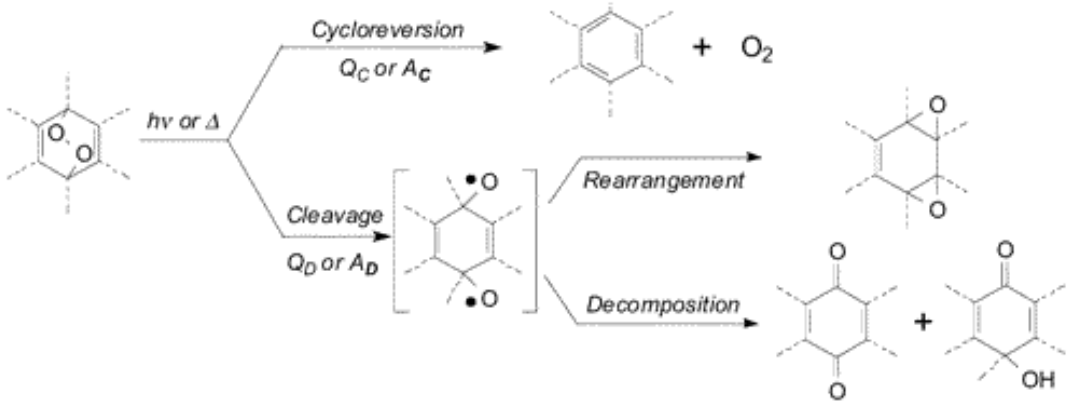

Figure 18. Two major dissociation mechanisms of endoperoxide structures. Reprinted (adapted) with permission from (81). Copyright © 2003 American Chemical Society.

Upon concerted cycloreversion, singlet oxygen is produced. However, there is another pathway which yields singlet and triplet oxygen; diradical formation.

Formed diradical at singlet state can form singlet oxygen, yet diradical that goes through intersystem crossing yields triplet oxygen as seen Figure 19 [86].

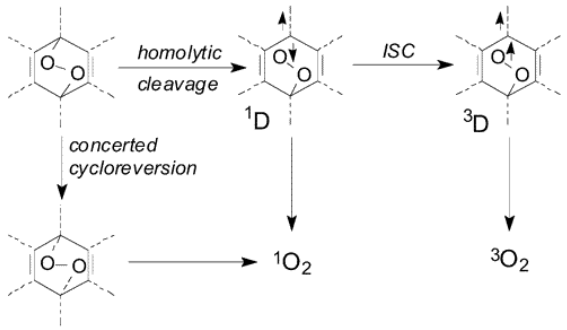

Figure 19. Mechanisms of singlet oxygen release from endoperoxides. Reprinted (adapted) with permission from (81). Copyright © 2003 American Chemical Society.

1.4.3 Singlet Oxygen Carriers

1,4-dimethylnaphthalene is an efficient singlet oxygen storage and release unit that is organic solvent soluble. This structure is widely applicable due to, commercially availability, chemical stability of endoperoxide, relatively fast reaction with singlet oxygen and release of singlet oxygen at 298 K with half-life of 5 hours. That is, stored singlet oxygen in this structure can be released with gentle warming. Also, this structure can be stored at 193 K for a long time [87].

9,10-diphenyl anthracene derivatives are also another type of singlet oxygen carriers. 9,10-antharacene derivative being connected to gold nanorods can store singlet oxygen at room temperature for several years, yet release of singlet oxygen upon heating of gold nanorods with light at 808 nm reported by Akkaya et. al. for photodynamic therapy application [88].

Another type of singlet oxygen storage unit is 2-pyridone. It was reported that N-substituted 2-pyridone can store singlet oxygen and release with high efficiency (>80%). Benzyl substituted 2-pyridone can release singlet oxygen with

96% efficiency at low conversion rates and with 81% efficiency at high conversion rates, so that its singlet oxygen release efficiency is higher than commercially available 1,4-dimethylnapthalene [89]. Turro et. al. reported that activation entropy of thermal release of singlet oxygen from endoperoxides varies from slightly positive to negative. Structures that have slightly positive activation entropy yields low singlet oxygen release, yet structures that have negative activation entropy yields high singlet oxygen release [90,91]. Therefore, high singlet oxygen yield of N-substituted 2-pyridone structures can be explained by activation entropies ranging from zero to slightly negative values. For example, benzyl substituted 2-pyridone has -5.3 cal K^{-1} mol^{-1} activation entropy, explaining its high singlet oxygen release capacity [81].

It was stated earlier that endoperoxides can be source of singlet oxygen for practical treatment of tumor. In this particular example, BNPE (1-methylnaphthalene-4-propionate endoperoxide), MNPE (1-methylnaphthalene-4-propionate endoperoxide) and NDPE (naphthalene-1,4-dipropionate endoperoxide) are employed in a study to understand the effect of singlet oxygen in cell death mechanism. Findings indicate that singlet oxygen released from endoperoxides triggered death mechanism resembling apoptosis [80]. By considering the release and storage capacity of endoperoxides (EPOs) and their capability of triggering cell death, these structures can be utilized for cancer treatment.

CHAPTER II

Experimental Procedures

This work has been partially described in the following publication:

Turan, I. S., Yildiz, D., **Turksoy, A.**, Gunaydin, G., & Akkaya, E. U. "A Bifunctional Photosensitizer for Enhanced Fractional Photodynamic Therapy: Singlet Oxygen Generation in the Presence and Absence of Light". *Angewandte Chemie*, 128.8 (2016) :2925-2928.

2.1 General Procedures

^{1}H NMR and ^{13}C NMR spectra were recorded on Bruker Spectrospin Avance DPX 400 spectrometer (operating at 400 MHz for ^{1}H NMR and 100 MHz for ^{13}C NMR) using $CDCl_3$ as the solvent with tetramethylsilane (TMS) as internal standard. Chemical shifts values are reported in ppm from tetramethylsilane as internal standard. Spin multiplicities are reported as the following: s (singlet), d (doublet), dd (doublet of doublet), ddd (doublet of doublet of doublet), dt (doublet of triplet), m (multiplet). HRMS data were acquired on an Agilent Technologies 6530 Accurate-Mass Q-TOF LC/MS. Electronic absorption spectra in solution were acquired using a Varian Cary-100 spectrophotometer and fluorescence spectra were determined on Varian Eclipse fluorospectrometer. Electrophoretic Light Scattering was performed with Malvern NanoZS zeta potential. Spectrophotometric grade solvents were used for spectroscopy experiments. Flash column chromatography (FCC) was performed by using glass columns with a flash grade silica gel (Merck Silica gel 60 (particle size: 0.040-0.063 mm, 230-400 mesh ASTM)). Reactions were monitored by thin layer chromatography (TLC) using precoated silica gel plates (Merck Silica Gel PF-254), visualized by UV light. All organic extracts were dehydrated over anhydrous Na_2SO_4 and concentrated by using rotary evaporator

before being subjected to FCC. In singlet oxygen measurements 1,3-diphenylisobenzofuran was used as a singlet oxygen trap in organic solvent measurements and was purchased from supplier. All other chemicals and solvents were supplied from commercial sources and used as received.

2.2 Synthesis Scheme

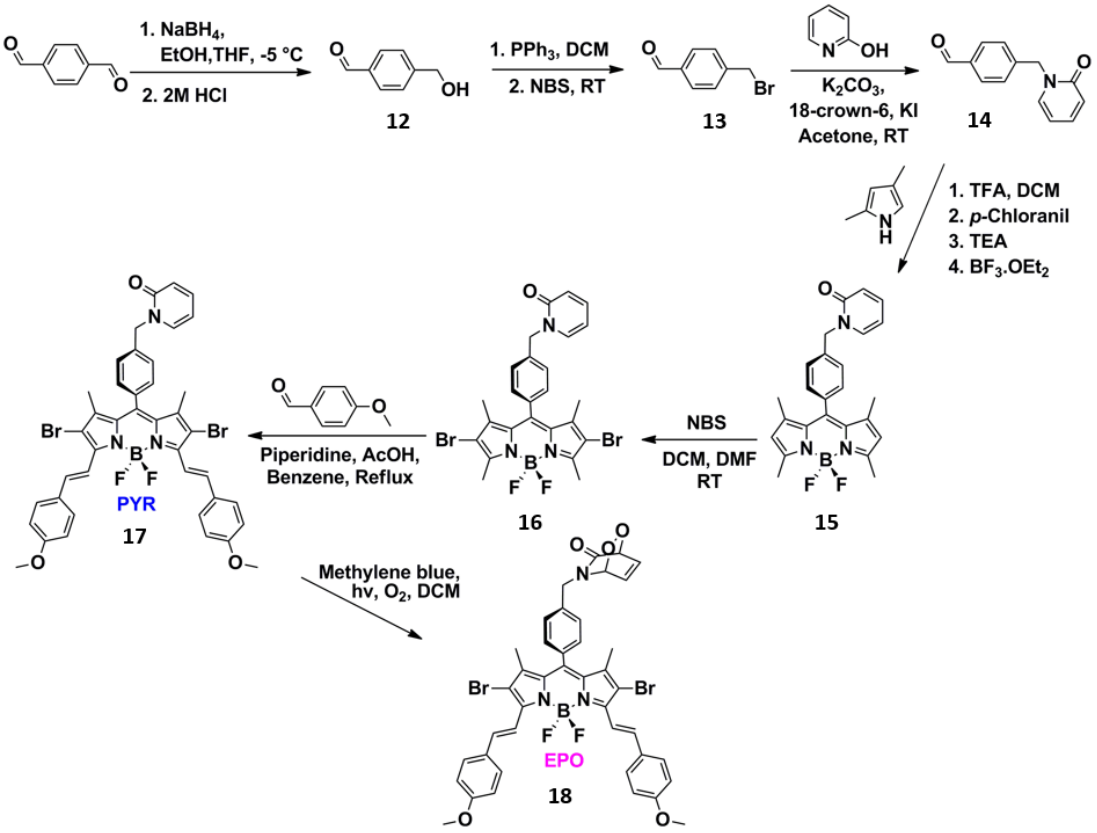

Figure 20. Synthesis scheme of 2-pyridone containing di-halogenated, di-styryl BODIPY PYR (**17**) and its endoperoxide version EPO (**18**). Copyright © 2016, Wiley- © 2016 WILEY-VCH Verlag GmbH & Co. KGaA, Weinheim. Reprinted with permission from ref (94).

2.2.1 Synthesis of Compound 12

Teraphthaldialdehyde (2.5 g, 18.6 mmol) was dissolved in EtOH-THF (35.0 ml-50.0 ml) solvent mixture and cooled to -5 ^{0}C. $NaBH_4$ (0.175 g, 4.63 mmol) was

added to reaction mixture in two portions and reaction mixture was stirred at 0 ^{0}C. The progress of the reaction was monitored by TLC using DCM:MeOH (98:2) as the eluent. When the reaction was completed, pH of the mixture was adjusted to 3 by using 2 M HCl that was extracted with EtOAc. Combined organic phases were dried over anhydrous Na_2SO_4. After removal of the solvent, the residue was purified by silica gel flash column chromatography using DCM/MeOH (98:2, v/v) as the eluent. Compound **12** was obtained as colorless oil (0.96 g, 38%).

1H NMR (400 MHz, CDCl3): δ 9.92 (s, 1H), 7.80 (d, J = 8.1 Hz, 2H), 7.47 (d, J = 8.1 Hz, 2H), 4.74 (s, 2H), 3.25 (s, 1H). ^{13}C NMR (100 MHz, $CDCl_3$): δ 192.4, 148.2, 135.5, 130.0, 126.9, 64.3. MS (TOF- ESI): m/z Calcd for $C_8H_8O_2$ [M-H]$^-$: 135.04515, Found for [M-H]$^-$: 135.04782, Δ= -19.75 ppm

2.2.2 Synthesis of Compound 13

PPh_3 (3.90 g, 14.86 mmol) was added to the solution of compound **12** (1.0 g, 7.34 mmol) in 60.0 ml DCM at room temperature. The reaction was initiated with the portion-wise addition of N-bromosuccinimide (NBS) at room temperature. The progress of the reaction was monitored by TLC by using DCM: Hexane (1:1) as the eluent. When TLC showed no starting material, the reaction was diluted with DCM and extracted with water. Combined organic phases were dried over anhydrous Na_2SO_4. After removal of the solvent, the residue was purified by silica gel flash column chromatography using DCM/ Hexane (1:1, v/v) as the eluent. Compound **13** was obtained as white powder (0.76 g, 52%).

^{1}H NMR (400 MHz, $CDCl_3$): δ 10.01 (s, 1H), 7.86 (d, J = 8.1 Hz, 2H), 7.55 (d, J = 8.1 Hz, 2H), 4.51 (s, 2H). ^{13}C NMR (100 MHz, $CDCl_3$): δ 191.4, 144.2, 136.2, 130.1, 129.7, 31.9. MS (TOF- ESI):

2.2.3 Synthesis of Compound 14

K_2CO_3 (0.433 g, 3.14 mmol) was added to the reaction mixture of compound **13** (0.25 g, 1.26 mmol) and 2-pyridone (0.10 g, 1.05mmol) dissolved in acetone.

After adding catalytic amount of 18-benzocrown-6 and KI, reaction was left to stir at room temperature. The progress of the reaction was monitored by TLC by using EtOAc:Hexane (1:1) as the eluent. When TLC showed no starting material, the reaction was filtered and concentrated under vacuum. The residue was purified by silica gel flash column chromatography using EtOAc/ Hexane (1:1, v/v) as the eluent. Compound **14** was obtained as white powder (0.23 g, 87%).

^{1}H NMR (400 MHz, $CDCl_3$): δ10.01 (s, 1H), 7.87 (d, J = 8.3 Hz, 2H), 7.45 (d, J = 8.3 Hz, 2H), 7.41-7.34 (m, 1H), 7.30 (dd, J_{12} = 6.8 Hz, J_{23} = 2.0 Hz, 1H), 6.66 (d, J = 9.2 Hz, 1H), 6.21 (dt, J_{12} = 6.8 Hz, J_{23} = 1.4 Hz, 1H), 5.23 (s, 2H). ^{13}C NMR (100 MHz, $CDCl_3$): δ 191.7, 162.6, 143.1, 139.9, 137.4, 135.9, 130.2, 128.3, 121.4, 106.7, 52.0. MS (TOF- ESI): m/z Calcd for $C_{13}H_{11}NO_2$ $[M+H]^+$: 214.08626, Found for $[M+H]^+$: 214.08808, Δ= -8.52 ppm

2.2.4 Synthesis of Compound 15

Trifluoroacetic acid was added dropwise to a vigorously stirring solution of compound **14** (0.33 g, 1.55 mmol) and 2,4-dimethylpyrrole (0.35 ml, 3.4 mmol) in 350 ml Ar-bubbled dichloromethane (DCM). The resulting red solution was stirred at room temperature in the dark overnight. *p*-Chloranil (0.38 g, 1.55 mmol) was then added in one portion and reaction was stirred for an additional hour. Triethylamine (TEA) (5.0 ml) was then added dropwise to this mixture over a period of 15 min, and the resulting dark brown solution was allowed to stir for an additional 15 min. $BF_3 \bullet OEt_2$ (5.0 ml) was then added dropwise over a period of 15 min. and the resulting dark red solution was allowed to stir further for 2h at rt. The slurry reaction mixture was washed with water (3 $\times$ 300 ml) and dried over anhydrous Na_2SO_4. The solvent was evaporated and the residue was purified by silica gel flash column chromatography using EtOAc as the eluent. Compound **15** was obtained as a dark orange solid (0.23 g, 34% yield).

^{1}H NMR (400 MHz, $CDCl_3$): δ7.42 (d, J = 7.8 Hz, 2H), 7.36-7.40 (m, 1H), 7.27-7.31 (m, 3H), 6.68 (d, J = 9.2 Hz, 1H), 6.21 (t, J = 6.7 Hz, 1H) , 5.99 (s, 2H),

5.26 (s, 2H), 2.56 (s, 6H), 1.37 (s, 6H). ^{13}C NMR (100 MHz, $CDCl_3$): δ 162.6, 155.6, 143.0, 141.0, 139.6, 137.6, 137.0, 134.8, 131.4, 128.62, 128.57, 121.4, 121.3, 106.6, 51.6, 14.6, 14.4. MS (TOF- ESI): m/z Calcd for $C_{25}H_{24}BF_2N_3O$ [M-H]$^-$: 429.19440 Found for [M-H]$^-$: 429.19033, Δ= 9.49 ppm.

2.2.5 Synthesis of Compound 16

Compound **15** (0.10 g, 0.232 mmol) was dissolved in 20 ml mixture (DMF/DCM, 3:1, v/v). Then, NBS (0.10 g, 0.56 mmol) dissolved in DCM (10 ml) was added dropwise to reaction mixture at room temperature. The progress of the reaction was monitored with TLC. When TLC showed no starting material, the reaction was extracted with water (3x100 ml) and combined organic phases were dried over anhydrous Na_2SO_4. After removal of the solvent, the residue was purified by silica gel flash column chromatography using EtOAc as the eluent. Compound **16** was obtained as red solid (0.11 g, 78%).

^{1}H NMR (400 MHz, $CDCl_3$): δ 7.46 (d, J = 7.9 Hz, 2H), 7.37-7.42 (m, 1H), 7.32 (dd, J_{12} = 6.8 Hz, J_{23} = 2.1 Hz, 1H), 7.26 (d, J = 7.9 Hz, 2H), 6.70 (d, J = 9.2 Hz, 1H), 6.24 (t, J = 6.8 Hz, 1H), 5.28 (s, 2H), 2.61 (s, 6H), 1.36 (s, 6H). ^{13}C NMR (100 MHz, $CDCl_3$): δ 162.7, 154.1, 150.0, 141.4, 140.5, 139.9, 138.3, 137.0, 134.0, 128.8, 128.4, 121.4, 106.8, 51.7, 13.8, 13.7. MS (TOF- ESI): m/z Calcd for $C_{25}H_{22}B\,Br_2\,F_2\,N_3\,O$ [M-H]$^-$: 585.01543, Found for [M-H]$^-$: 585.00912, Δ= 10.79 ppm.

2.2.6 Synthesis of Compound 17

p-methoxybenzaldehyde (0.092 ml, 0.75 mmol) was added to a solution of compound **16** (0.185 g, 0.314 mmol) in 25 ml of benzene containing piperidine (0.2 ml) and acetic acid (0.2 ml). Mixture was refluxed until all the starting material was consumed and the progress of the reaction was monitored by TLC using DCM:MeOH (98:2) as the eluent. When all the starting compound was consumed; the reaction was diluted with DCM and extracted with water. Combined organic phases were dried over anhydrous Na_2SO_4. After removal of the solvent, the residue was purified by silica gel flash column chromatography

using DCM:MeOH (98:2, v/v) as the eluent. Compound **17** was obtained as green waxy solid (0.168 g, 65%).

^{1}H NMR (400 MHz, $CDCl_3$): δ 8.13 (d, J = 16.7 Hz, 2H), 7.60 -7.68 (m, 6H), 7.46 (d, J = 7.7 Hz, 2H), 7.35-7.41 (m, 1H), 7.28-7.33 (m, 3H), 6.97 (d, J = 8.5 Hz, 4H), 6.68 (d, J = 9.4 Hz, 1H), 6.22 (t, J = 6.7 Hz, 1H), 5.28 (s, 2H), 3.88 (s, 6H), 1.40 (s, 6H). ^{13}C NMR (100 MHz, $CDCl_3$): δ 162.6, 160.9, 148.6, 140.8, 139.7, 139.0, 138.2, 137.9, 137.0, 134.6, 131.9, 129.8, 129.3, 129.0, 128.8, 121.5, 116.1, 114.4, 110.2, 106.6, 55.4, 13.8. MS (TOF- ESI): m/z Calcd for $C_{41}H_{34}B\,Br_2\,F_2\,N_3\,O_3$ [M]: 822.10644, Found for [M]: 822.09301, Δ= 16.33 ppm.

2.2.7 Synthesis of compound 18

Compound **17** (0.55 g, 0.067 mmol) was dissolved in DCM. Methylene blue (5 mg) was added to the reaction mixture which was irradiated while oxygen gas was passing through it. The progress of the reaction was monitored with TLC by using DCM as the eluent. When TLC showed no starting material, the mixture was concentrated under vacuum and the residue was subjected to the silica gel flash column chromatography by using DCM as the eluent. Compound **18** was obtained as green waxy solid (0.053 g, 93%).

^{1}H NMR (400 MHz, $CDCl_3$): δ 8.14 (d, J = 16.7 Hz, 2H), 7.61-7.68 (m, 6H), 7.44 (d, J = 7.9 Hz, 2H), 7.34 (d, J = 7.9 Hz, 2H), 6.98 (d, J = 8.6 Hz, 4H), 6.81-6.86 (m, 1H), 6.74-6.79 (m, 1H), 5.63 (dd, J_{12} = 5.6 Hz, J_{23} = 2.0 Hz, 1H), 5.15 (dd, J_{12} = 5.6 Hz, J_{23} = 1.9 Hz, 1H), 4.89 (d, J = 15.1 Hz, 1H), 4.68 (d, J = 15.1 Hz, 1H), 3.89 (s, 6H), 1.43 (s, 6H). ^{13}C NMR (100 MHz, $CDCl_3$): δ 139.1, 137.2, 134.1, 129.8, 139.4, 129.2, 129.1, 129.0, 116.1, 114.4, 100.0, 83.6, 55.4, 13.8. MS (TOF- ESI): Data cannot be obtained.

2.2.8 Preparation of Micelle of 17 (m-PYR)

Micelle structure of compound **17** was prepared with Cremophor EL by following the procedure in literature [92]. **17** (8.25 mg, 10 µmol) and 50 mg (47.6 µl) Cremephor EL were dissolved in 1 ml dry tetrahydrofuran. The solution was sonicated for 30 min at room temperature. Following sonication, THF was

evaporated under reduced pressure. Remaining solid was dissolved in water (5 ml). The suspension was filtered through 0.45 µm PTFE filter. Concentration of solution of the compound in micelle was estimated by using its extinction coefficient in DMSO.

2.2.9 Preparation of Micelle of 18 (m-EPO)

Micelle structure of compound **18** was prepared with Cremophor EL by following the procedure in literature [92]. **18** (6.5 mg, 9.1 µmol) and 50 mg (47.6 µl) Cremephor EL were dissolved in 1 ml freshly distilled tetrahydrofuran. The solution was sonicated for 30 min by maintaining temperature of sonication water bath below 4 °C. Following sonication, THF was evaporated under reduced pressure. Remaining solid was dissolved in water (5 ml). The suspension was filtered through 0.45 µm PTFE filter. Concentration of solution of the compound in micelle was estimated by using its extinction coefficient in DMSO.

2.3 Singlet Oxygen Trap Experiments

In singlet oxygen measurements 1,3-diphenylisobenzofuran (DPBF) was used as a singlet oxygen trap in DMSO and was purchased from a supplier. In a typical procedure for the detection of singlet oxygen generation by using trap molecules, a photosensitizer (~5 µM) and a trap molecule (O.D ~ 1.0) were mixed in O_2 bubbled DMSO. Initially several dark measurements were taken followed by irradiation of the mixture at absorption maximum of a sensitizer. Absorbance decrease of trap molecules was monitored suggesting singlet oxygen generation in the presence of light and sensitizers. Measurements were performed using 655 nm LED (1.2 W/m^2) and samples were irradiated with the light source from a 15 cm distance. All samples were homogenized for 1 min before measurements.

2.4 Singlet Oxygen Quantum Yield Calculations

Calculation of relative singlet oxygen quantum yields was carried out by following the literature [95]. Relative singlet oxygen quantum yields were calculated compared to methylene blue whose singlet oxygen quantum yield is 0.52 in ethanol. The absorbance of DPBF (singlet oxygen trap molecule) was adjusted around 1.0 in cuvette by using oxygen saturated ethanol. The photosensitizer was placed into cuvette by satisfying its absorbance is below 0.2. Solution was kept in dark and mixed by micropipette until absorbance readings were stable. After stabilization, absorbance readings were recorded for 4 minutes by exposing cuvette to light (655 nm) for 30 seconds (from 15 cm distance).

2.5 Emission and Fluorescence Measurements

The fluorescence quantum yield (Φ_F) of the samples was calculated by using an equation shown below.

$$\Phi_F = \Phi_F^0 \frac{I}{I_0} \frac{A}{A_0} \frac{n^2}{n_0^2}$$

I is the integrated fluorescence intensity, A is the absorbance at excitation wavelength, n is the refractive index of the solvent used, the subscript "0" stands for a reference compound. Cresyl violet was used as the reference compound (Φf = 0.66 in MeOH). BODIPY dyes (PYR (**17**) and EPO (**18**)) were dissolved in DMSO. BODIPY dyes and reference compound were prepared with the same absorbance (Ai) at the excitation wavelength (less than 0.05 in a 1.0 cm quartz cell). Reference and compound **17** and **18** are excited at 610nm.

2.6 Cell Studies

In order to investigate the cellular effects of the micellar compounds of **17** and **18**, cell culture assays were performed with a human cervical cancer cell line. HeLa cells were incubated with complete Dulbecco's Modified Eagle Medium (DMEM) at the environmental conditions of 37 ^{o}C, 5% CO_2 and 60% humidity. Cells were exposed to varying concentrations of the compounds (9 nM – 2.5 µM) and illuminated with a red light source (light-emitting diode, 655 nm, 324 µmol.m^{-2}.s^{-1} wavelength, flux) for 10 minutes in every 1 hour for a repeated 24 times. Thus, the final total illumination time was exactly 4 hours. This 24-h period of light - dark cycles was followed by a 24-h incubation solely in the dark (total 48 h). The control group of the cells were incubated in the dark, for the duration of 48 hours under identical environmental conditions. The MTT assay was utilized in order to assess cell viability and cytotoxicity. Even the low doses of the compound **18** seem to have resulted in a significant decrease of the cell viability. The CC_{50} (50% cytotoxic concentration) values of the compounds both in the dark and illuminated conditions were estimated by fitting a model with non-linear regression. The CC_{50} of compound **18** was significantly less than that of **17**, when they were both illuminated (approximately 8.59 nM vs. 49.04 nM).

2.6.1 Cell Culture and MTT Assay

HeLa human cervix cancer cells were cultured in 25 cm^2 culture flasks containing Dulbecco's Modified Eagle Medium supplemented with 2 mM L-glutamine, 10% fetal bovine serum, 100 units/ml penicillin and 100 µg/ml streptomycin in a cell culture incubator at 37 ^{o}C, 5% CO_2 and 60% humidity. Compounds **17** and **18** were diluted in complete medium and assay concentrations were freshly prepared. Cell viability/death was evaluated by MTT (3-(4,5-dimethylthiazolyl-2)-2,5-diphenyltetrazolium bromide) assay. Briefly, 50 µl cell suspensions in

complete DMEM containing 3 x 10^3 HeLa cells were plated in 96-well flat-bottom culture plates (Corning, MA, USA) and incubated for 12 hours to recover from handling. Varying concentrations of the chemical compounds in complete DMEM were added into each well (the final concentrations were 9 nM – 2.5 µM) in triplicate. The experimental group of the cells were illuminated with a red light source (655 nm, 324 µmol.m^{-2}.s^{-1}, distance between light source and cells: 10 cm) for 10 minutes in every 1 hour for a repeated 24 times (final total illumination time was exactly 4 hours) in a culture incubator (37 ^{o}C, 5% CO_2, 60% humidity). This 24-h period of light - dark cycles was followed by a 24-h incubation solely in the dark (total 48 h) also in the incubator. The control group of the cells were incubated in the dark, for the duration of 48 hours under identical environmental conditions except illumination. According to the assay protocol, 25 µl of the MTT reagent (Sigma-Aldrich, MO, USA) was added to each well in order to assess cell viability (final concentration: 1 mg/ml) at the end of the 48 h incubation period. Following a 4 h incubation of the cells with the MTT reagent, the generated formazan precipitates were solubilized by the addition of the lysing buffer (80 µl, pH: 4.7), which is composed of 23% SDS (Sodium dodecyl sulfate) dissolved in a solution of 45% DMF (N,N-Dimethylformamide). After an overnight incubation at 37 ^{o}C, the absorbance values (of each well) were measured at 570 nm in a microtiter plate reader (Spectramax Plus, Molecular Devices, CA, USA) at 25 ^{o}C. Cells incubated in culture medium only (without any chemical compounds) served as the control for cell viability both for the illuminated plates and for the ones kept in the dark; whereas DMSO (50%, v/v) was used to observe maximum cell death. Cell death (%) was assessed with the normalization of the values calculated by the formula "optical density (OD) of control cells – OD of treated cells". The CC_{50} values of the compounds both in the dark and illuminated conditions were estimated by fitting a model with non-linear regression.

CHAPTER III

Results and Discussion

This work has been partially described in the following publication:

Turan, I. S., Yildiz, D., **Turksoy, A.**, Gunaydin, G., & Akkaya, E. U. "A Bifunctional Photosensitizer for Enhanced Fractional Photodynamic Therapy: Singlet Oxygen Generation in the Presence and Absence of Light". *Angewandte Chemie*, 128.8 :2925-2928.

3.1 Insight into the Structure

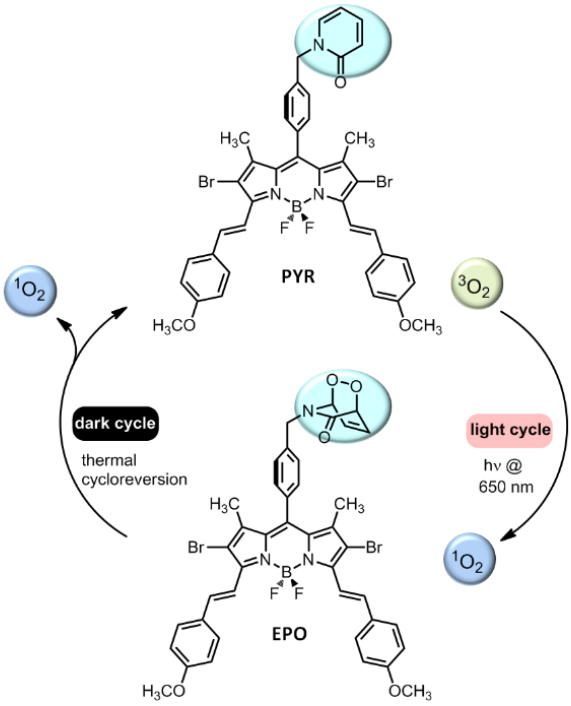

Figure 21. Operation principle of multifunctional agent which produces, stores and releases singlet oxygen. Copyright © 2016, WILEY-VCH Verlag GmbH & Co. KGaA, Weinheim. Reprinted with permission from ref (94).

BODIPY type dye is functionalized with 2-pyridone moiety at meso position in order to achieve the structure that can produce and store singlet oxygen, so that during light cycle of fractional photodynamic therapy photosensitizer being excited at longer wavelengths (relevant to therapeutic window) exhaustively produces singlet oxygen. In the meantime, it stores some of produced singlet oxygen to 2-pyridone moiety which goes through thermal cycloreversion to release stored singlet oxygen so as to be employed as cytotoxic agent in dark cycle of treatment, aiming to keep treatment ongoing while cells replenishing intracellular oxygen as depicted in Figure 21.

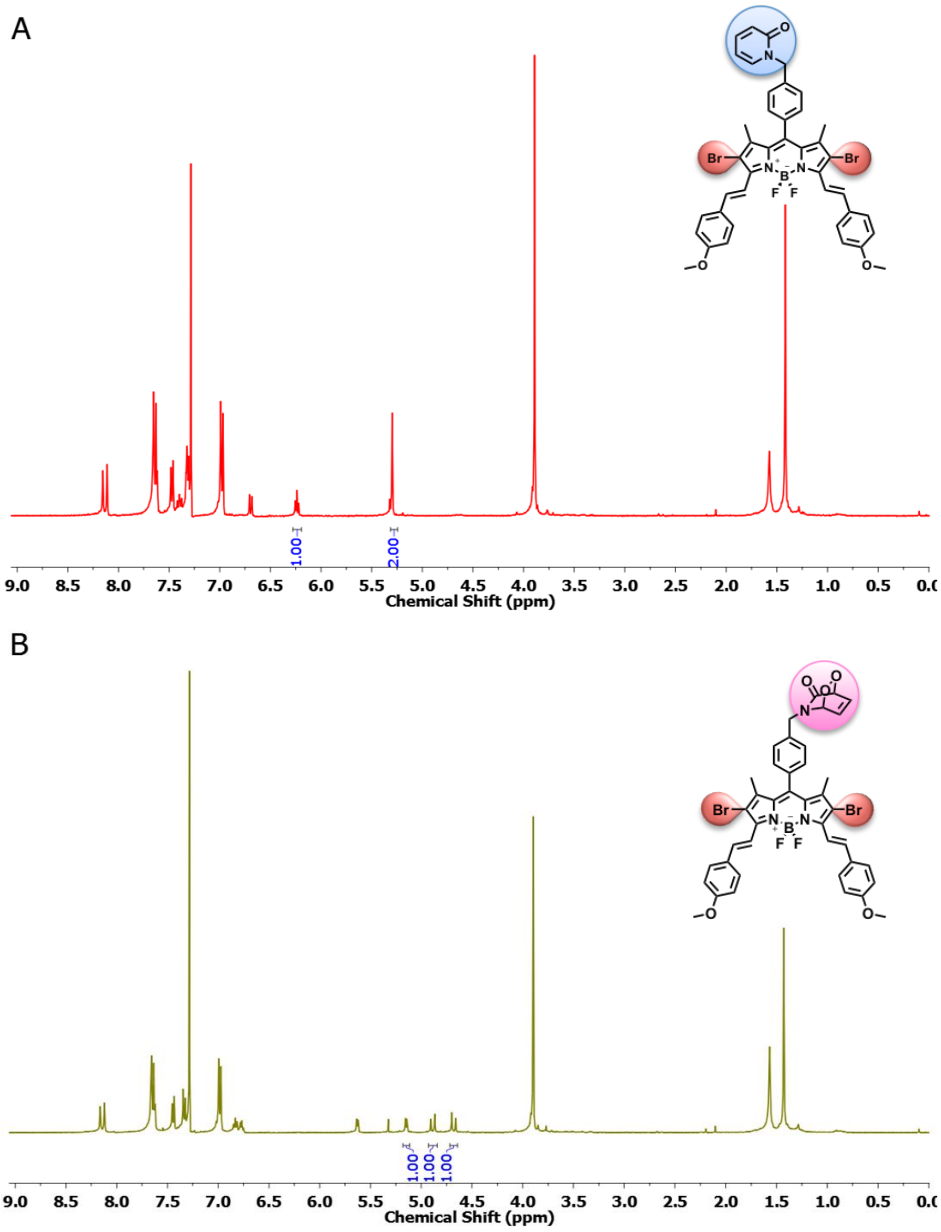

Figure 22. ^{1}H NMR spectra of PYR (**17**) and EPO (**18**) with highlighted structure specific peaks. Copyright © 2016, WILEY-VCH Verlag GmbH & Co. KGaA, Weinheim. Reprinted with permission from ref (94).

3.2 Initial Characterization of Structures

BODIPY type dye abbreviated as PYR (**17**) was synthesized following synthesis scheme in Experimental Part. In order to evaluate the capability of storing singlet oxygen as endoperoxides PYR (**17**) is reacted with singlet oxygen produced by methylene blue to form endoperoxide version of PYR (**17**) abbreviated as EPO (**18**). Figure 22 contains the NMR spectra of PYR (**17**) and EPO to evaluate changes upon formation of endoperoxide. Panel A belongs to PYR (**17**) and panel B belongs to EPO (**18**). In PYR (**17**) spectrum, peak at 6.22 ppm belongs to 2-pyridone moiety and peak at 5.28 ppm belongs to CH_2 group connected to nitrogen of 2-pyridone moiety. Upon endoperoxide formation these two particular peak positions change such that hydrogen peak of pyridone shifts to 5.15 ppm and methanediyl shifts to between 4.6 and 4.9 ppm as an AB system. Hereon, for further analysis ratios of these peaks will be used.

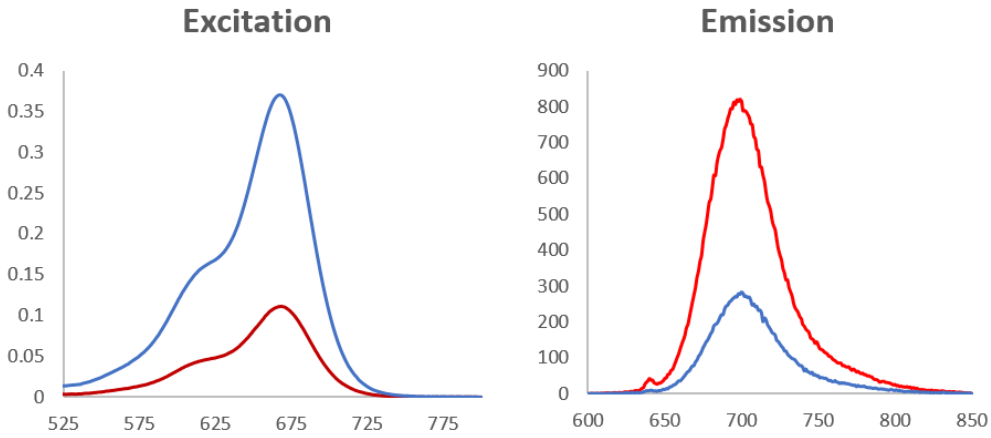

Figure 23. Excitation and emission spectra of PYR (red, **17**) and EPO (blue, **18**). Copyright © 2016, 2016 WILEY-VCH Verlag GmbH & Co. KGaA, Weinheim. Reprinted with permission from ref (94).

3.3 Emission and Fluorescence Measurements

Excitation and emission maxima of PYR (**17**) and EPO (**18**) structures were obtained for further characterization and measurements. Figure 23 contains the excitation and emission spectra of PYR (**17**) and EPO (**18**).

Absorption and emission maxima of PYR are 668 nm and 697 nm, respectively. EPO (**18**) also has similar absorption and emission maxima; 697 nm, and 700 nm, respectively. Molar absorption coefficient of PYR (**17**) and EPO (**18**) were calculated as 22 200 and 74 200 $M^{-1}cm^{-1}$. Relative fluorescence quantum yields of PYR (**17**) and EPO (**18**) in DMSO were obtained compared to Cresyl Violet in MEOH (with fluorescence quantum yield 0.66) as 0.14 and 0.10, respectively.

In order to evaluate singlet oxygen production capabilities of PYR (**17**) and EPO (**18**), DPBF was used as trap molecule for PYR (**17**), EPO (**18**) and standard methylene blue. Figure 24 contains the absorbance readings of DPBF at its absorbance maximum recorded against time for PYR (**17**), EPO (**18**) and methylene blue as standard.

Singlet oxygen quantum yields were calculated according to the equation:

$$\Phi_{\Delta}(PS) = \Phi_{\Delta}(MB) x \frac{m(PS)}{m(MB)} x \frac{F(MB)}{F(PS)} x \frac{PF(MB)}{PF(PS)}$$

where PS and MB designate photosensitizer and methylene blue respectively. m is the slope of difference in change in absorbance of DPBF at absorbance maxima with the irradiation time [93]. F is the absorption correction factor, given as $F=1-10^{-OD}$, and PF is absorbed photonic flux. Calculated singlet oxygen quantum yields of PYR and EPO are 0.15 and 0.20, respectively.

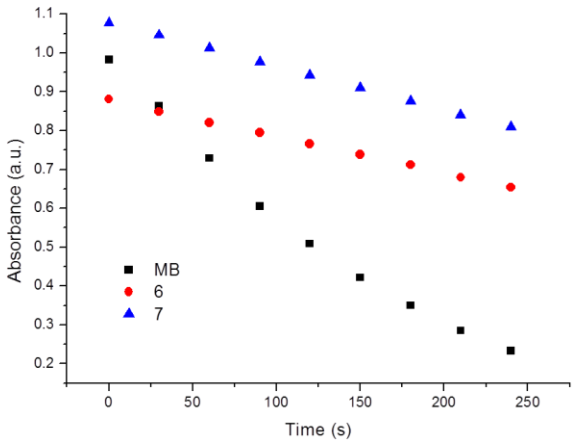

Figure 24. Relative singlet oxygen quantum yield experiment. Absorbance decrease of DPBF at absorbance maxima with time in ethanol in the presence of compound PYR (**17**) and EPO (**18**) as photosensitizers and methylene blue as reference. Copyright © 2016, 2016 WILEY-VCH Verlag GmbH & Co. KGaA, Weinheim. Reprinted with permission from ref (94).

3.4 Reversibility of the Transformations

Initial evaluation of the design is reversibility of transformations between PYR (**17**) and EPO (**18**). As stated earlier, the ^{1}H NMR spectra of the two compounds have well-resolved characteristic signals for both the PYR (**17**) and EPO (**18**) forms. Figure 25 contains partial ^{1}H NMR data. Spectrum A belongs to PYR (**17**) since there is no endoperoxide related peaks. Upon irradiation at $\lambda = 655$ nm of NMR tube while bubbling with O_2 for 30 minutes, ^{1}H NMR spectrum B indicates that full conversion of PYR (**17**) to EPO (**18**) is accomplished since there is no peak at 6.22 ppm being indicator of PYR (**17**) structure. From spectrum B to spectrum F, NMR tube in dark was placed in heating bath (37 ^{0}C) and spectra were recorded in 15 minutes intervals. Thermal cycloreversion produced PYR (**17**) structure as seen in increase of percentage of PYR (**17**) in given table. After recording F, NMR tube was again irradiated at $\lambda = 655$ nm under oxygen bubbling for 5 minutes and spectrum G is obtained, proving that singlet oxygen can be stored again to 2-pyridone moiety. Thus, it is clear that interconversion between the two forms occurred as long as there was dissolved oxygen present during the irradiation.

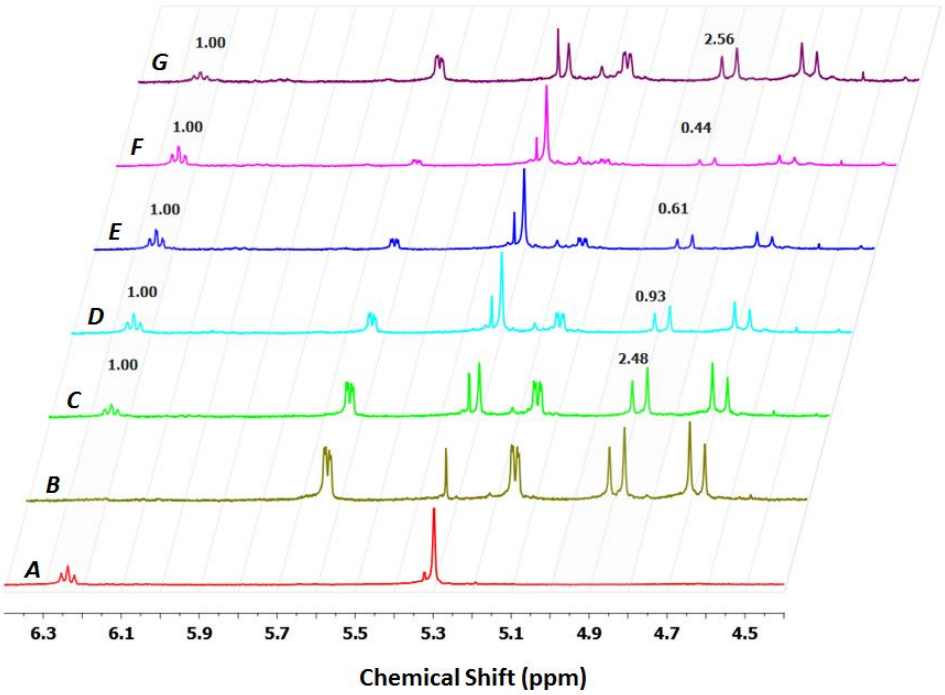

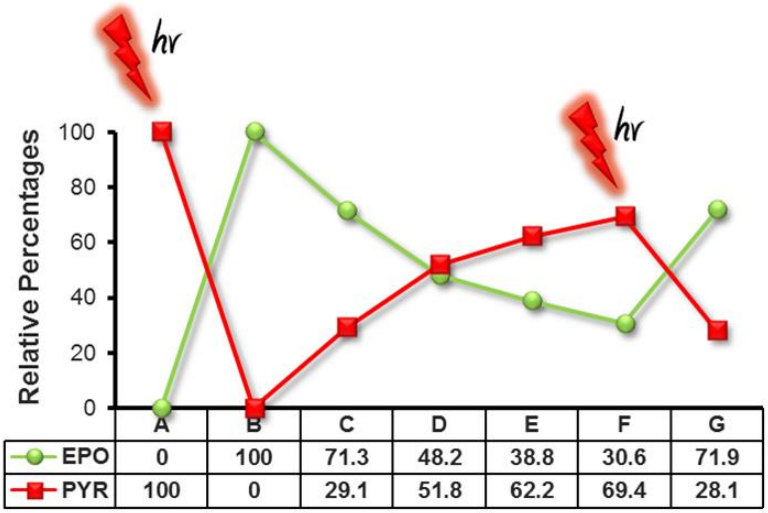

	A	B	C	D	E	F	G
EPO	0	100	71.3	48.2	38.8	30.6	71.9
PYR	100	0	29.1	51.8	62.2	69.4	28.1

Figure 25. ^{1}H NMR study showing reversibility of transformation between PYR (**17**) and EPO (**18**). Table contains percentages of each structure in corresponding NMR. Copyright © 2016, WILEY-VCH Verlag GmbH & Co. KGaA, Weinheim. Reprinted with permission from ref (94).

3.5 Power of the Dark Side in Action

The formation of singlet oxygen by light and dark cycles was further studied by using singlet-oxygen trap molecule DPBF (1,3-diphenylisobenzofuran). Upon irradiation with an LED array at $\lambda = 655$ nm, synthesized BODIPY sensitizes singlet oxygen from ground state oxygen by energy transfer. Produced singlet oxygen reacts with singlet oxygen trap DPBF, causing decrease in the absorbance at $\lambda = 416$ nm. As verified before transformation from PYR (**17**) to

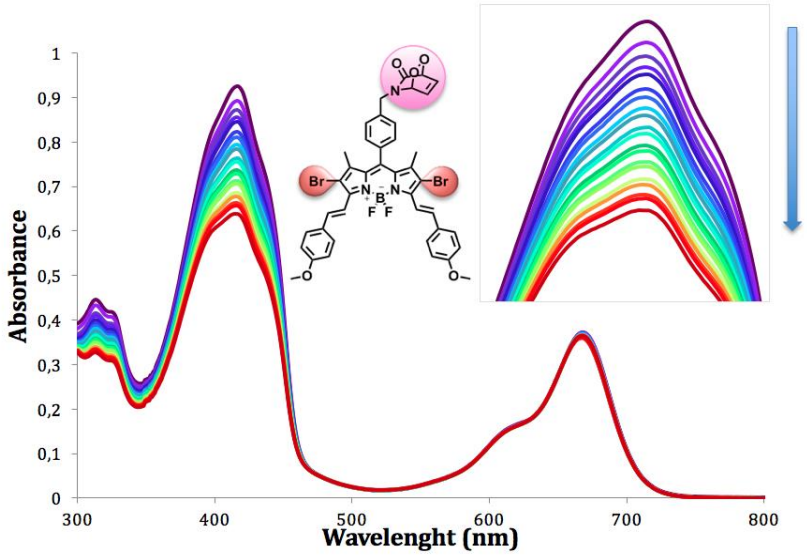

Figure 26. Singlet oxygen mediated bleaching of trap molecule (1,3-diphenylisobenzofuran) in the presence of EPO (**18**) (5 µM) in DMSO. Two cycles are introduced in sequence: Light cycle (LED applied at 655 nm for 30 seconds at 37 °C) and dark cycle (at 37 °C for 30 minutes). Copyright © 2016, WILEY-VCH Verlag GmbH & Co. KGaA, Weinheim. Reprinted with permission from ref (94).

EPO (**18**) under light irradiation occurs. During dark cycle EPO (**18**) structure can go through cycloreversion to release singlet oxygen. Figure 26 and 27 contain absorbance decrease of singlet oxygen trap molecule consecutive light and dark cycles, indicating that stored singlet oxygen can be released and further treatment of the structure with light irradiation not only produces singlet oxygen

but also stores some which further can be released. Therefore, this structure is capable of producing and storing singlet oxygen and stored singlet oxygen can be released with mild heat treatment, proving that this design is capable of producing cytotoxic agent during dark cycles of fractional photodynamic therapy.

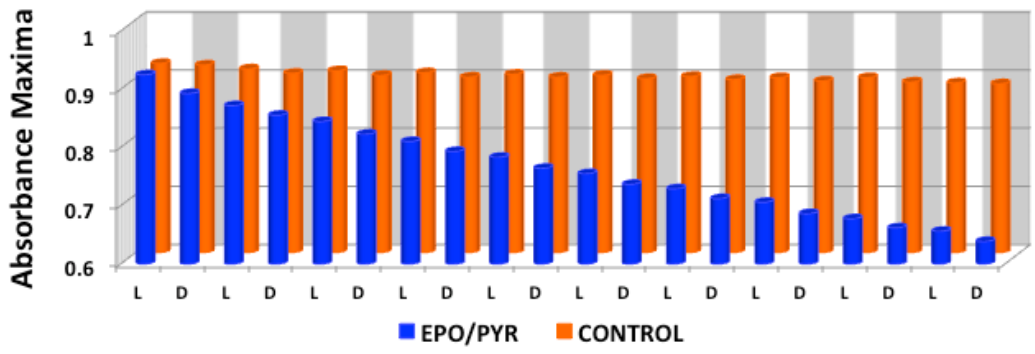

Figure 27. Comparison of singlet oxygen mediated bleaching of trap molecule (1,3-diphenylisobenzofuran) in the presence of EPO (**18**) (5 µM) in DMSO and trap molecule as control group. Two cycles are introduced in sequence: Light cycle (L) (LED applied at 655 nm for 30 seconds at 37 °C) and dark cycle (D) (at 37 °C for 30 minutes).

3.6 Cell Study

(This work has been conducted in collaboration with Dr. Gürcan Günaydın)

The performance of the bifunctional photosensitizer was also studied in HeLa (human cervical cancer cell line) cell cultures. Our expectation was that EPO (**18**) would be a more effective cytotoxic agent compared to a simple photosensitizer in when employed in the dark–light cycle regime (as is done in fractional PDT). Since the apoptotic response is time-dependent, a more fair comparison would be to compare the effects of PYR (**17**) and EPO (**18**). Since

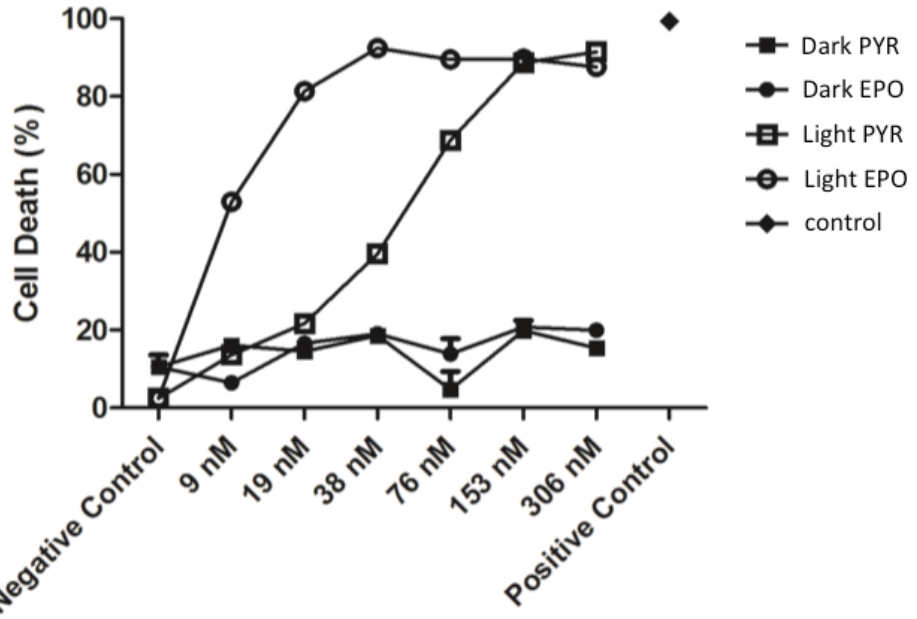

Figure 28. Cell viabilities as determined by MTT assays. Data labeled as "light" refers to results obtained when indicated concentrations of micelle-delivered agents PYR (**17**) and EPO (**18**) were exposed to cycles of light (λ= 655 nm, 10 min) and dark (50 min) with a total of 4 h of light exposure, followed by 24 h of incubation in the dark. The label "dark" indicates compounds which had been incubated in the dark only for 48 h. Reprinted with permission from ref (94).

both compounds had very limited water solubility, the non-ionic surfactant cremophor EL was used to deliver the agents within a micellar structure.

Micelles were prepared following literature procedures [92]. The size distribution of the micelles was studied by using dynamic light scattering, which showed that the average size of the micelles carrying embedded **17** or **18** is about 50 nm. HeLa cells were incubated with complete Dulbecco's modified Eagle's medium (DMEM) under environmental conditions of 37 °C, 5% CO_2, and 60% humidity. Cells were exposed to varying concentrations of the compounds in cremophor EL micelles (9 nm–2.5 μm) and illuminated with a red light source (λ=655 nm LED array, 324 μmol m^{-2} s^{-1} photon flux) for 10 min in every one hour, which was repeated 24 times. Thus, the total illumination time was exactly 4 h. This 24 h period of light–dark cycles was then followed by a 24 h incubation period in the dark (total 48 h). The control group of cells were incubated in the dark for 48 h under identical environmental conditions. MTT assays were performed to assess cell viability and cytotoxicity (Figure 28). It was found that even low doses of compound EPO (**18**) results in a significant decrease of the cell viability. The CC_{50} values (50% cytotoxic concentration) of the compounds both in the dark and after irradiation were estimated by fitting a model with nonlinear regression. The CC_{50} value of compound EPO (**18**) was found to be significantly less than that of PYR (**17**) after intermittent illumination of both (approximately 8.6 nm versus 49.0 nm). This result validates our design as it suggests that initial EPO (**18**) cycloreversion results in a large difference in singlet oxygen generation when followed by the application of a light–dark cycle. Additionally, when considering the reported CC_{50} values, EPO (**18**) is, as expected, much more active as a photosensitizing cytotoxic agent compared to reported BODIPY-based long-wavelength photosensitizers which do not have reversible singlet-oxygen storage modules.

CHAPTER IV

Conclusion

In this study, in order to create more effective fractional photodynamic therapy agent halogenated di-styryl BODIPY dye containing 2-pyridone module was synthesized, characterized and analyzed. Synthesized PYR (**17**) and EPO (**18**) structures are capable of producing singlet oxygen at relatively comparable wavelength with therapeutic window.

^{1}H NMR study conducted on PYR (**17**) structure showed that upon light illumination, the structure stores singlet oxygen in 2-pyridone moiety via self-sensitization. Thermal treatment of endoperoxide version EPO (**18**) indicated stored singlet oxygen can be released. Also, further light treatment proved the point that PYR (**17**) and EPO (**18**) are interconvertible.

Cell studies conducted on these structure have proved to effect of storage of singlet oxygen in CC_{50} values of PYR (**17**) (49.0 nm) and EPO (**18**) (8.6 nm), indicating that EPO (**18**) performed better compared to PYR (**17**).

As a final remark, in order to benefit from dark cycle of fractional photodynamic therapy to overcome intrinsic limitations of PDT even more, multifunctional agent EPO (**18**) being capable of producing, storing and releasing singlet oxygen was shown to be a promising fractional photodynamic therapy drug.

References

1. Zeitouni, Nathalie C., Allan R. Oseroff, and Sherry Shieh. "Photodynamic therapy for nonmelanoma skin cancers: current review and update." *Molecular Immunology* 39.17 (2003): 1133-1136.
2. Huang, Zheng. "A review of progress in clinical photodynamic therapy." *Technology in Cancer Research & Treatment* 4.3 (2005): 283-293.
3. Dolmans, Dennis EJGJ, Dai Fukumura, and Rakesh K. Jain. "Photodynamic therapy for cancer." *Nature Reviews Cancer* 3.5 (2003): 380-387.
4. Brown, Stanley B., Elizabeth A. Brown, and Ian Walker. "The present and future role of photodynamic therapy in cancer treatment." *The Lancet Oncology* 5.8 (2004): 497-508.
5. Dougherty, T. Jâ, et al. "Photoradiation therapy. II. Cure of animal tumors with hematoporphyrin and light." *Journal of the National Cancer Institute* 55.1 (1975): 115-121.
6. Kelly, J. F., and M. E. Snell. "Hematoporphyrin derivative: a possible aid in the diagnosis and therapy of carcinoma of the bladder." *The Journal of Urology* 115.2 (1976): 150-151.
7. Hayata, Yoshihiro, et al. "Hematoporphyrin derivative and laser photoradiation in the treatment of lung cancer." *Chest* 81.3 (1982): 269-277.
8. McCaughan, James S., et al. "Palliation of esophageal malignancy with photoradiation therapy." *Cancer* 54.12 (1984): 2905-2910.
9. Hayata, Yoshihiro, et al. "Photodynamic therapy with hematoporphyrin derivative in cancer of the upper gastrointestinal tract." *Seminars in Surgical Oncology*. Vol. 1. No. 1. John Wiley & Sons, Inc., 1985.

10. Sandeman, D. R. "Photodynamic therapy in the management of malignant gliomas: a review." *Lasers in Medical Science* 1.3 (1986): 163-174.
11. Hill, John S., et al. "Selective uptake of hematoporphyrin derivative into human cerebral glioma." *Neurosurgery* 26.2 (1990): 248-254.
12. Popovic, Emil A., Andrew H. Kaye, and John S. Hill. "Photodynamic therapy of brain tumors." *Journal of Clinical Laser Medicine & Surgery* 14.5 (1996): 251-261.
13. Rosenthal, Mark A., et al. "Phase I and pharmacokinetic study of photodynamic therapy for high-grade gliomas using a novel boronated porphyrin." *Journal of Clinical Oncology* 19.2 (2001): 519-524.
14. Gomer, Charles J., et al. "Hematoporphyrin derivative photoradiation therapy for the treatment of intraocular tumors: examination of acute normal ocular tissue toxicity." *Cancer Research* 43.2 (1983): 721-727.
15. Favilla, I., et al. "Photodynamic therapy: a 5-year study of its effectiveness in the treatment of posterior uveal melanoma, and evaluation of haematoporphyrin uptake and photocytotoxicity of melanoma cells in tissue culture." *Melanoma Research* 5.5 (1995): 355-364.
16. Landau, Irene ME, Björn Steen, and Stefan Seregard. "Photodynamic therapy for circumscribed choroidal haemangioma." *Acta Ophthalmologica Scandinavica* 80.5 (2002): 531-536.
17. Dougherty, Thomas J., et al. "Photoradiation in the treatment of recurrent breast carcinoma." *Journal of the National Cancer Institute* 62.2 (1979): 231-237.
18. Mang, Thomas S., et al. "A phase II/III clinical study of tin ethyl etiopurpurin (purlytin)--Induced photodyanmic therapy for the treatment of recurrent cutaneous metastatic breast cancer." *The Cancer Journal* 4.6 (1998): 378.
19. Dimofte, Andreea, et al. "In vivo light dosimetry for motexafin lutetium-mediated PDT of recurrent breast cancer." *Lasers in Surgery and Medicine* 31.5 (2002): 305-312.

20. Schweitzer, Vanessa Gayl. "Photodynamic therapy for treatment of head and neck cancer." *Otolaryngology Head and Neck Surgery* 102.3 (1990): 225-232.
21. Biel, Merrill A. "Photodynamic therapy and the treatment of head and neck neoplasia." *The Laryngoscope* 108.9 (1998): 1259-1268.
22. Bown, S. G., et al. "Photodynamic therapy for cancer of the pancreas." *Gut* 50.4 (2002): 549-557.
23. Hornung, R. "Photomedical approaches for the diagnosis and treatment of gynecologic cancers." *Current Drug Targets-Immune, Endocrine & Metabolic Disorders* 1.2 (2001): 165-177.
24. Fehr, Mathias K., et al. "Photodynamic therapy of vulvar intraepithelial neoplasia III using topically applied 5-aminolevulinic acid." *Gynecologic Oncology* 80.1 (2001): 62-66.
25. Hasan, Tayyaba, et al. "Photodynamic therapy of cancer." *Cancer Medicine* 7 (2003): 48-537.
26. Castano, Ana P., Tatiana N. Demidova, and Michael R. Hamblin. "Mechanisms in photodynamic therapy: part one—photosensitizers, photochemistry and cellular localization." *Photodiagnosis and Photodynamic Therapy* 1.4 (2004): 279-293.
27. Robertson, Claudine A., D. Hawkins Evans, and Heidi Abrahamse. "Photodynamic therapy (PDT): a short review on cellular mechanisms and cancer research applications for PDT." *Journal of Photochemistry and Photobiology B: Biology* 96.1 (2009): 1-8.
28. Agostinis, Patrizia, et al. "Photodynamic therapy of cancer: an update." *CA: A Cancer Journal for Clinicians* 61.4 (2011): 250-281.
29. Monguzzi, A., R. Tubino, and F. Meinardi. "Upconversion-induced delayed fluorescence in multicomponent organic systems: Role of Dexter energy transfer." *Physical Review B* 77.15 (2008): 155122.
30. Henderson, Barbara W., and Thomas J. Dougherty. "How does photodynamic therapy work?" *Photochemistry and Photobiology* 55.1 (1992): 145-157.

31. Foote, Christopher S. "Mechanisms of photosensitized oxidation." *Science* 162.3857 (1968): 963-970.
32. Bilski, P., et al. "The photooxidation of diethylhydroxylamine by rose bengal in micellar and nonmicellar aqueous solutions." *Photochemistry and Photobiology* 58.1 (1993): 11-18.
33. Ma, Jianghua, and Lijin Jiang. "Photogeneration of singlet oxygen (1O2) and free radicals ($Sen^{\cdot -}$, $O^{\cdot -2}$) by tetra-brominated hypocrellin B derivative." *Free Radical Research* 35.6 (2001): 767-777.
34. Pazos, M. D. C., and Helena Bonciani Nader. "Effect of photodynamic therapy on the extracellular matrix and associated components." *Brazilian Journal of Medical and Biological Research* 40.8 (2007): 1025-1035.
35. Geze, M., et al. "Lysosomes, a key target of hydrophobic photosensitizers proposed for photochemotherapeutic applications." *Journal of Photochemistry and Photobiology B: Biology* 20.1 (1993): 23-35.
36. Berg, Kristian, and Johan Moan. "Lysosomes as photochemical targets." *International Journal of Cancer* 59.6 (1994): 814-822.
37. MacDonald, Ian J., et al. "Subcellular Localization Patterns and Their Relationship to Photodynamic Activity of Pyropheophorbide-a Derivatives." *Photochemistry and Photobiology* 70.5 (1999): 789-797.
38. Berg, K., Madslien, K., Bommer, J. C., Oftebro, R., Winkelman, J. W., & Moan, J. (1991). "Light induced relocalization of sulfonated meso-tetraphenylporphirines in NHIK 3025 Cells and effects of dose fractionation" *Photochemistry and Photobiology*, *53*(2), 203-210. *Photochemistry and photobiology* 53.2 (1991): 203-210.
39. Peng, Q., et al. "Subcellular localization, redistribution and photobleaching of sulfonated aluminum phthalocyanines in a human melanoma cell line." *International Journal of Cancer* 49.2 (1991): 290-295.
40. Horobin, R. W., and F. Rashid. "Interactions of molecular probes with living cells and tissues. Part 1. Some general mechanistic proposals, making use of a simplistic Chinese box model." *Histochemistry and Cell Biology* 94.2 (1990): 205-209.

41. Castano, Ana P., Tatiana N. Demidova, and Michael R. Hamblin. "Mechanisms in photodynamic therapy: part two—cellular signaling, cell metabolism and modes of cell death." *Photodiagnosis and Photodynamic Therapy* 2.1 (2005): 1-23.
42. Davids, Lester M., et al. "Hypericin phototoxicity induces different modes of cell death in melanoma and human skin cells." *Journal of Photochemistry and Photobiology B: Biology* 91.2 (2008): 67-76.
43. Castano, Ana P., Tatiana N. Demidova, and Michael R. Hamblin. "Mechanisms in photodynamic therapy: part three—photosensitizer pharmacokinetics, biodistribution, tumor localization and modes of tumor destruction." *Photodiagnosis and Photodynamic Therapy* 2.2 (2005): 91-106.
44. Pazos, M. D. C., and Helena Bonciani Nader. "Effect of photodynamic therapy on the extracellular matrix and associated components." *Brazilian Journal of Medical and Biological Research* 40.8 (2007): 1025-1035.
45. Nowis, Dominika, et al. "The influence of photodynamic therapy on the immune response." *Photodiagnosis and Photodynamic Therapy* 2.4 (2005): 283-298.
46. Buytaert, Esther, Michael Dewaele, and Patrizia Agostinis. "Molecular effectors of multiple cell death pathways initiated by photodynamic therapy." *Biochimica et Biophysica Acta (BBA)-Reviews on Cancer* 1776.1 (2007): 86-107.
47. De Rosa, Fernanda S., and M. Vitória LB Bentley. "Photodynamic therapy of skin cancers: sensitizers, clinical studies and future directives." *Pharmaceutical Research* 17.12 (2000): 1447-1455.
48. Ketabchi, A., et al. "Induction of apoptotic cell death by photodynamic therapy in human keratinocytes." *Archives of Oral Biology* 43.2 (1998): 143-149.
49. Kamkaew, Anyanee, et al. "BODIPY dyes in photodynamic therapy." *Chemical Society Reviews* 42.1 (2013): 77-88.

50. Hajri, A., et al. "In Vitro and In Vivo Efficacy of Photofrin® and Pheophorbide a, a Bacteriochlorin, in Photodynamic Therapy of Colonic Cancer Cells." *Photochemistry and Photobiology* 75.2 (2002): 140-148.

51. Garland, Martin J., et al. "Designing photosensitizers for photodynamic therapy: strategies, challenges and promising developments." *Future Medicinal Chemistry* 1.4 (2009): 667-691.

52. Allison, Ron R., and Claudio H. Sibata. "Oncologic photodynamic therapy photosensitizers: a clinical review." *Photodiagnosis and Photodynamic Therapy* 7.2 (2010): 61-75.

53. Wilson, Brian C., W. Patrick Jeeves, and Diane M. Lowe. "In vivo and post mortem measurements of the attenuation spectra of light in mammalian tissues." *Photochemistry and Photobiology* 42.2 (1985): 153-162.

54. Schmidt, Meic H., et al. "Light-emitting diodes as a light source for intraoperative photodynamic therapy." *Neurosurgery* 38.3 (1996): 552-557.

55. DeRosa, Maria C., and Robert J. Crutchley. "Photosensitized singlet oxygen and its applications." *Coordination Chemistry Reviews* 233 (2002): 351-371.

56. Arnold, S. J., M. Kubo, and E. A. Ogryzlo. "Relaxation and reactivity of singlet oxygen." *Advances in Chemistry* 1968. 133-142.

57. Merkel, Paul B., and David R. Kearns. "Remarkable solvent effects on the lifetime of 1. DELTA. g oxygen." *Journal of the American Chemical Society* 94.3 (1972): 1029-1030.

58. Bregnhøj, Mikkel, et al. "Solvent-dependent singlet oxygen lifetimes: temperature effects implicate tunneling and charge-transfer interactions." *Physical Chemistry Chemical Physics* 18.33 (2016): 22946-22961.

59. Young, Robert H., David Brewer, and Richard A. Keller. "Determination of rate constants of reaction and lifetimes of singlet oxygen in solution by a flash photolysis technique." *Journal of the American Chemical Society* 95.2 (1973): 375-379.

60. Ogilby, Peter R., and Christopher S. Foote. "Chemistry of singlet oxygen. 42. Effect of solvent, solvent isotopic substitution, and temperature on the lifetime of singlet molecular oxygen (1Δg)." *Journal of American Chemical Society* 105.11 (1983): 3423-3430.
61. Usui, Yoshiharu. "Determination of quantum yield of singlet oxygen formation by photosensitization." *Chemistry Letters* 2.7 (1973): 743-744.
62. Xiao, Zhengwen, et al. "Fractionated versus standard continuous light delivery in interstitial photodynamic therapy of dunning prostate carcinomas." *Clinical Cancer Research* 13.24 (2007): 7496-7505.
63. Yang, Liyong, et al. "Increasing the efficiency of photodynamic therapy by improved light delivery and oxygen supply using an anticoagulant in a solid tumor model." *Lasers in Surgery and Medicine* 42.7 (2010): 671-679.
64. Gibson, Scott L., et al. "Effects of various photoradiation regimens on the antitumor efficacy of photodynamic therapy for R3230AC mammary carcinomas." *Cancer Research* 50.22 (1990): 7236-7241.
65. Treibs, Alfred, and Franz-Heinrich Kreuzer. "Difluorboryl-Komplexe von Di-und Tripyrrylmethenen." *European Journal of Organic Chemistry* 718.1 (1968): 208-223.
66. Kolemen, Safacan, et al. "Optimization of distyryl-Bodipy chromophores for efficient panchromatic sensitization in dye sensitized solar cells." *Chemical Science* 2.5 (2011): 949-954.
67. Rousseau, Theodulf, et al. "BODIPY derivatives as donor materials for bulk heterojunction solar cells." *Chemical Communications* 13 (2009): 1673-1675.
68. Barin, Gokhan, M. Deniz Yilmaz, and Engin U. Akkaya. "Boradiazaindacene (Bodipy)-based building blocks for the construction of energy transfer cassettes." *Tetrahedron Letters* 50.15 (2009): 1738-1740.
69. Ozlem, Suriye, and Engin U. Akkaya. "Thinking outside the silicon box: molecular and logic as an additional layer of selectivity in singlet oxygen generation for photodynamic therapy." *Journal of the American Chemical Society* 131.1 (2008): 48-49.

70. Bozdemir, O. Altan, et al. "Synthesis of symmetrical multichromophoric BODIPY dyes and their facile transformation into energy transfer cassettes." *Chemistry-A European Journal* 16.21 (2010): 6346-6351.
71. Gorman, Aoife, et al. "In vitro demonstration of the heavy-atom effect for photodynamic therapy." *Journal of the American Chemical Society* 126.34 (2004): 10619-10631.
72. Atilgan, Serdar, et al. "Water soluble distyryl-boradiazaindacenes as efficient photosensitizers for photodynamic therapy." *Chemical Communications* 42 (2006): 4398-4400.
73. Yogo, Takatoshi, et al. "Highly efficient and photostable photosensitizer based on BODIPY chromophore." *Journal of the American Chemical Society* 127.35 (2005): 12162-12163.
74. Cakmak, Yusuf, et al. "Designing Excited States: Theory-Guided Access to Efficient Photosensitizers for Photodynamic Action." *Angewandte Chemie* 123.50 (2011): 12143-12147.
75. Huang, Ling, et al. "Styryl Bodipy-C60 dyads as efficient heavy-atom-free organic triplet photosensitizers." *Organic Letters* 14.10 (2012): 2594-2597.
76. Thoresen, Lars H., et al. "Synthesis of 3, 5-Diaryl-4, 4-difluoro-4-bora-3a, 4a-diaza-s-indacene (BODIPY®) dyes." *Synlett* 1998.11 (1998): 1276-1278.
77. Burghart, Armin, et al. "3,5-Diaryl-4,4-difluoro-4-bora-3a,4a-diaza-s-indacene (BODIPY) dyes: synthesis, spectroscopic, electrochemical, and structural properties." *The Journal of Organic Chemistry* 64.21 (1999): 7813-7819.
78. Loudet, Aurore, and Kevin Burgess. "BODIPY dyes and their derivatives: syntheses and spectroscopic properties." *Chemical Reviews* 107.11 (2007): 4891-4932.
79. Dost, Zeynep, Serdar Atilgan, and Engin U. Akkaya. "Distyryl-boradiazaindacenes: facile synthesis of novel near IR emitting fluorophores." *Tetrahedron* 62.36 (2006): 8484-8488.
80. Otsu, Kaoru, et al. "Impaired activation of caspase cascade during cell death induced by newly synthesized singlet oxygen generator, 1-

buthylnaphthalene-4-propionate endoperoxide." *Cell Biology International* 32.11 (2008): 1380-1387.

81. Aubry, Jean-Marie, et al. "Reversible binding of oxygen to aromatic compounds." *Accounts of Chemical Research* 36.9 (2003): 668-675.
82. Van den Heuvel, C.J.M., et al. "The photo-oxidation of hexamethylbenzene and pentamethylbenzene by singlet oxygen." *Recueil des Travaux Chimiques des Pays-Bas* 99.9 (1980): 275-278.
83. Seip, M., and H-D. Brauer. "Endoperoxide formation of helianthrene with triplet molecular oxygen. A spin-forbidden reaction." *Journal of the American Chemical Society* 114.12 (1992): 4486-4490.
84. Van den Heuvel, C. J. M., J. W. Verhoeven, and Th J. de Boer. "A frontier orbital description of the reaction of singlet oxygen with simple aromatic systems." *Recueil des Travaux Chimiques des Pays-Bas* 99.9 (1980): 280-284.
85. Bobrowski, Maciej, et al. "CAS MCSCF/CAS MCQDPT2 study of the mechanism of singlet oxygen addition to 1, 3-butadiene and benzene." *Journal of the American Chemical Society* 122.34 (2000): 8112-8119.
86. Turro, Nicholas J., Ming Fea Chow, and Jean Rigaudy. "Mechanism of thermolysis of endoperoxides of aromatic compounds. Activation parameters, magnetic field, and magnetic isotope effects." *Journal of American Chemical Society* 103.24 (1981).
87. Ben-Shabat, Shimon, et al. "Formation of a nonaoxirane from A2E, a lipofuscin fluorophore related to macular degeneration, and evidence of singlet oxygen involvement." *Angewandte Chemie International Edition* 41.5 (2002): 814-817.
88. Kolemen, Safacan, et al. "Remote-Controlled Release of Singlet Oxygen by the Plasmonic Heating of Endoperoxide-Modified Gold Nanorods: Towards a Paradigm Change in Photodynamic Therapy." *Angewandte Chemie International Edition* 55.11 (2016): 3606-3610.
89. Matsumoto, Masakatsu, Masayo Yamada, and Nobuko Watanabe. "Reversible 1, 4-cycloaddition of singlet oxygen to N-substituted 2-

pyridones: 1, 4-endoperoxide as a versatile chemical source of singlet oxygen." *Chemical Communications* 4 (2005): 483-485.

90. N. J. Turro,M.-F. Chow and J. Rigaudy, *Journal of American Chemical Society*, 1977, 101,1300–1301.

91. N. J. Turro,M.-F. Chow and J. Rigaudy, *Journal of American Chemical Soiety*, 1979, 103,7218–7224.

92. McDonnell, Shane O., et al. "Supramolecular photonic therapeutic agents." *Journal of the American Chemical Society* 127.47 (2005): 16360-16361.

93. Adarsh, Nagappanpillai, Rekha R. Avirah, and Danaboyina Ramaiah. "Tuning photosensitized singlet oxygen generation efficiency of novel aza-BODIPY dyes." *Organic Letters* 12.24 (2010): 5720-5723.

94. Turan, I. S., Yildiz, D., Turksoy, A., Gunaydin, G., & Akkaya, E. U. "A Bifunctional Photosensitizer for Enhanced Fractional Photodynamic Therapy: Singlet Oxygen Generation in the Presence and Absence of Light". *Angewandte Chemie* 128.8 (2016): 2925-2928.

95. Adarsh, Nagappanpillai, Rekha R. Avirah, and Danaboyina Ramaiah. "Tuning photosensitized singlet oxygen generation efficiency of novel aza-BODIPY dyes." *Organic Letters* 12.24 (2010): 5720-5723.

Appendix-A

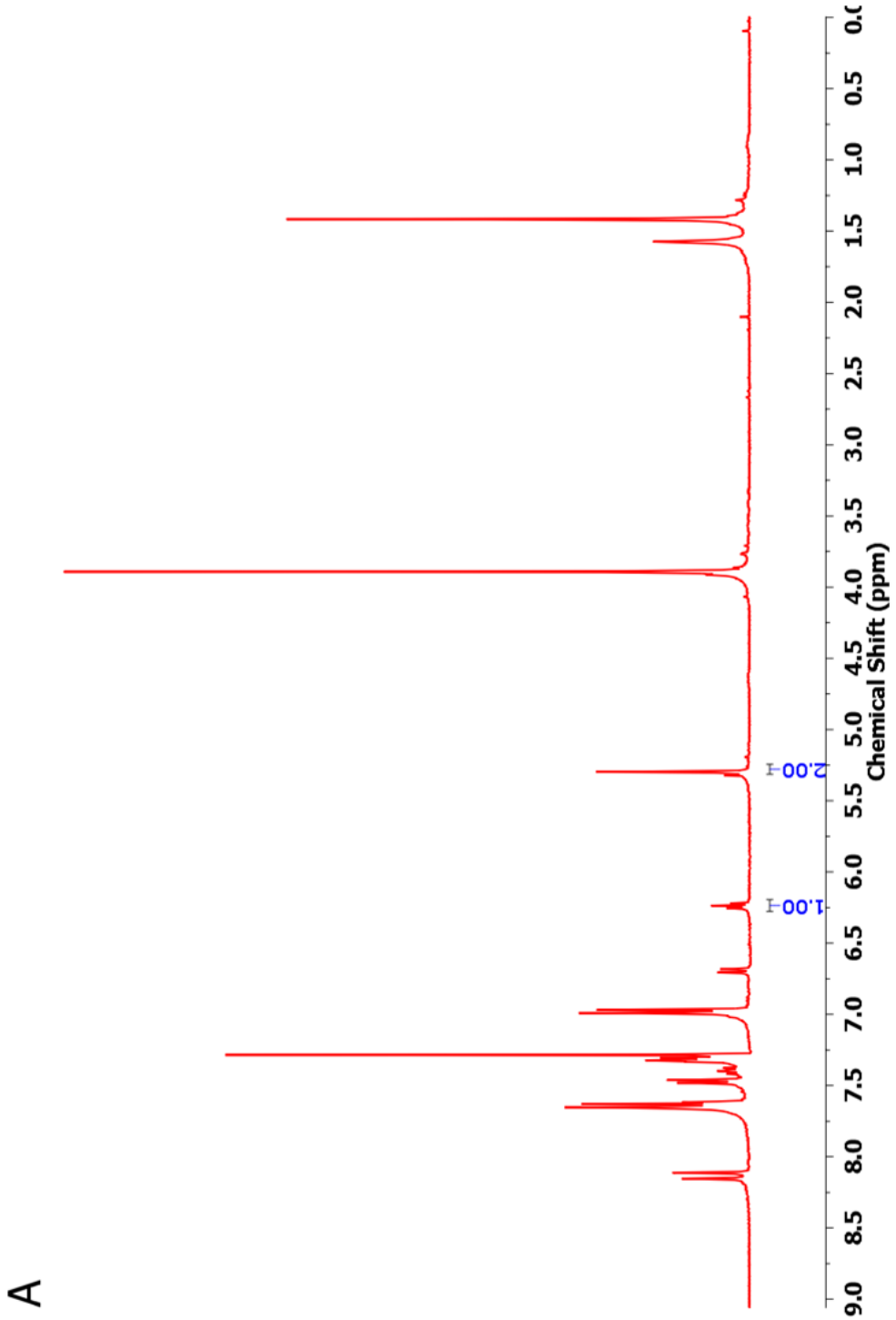

Figure 29. ^{1}H NMR Spectrum A of Cycloreversion Experiment in $CDCl_3$

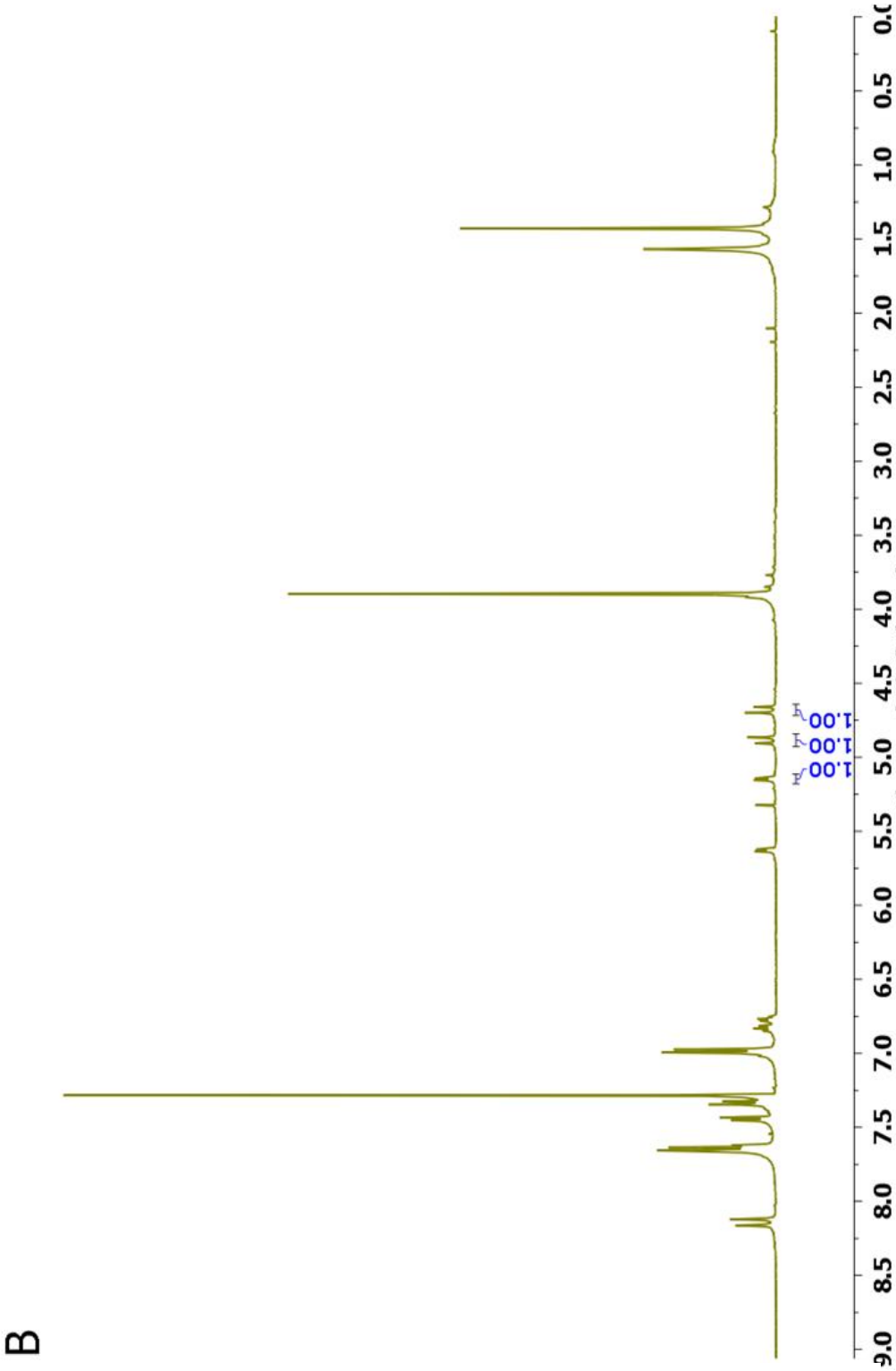

Figure 30. ^{1}H NMR Spectrum B of Cycloreversion Experiment in $CDCl_3$

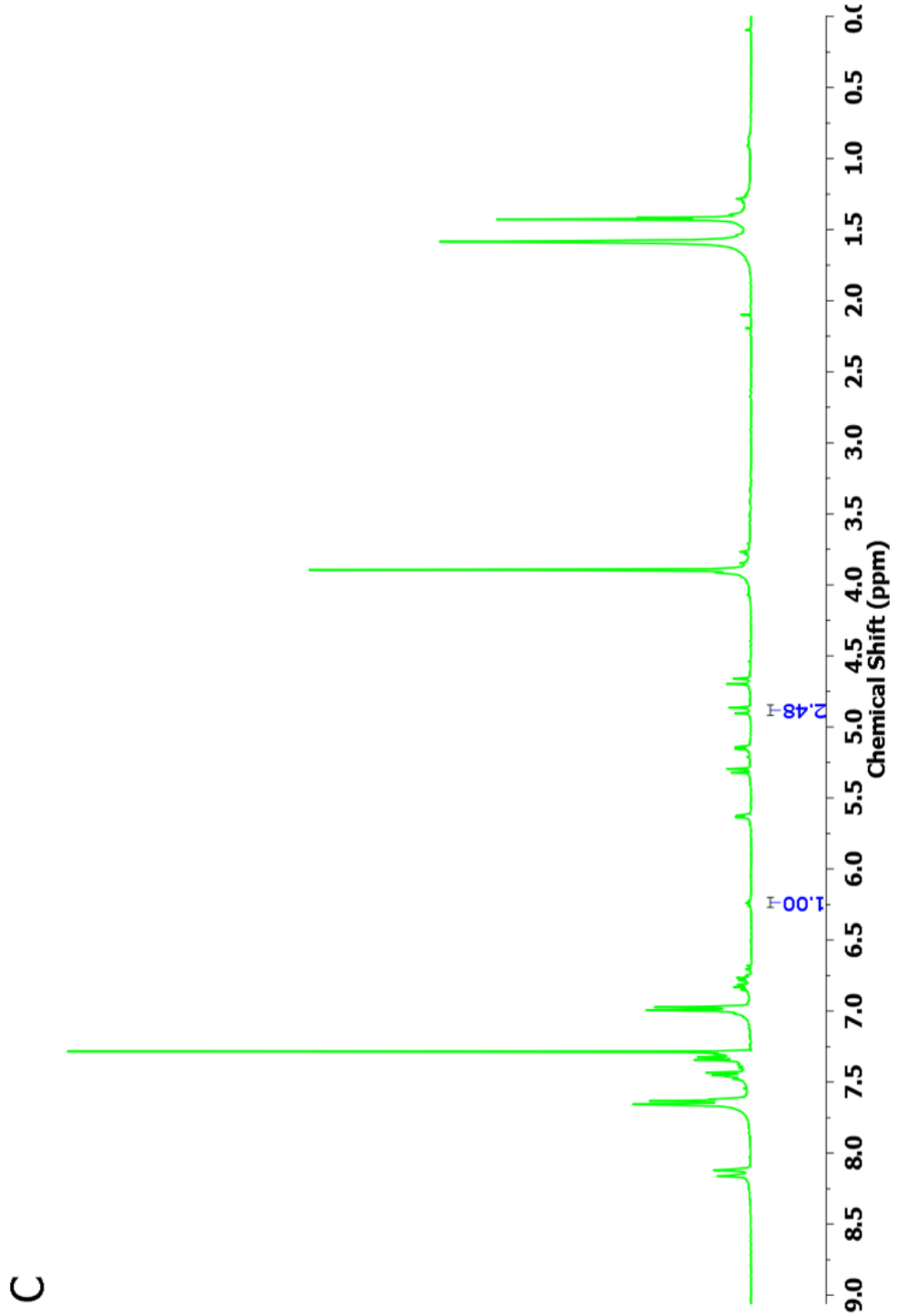

Figure 31. ^{1}H NMR Spectrum C of Cycloreversion Experiment in $CDCl_3$

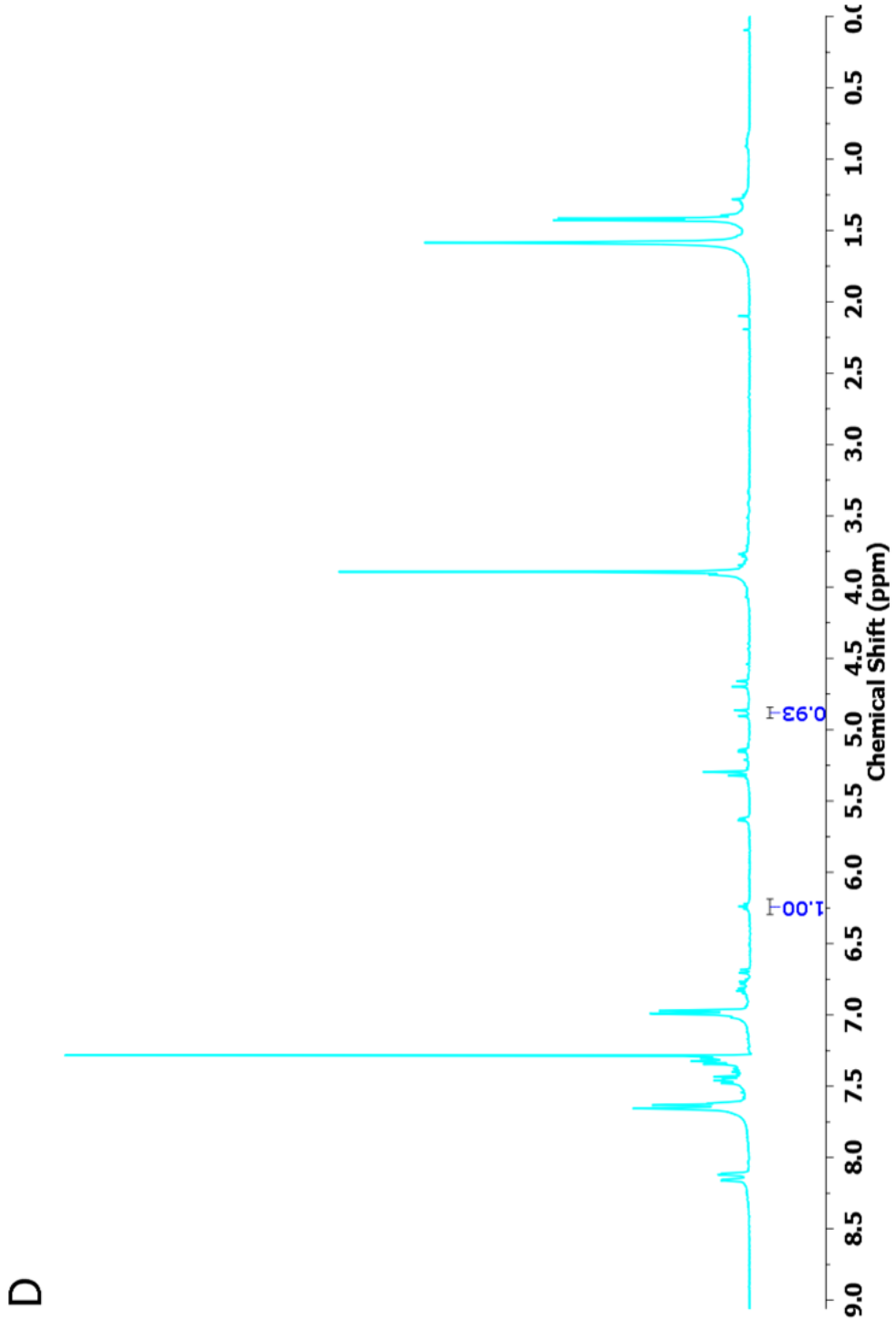

Figure 32. ^{1}H NMR Spectrum D of Cycloreversion Experiment in $CDCl_3$

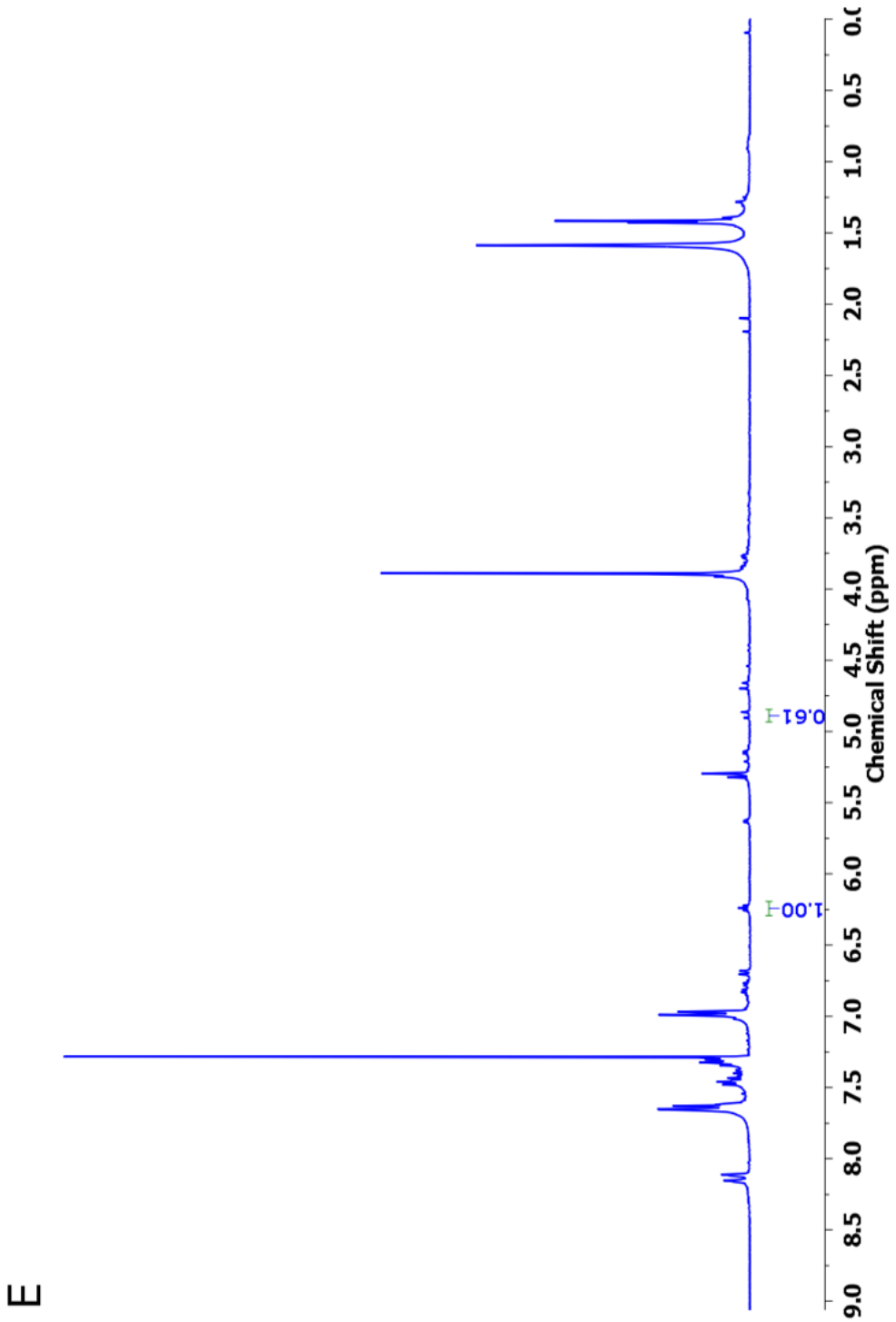

Figure 33. ^{1}H NMR Spectrum E of Cycloreversion Experiment in $CDCl_3$

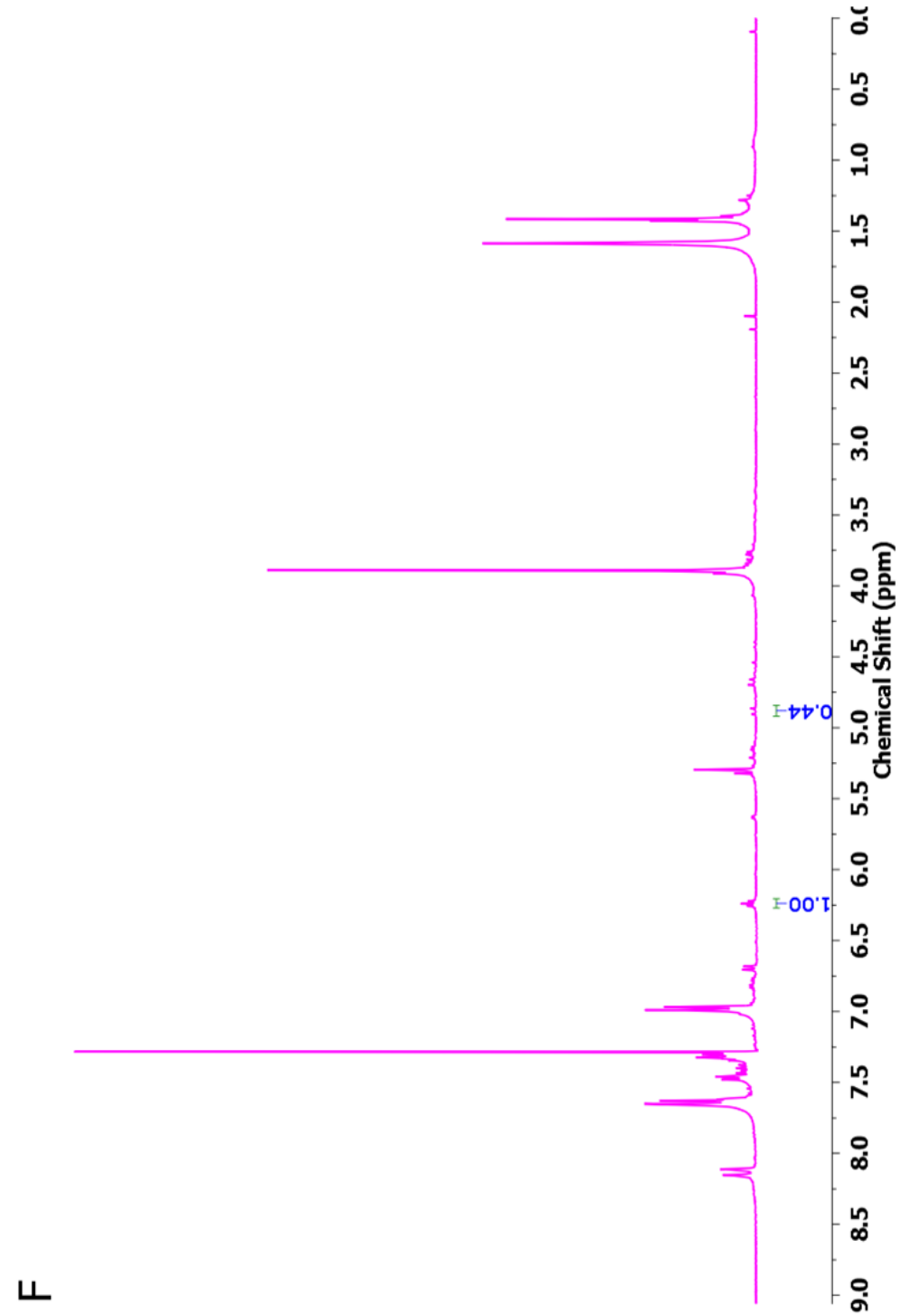

Figure 34. ^{1}H NMR Spectrum F of Cycloreversion Experiment in $CDCl_3$

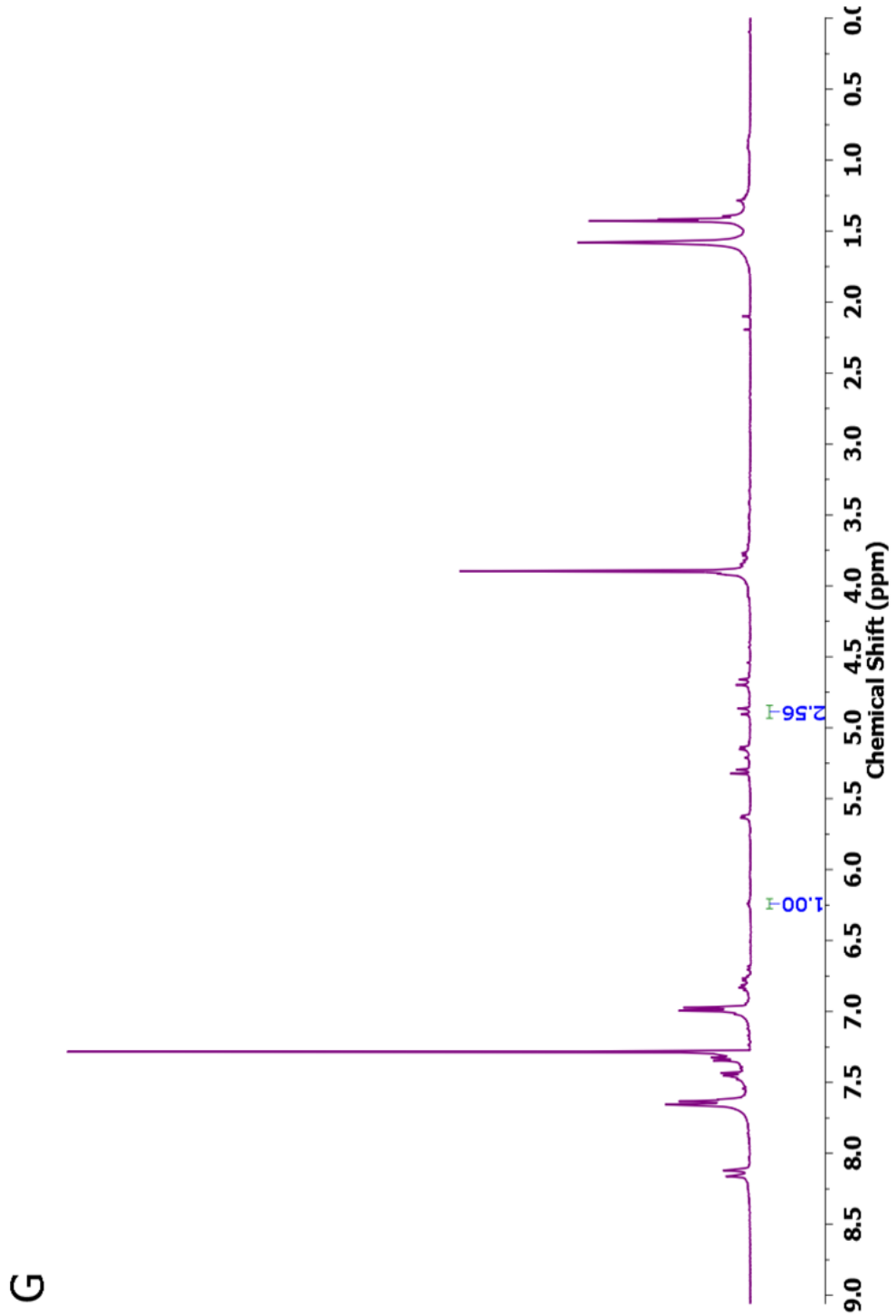

Figure 35. ^{1}H NMR Spectrum G of Cycloreversion Experiment in $CDCl_3$

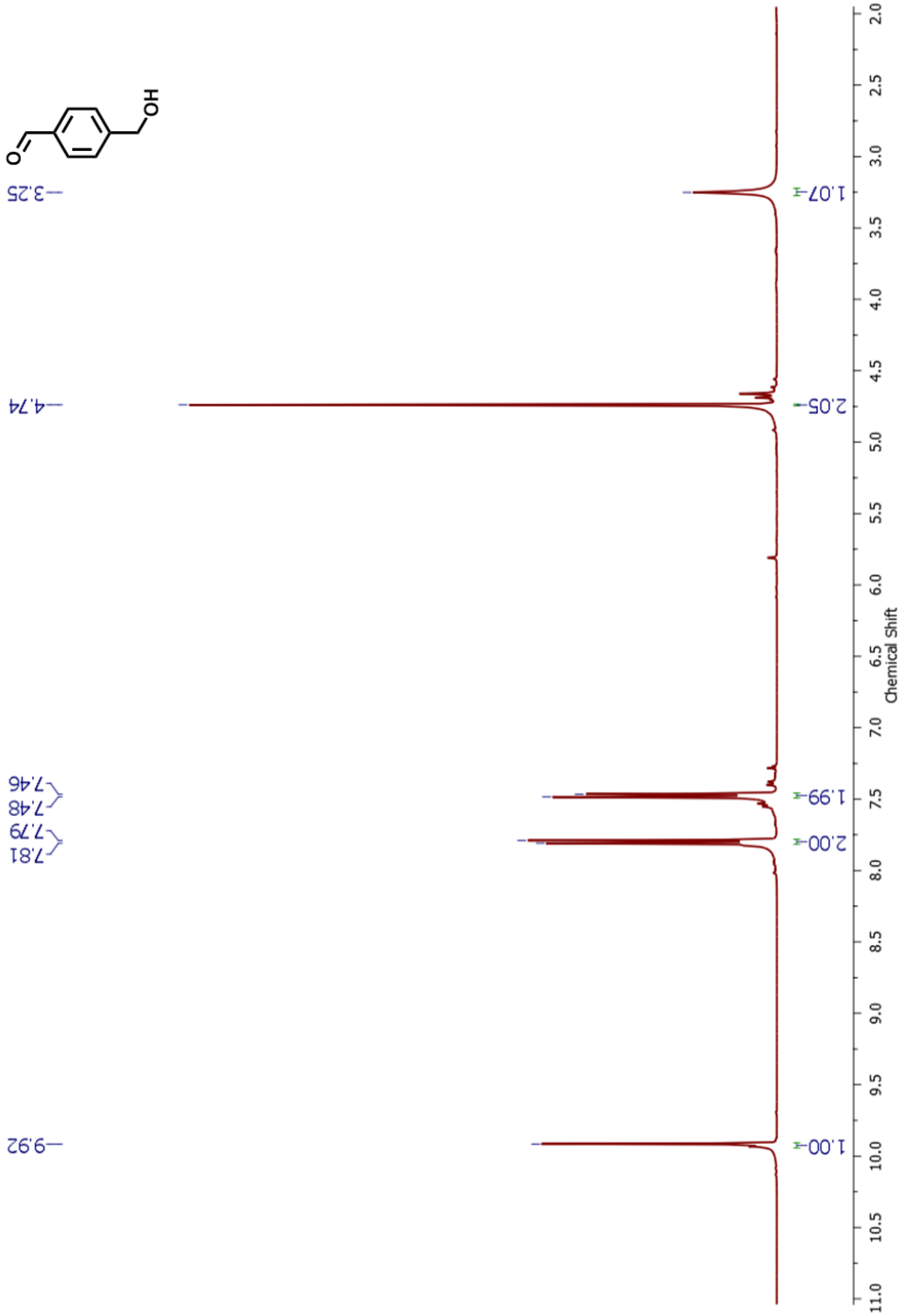

Figure 36. ^{1}H NMR Spectrum of Compound **12** in $CDCl_3$

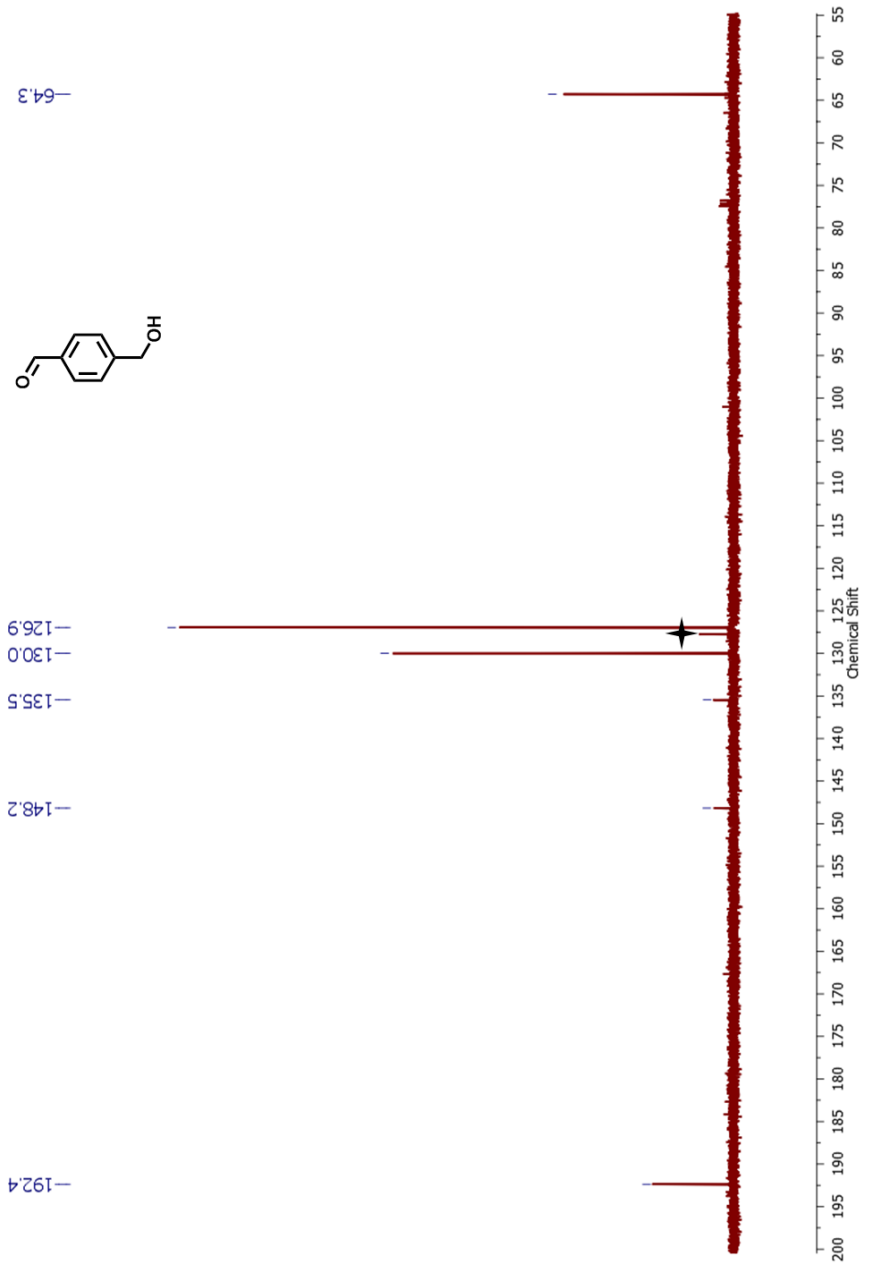

Figure 37. ^{13}C NMR Spectrum of Compound **12** in $CDCl_3$

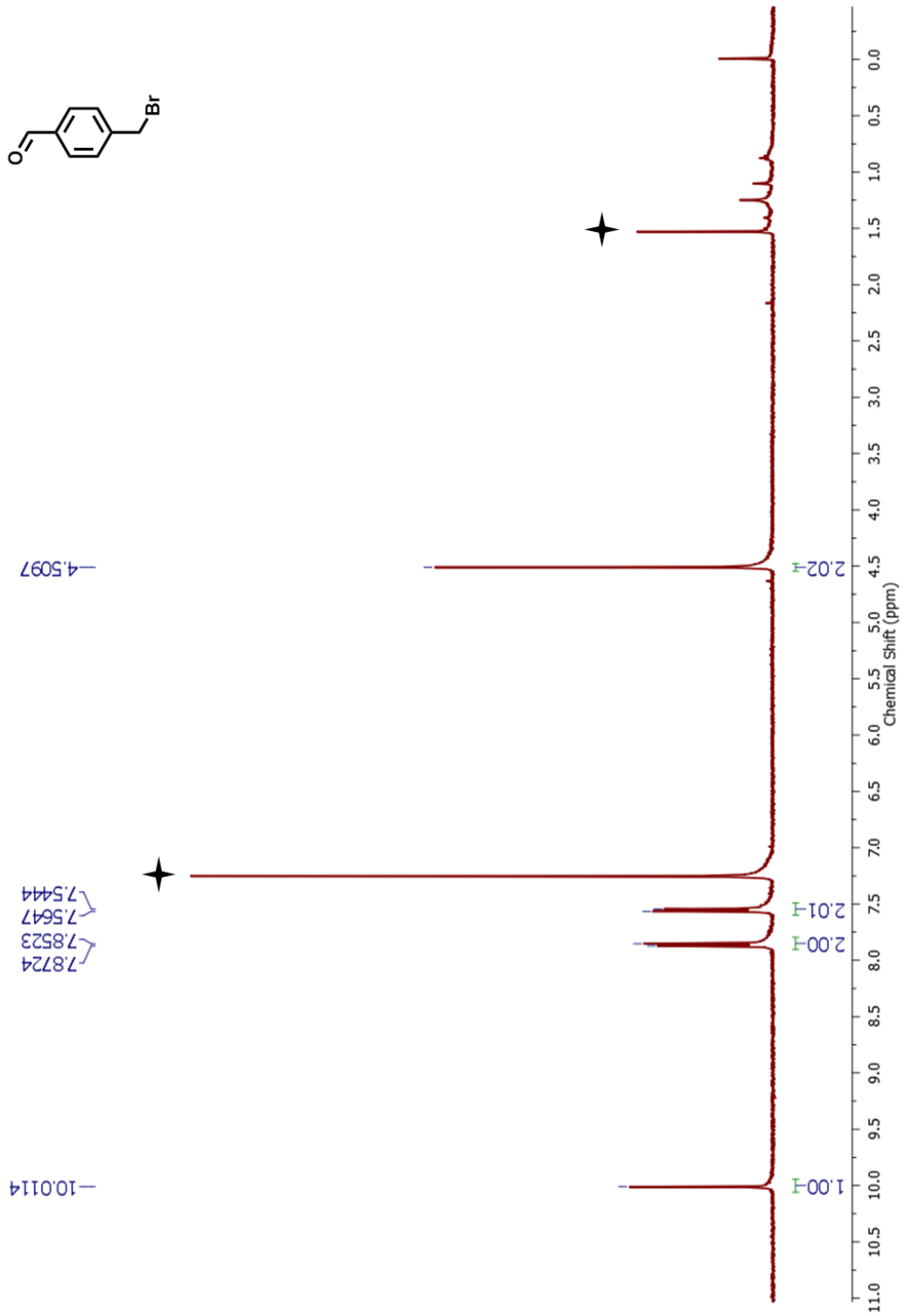

Figure 38. ^{1}H NMR Spectrum of Compound **13** in $CDCl_3$

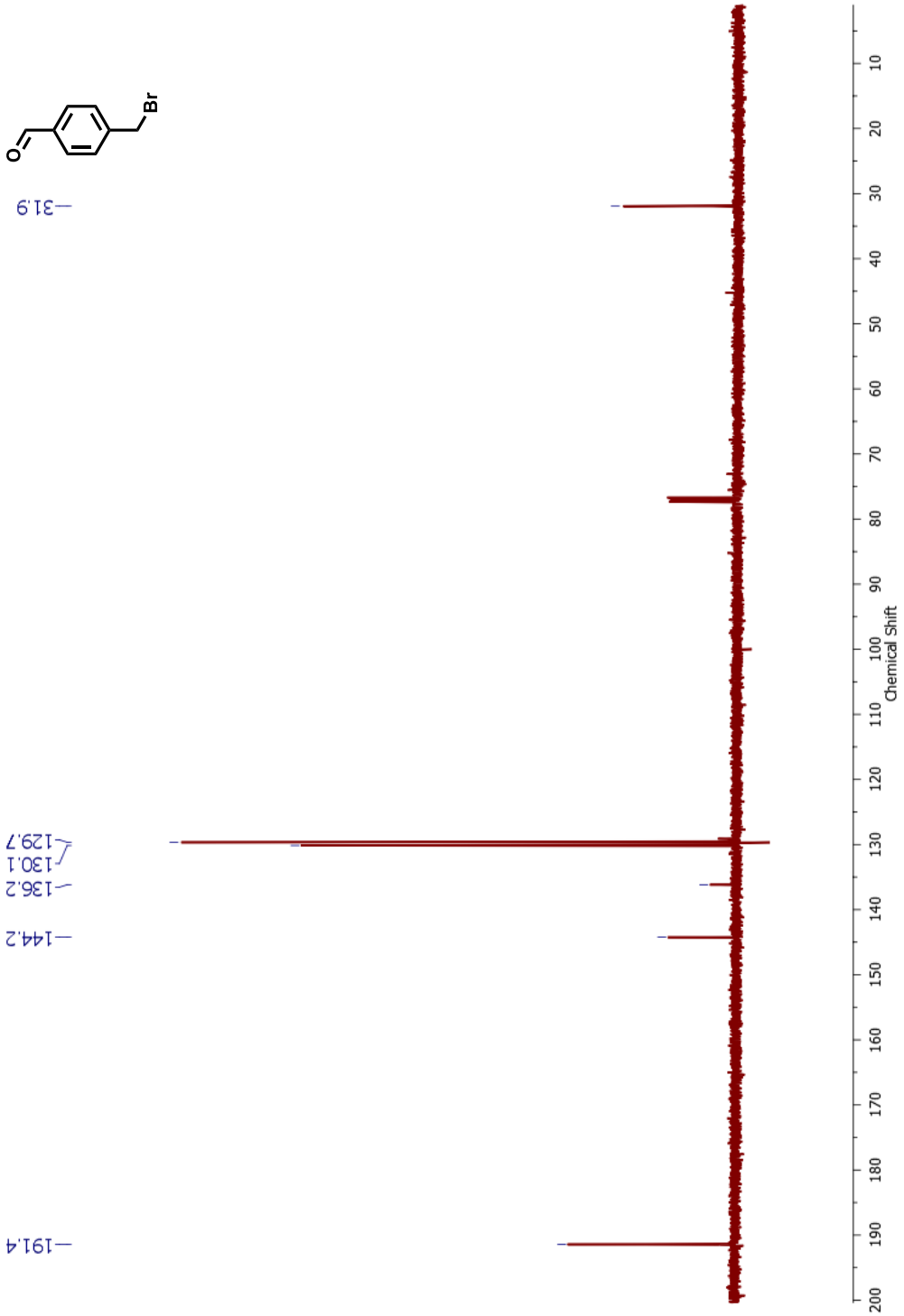

Figure 39. ^{13}C NMR Spectrum of Compound **13** in $CDCl_3$

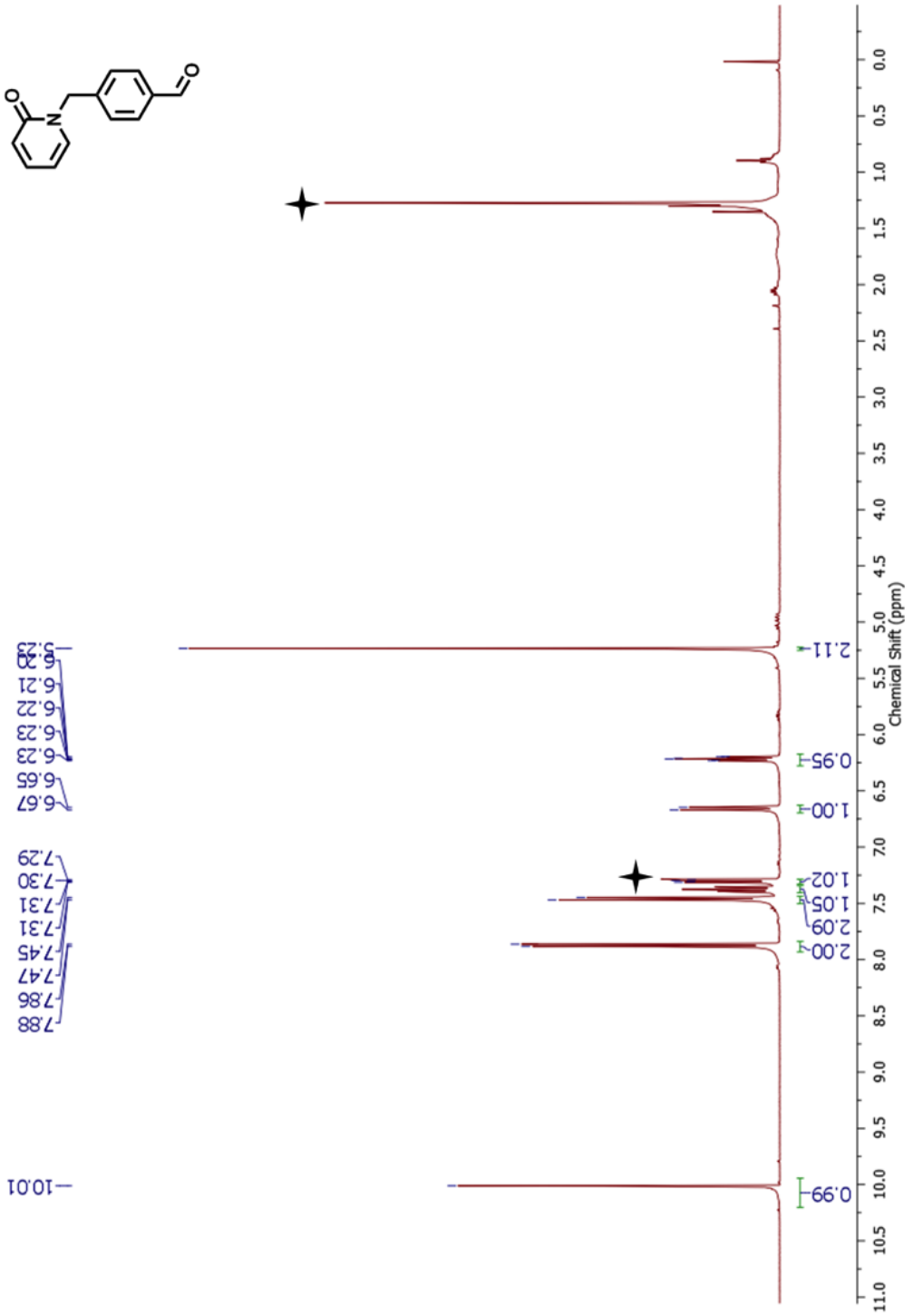

Figure 40. ^{1}H NMR Spectrum of Compound **14** in $CDCl_3$

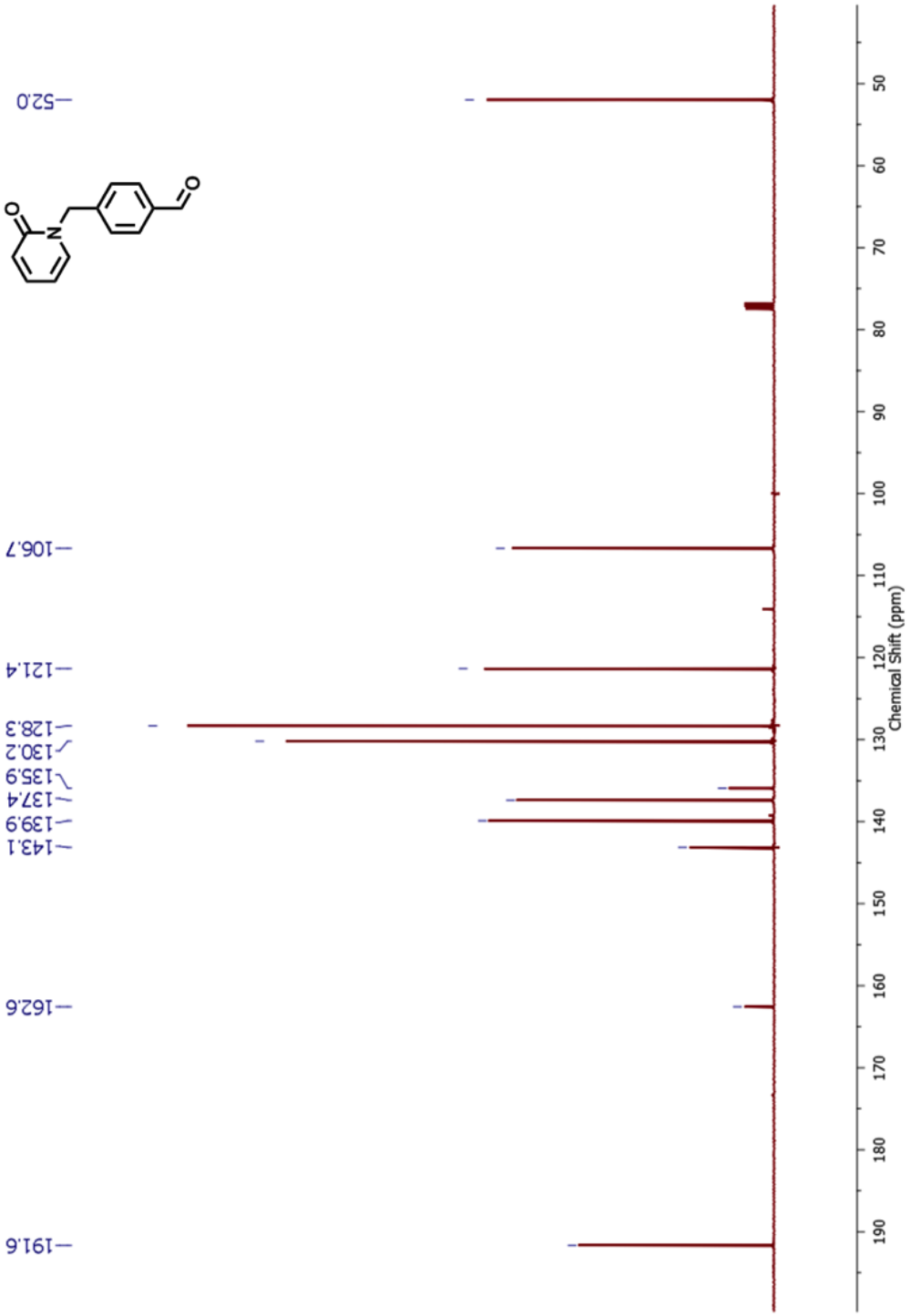

Figure 41. ^{13}C NMR Spectrum of Compound **14** in $CDCl_3$

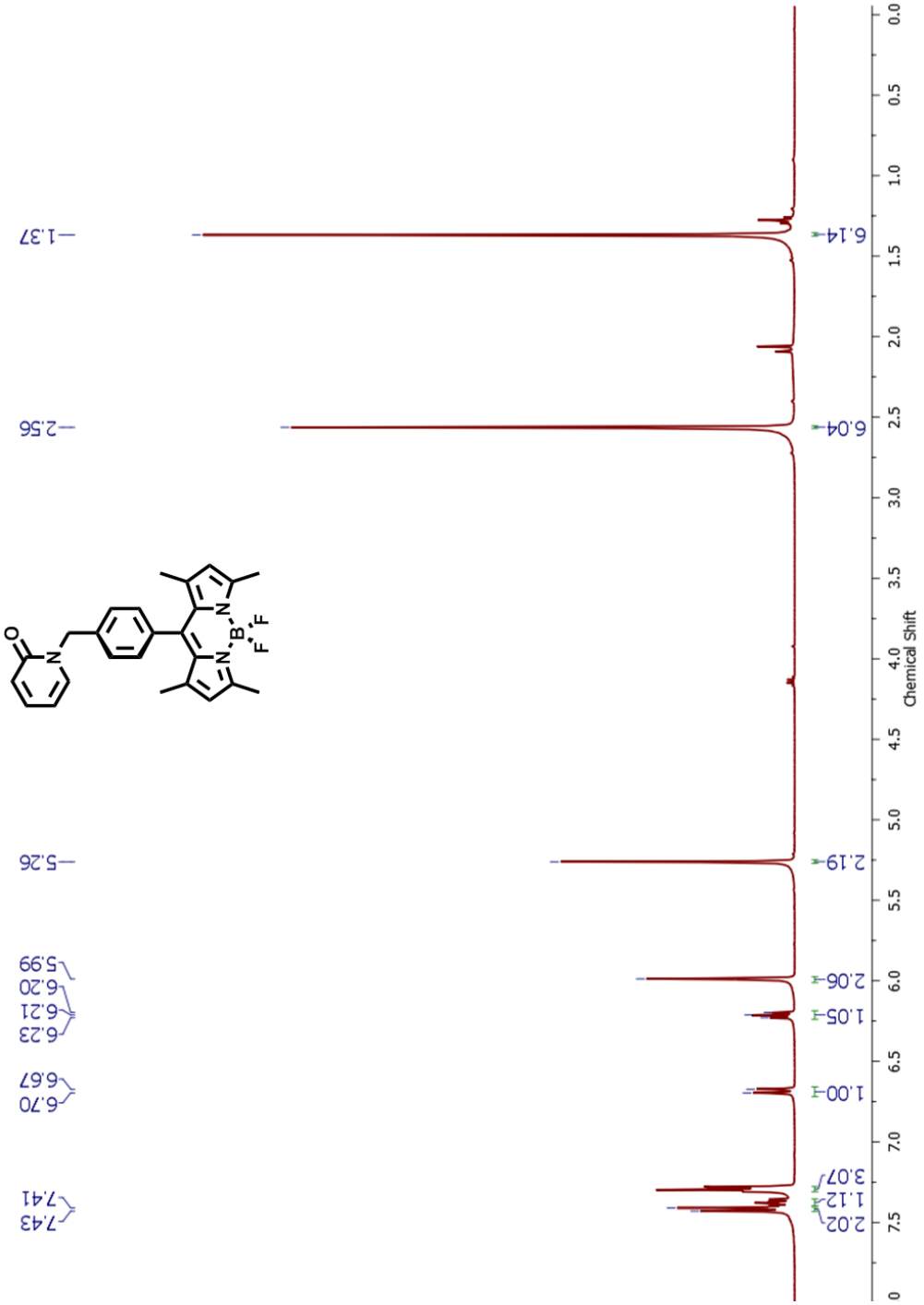

Figure 42. ^{1}H NMR Spectrum of Compound **15** in $CDCl_3$

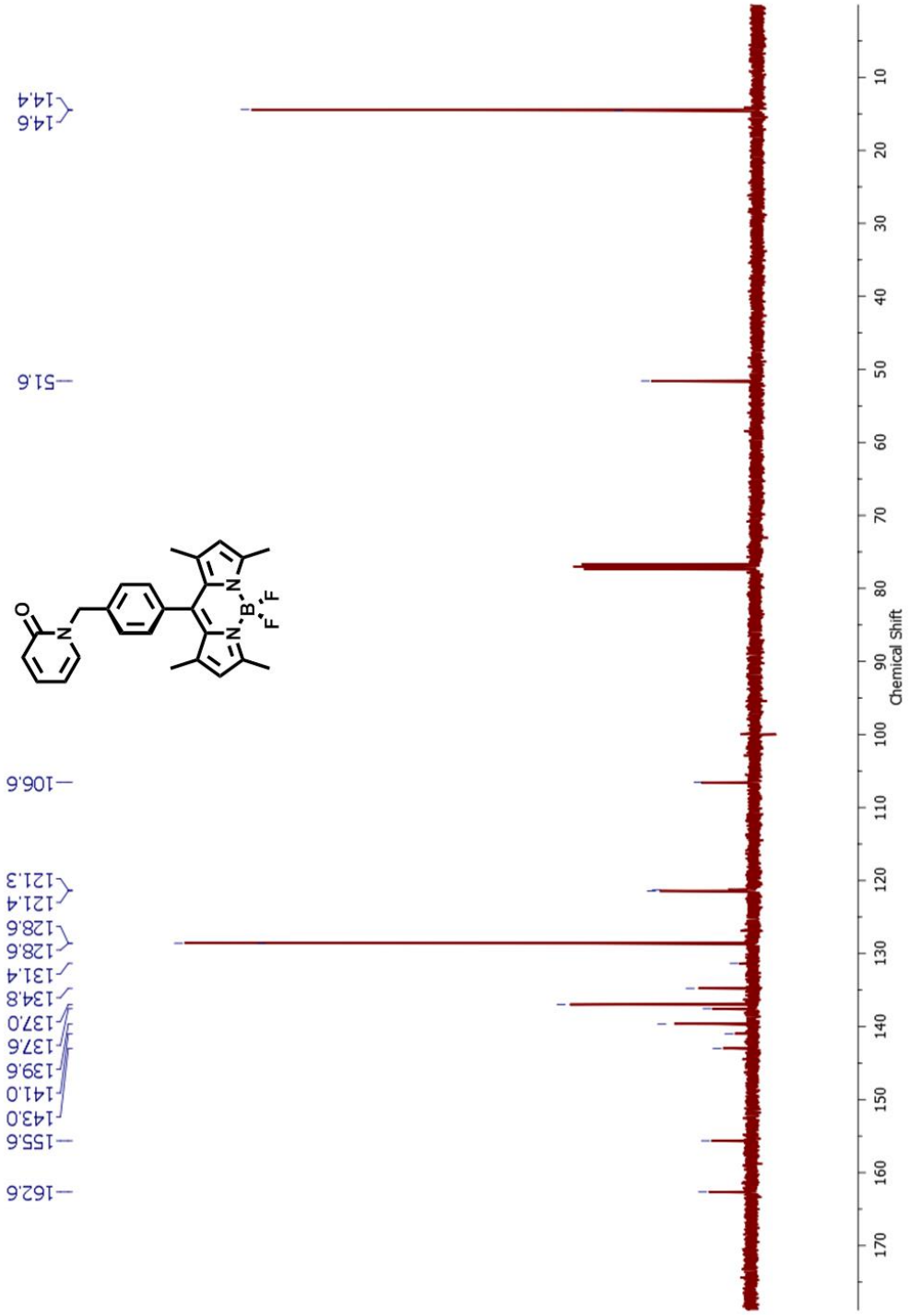

Figure 43. ^{13}C NMR Spectrum of Compound **15** in $CDCl_3$

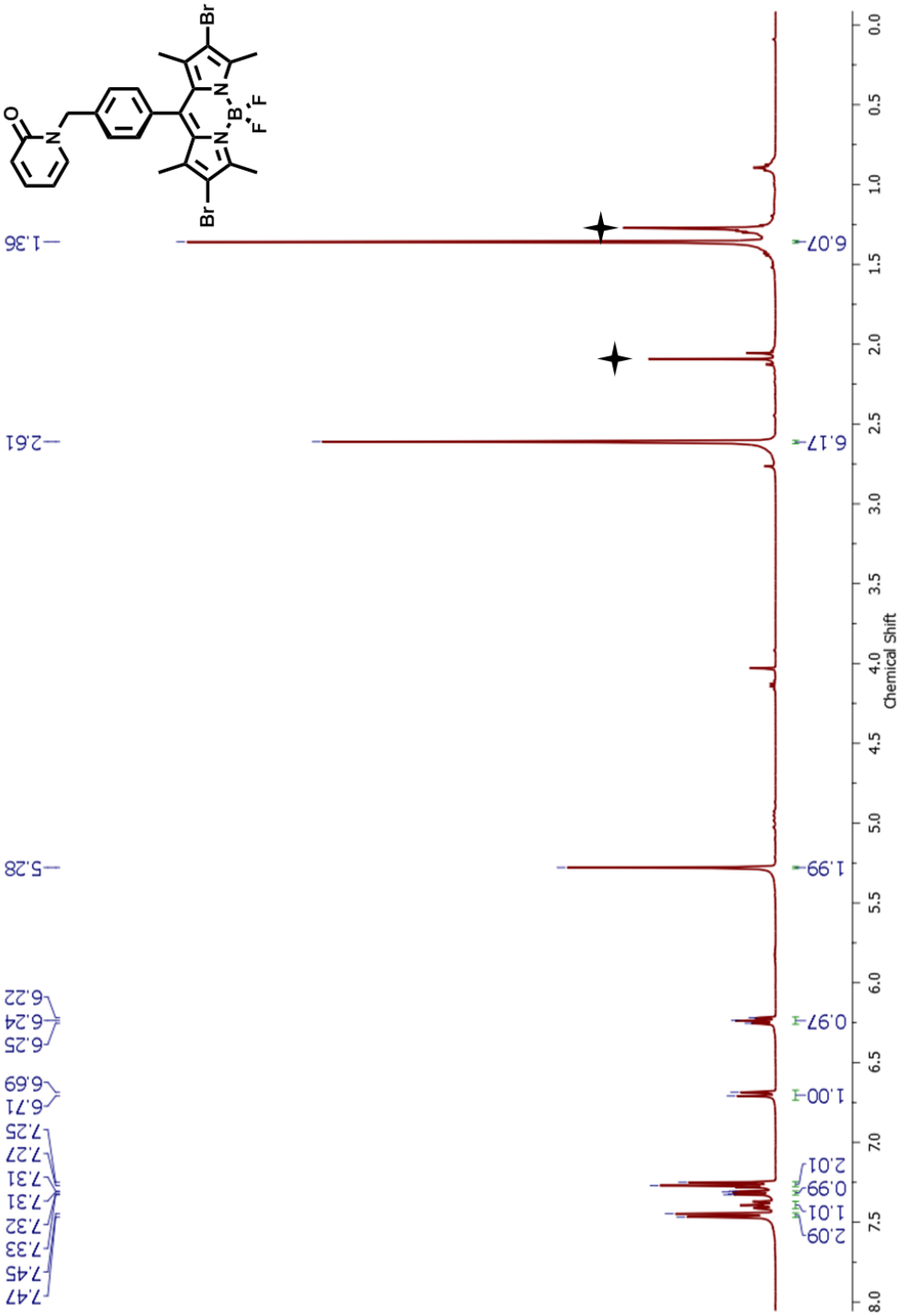

Figure 44. ^{1}H NMR Spectrum of Compound **16** in $CDCl_3$

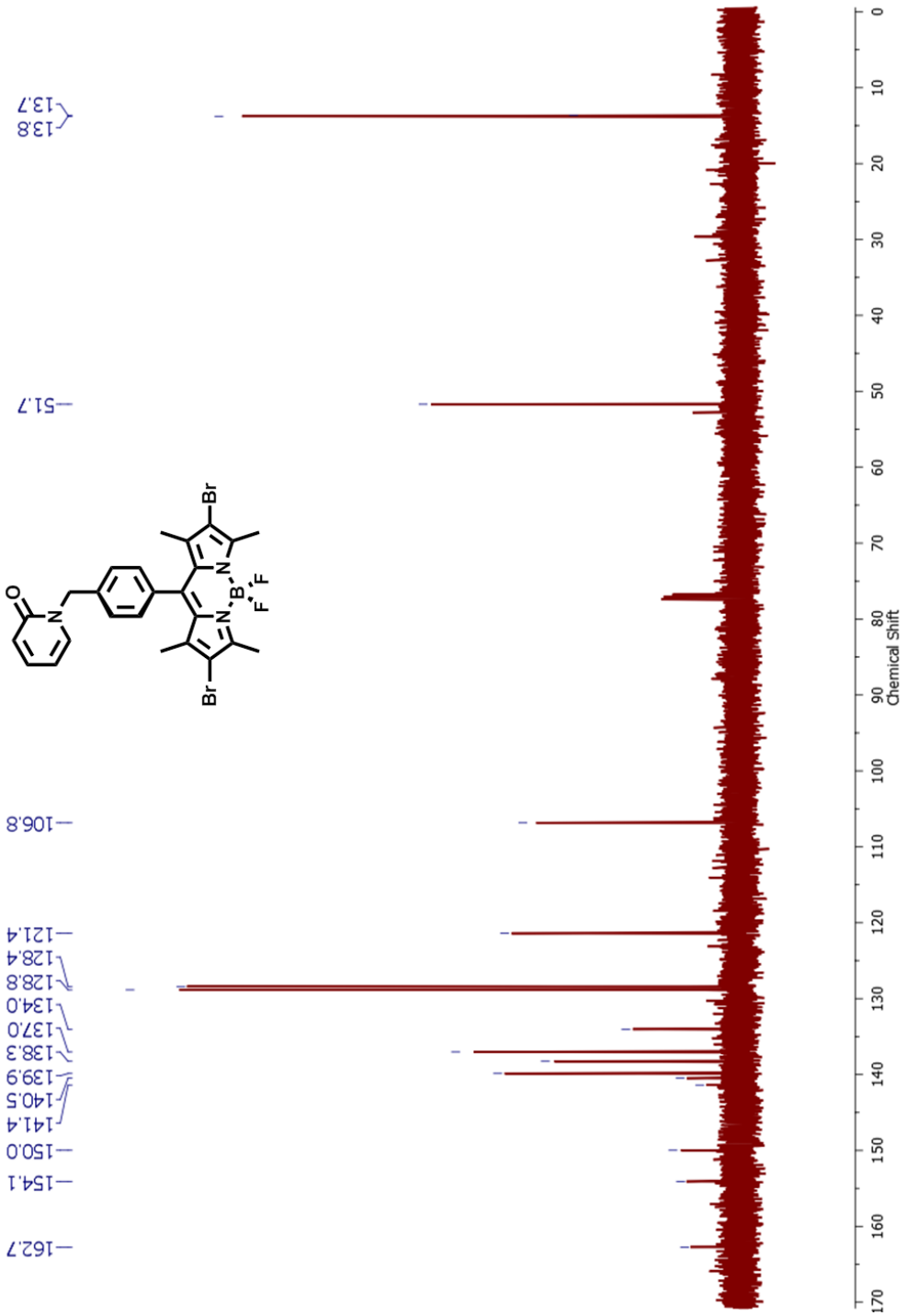

Figure 45. ^{13}C NMR Spectrum of Compound **16** in $CDCl_3$

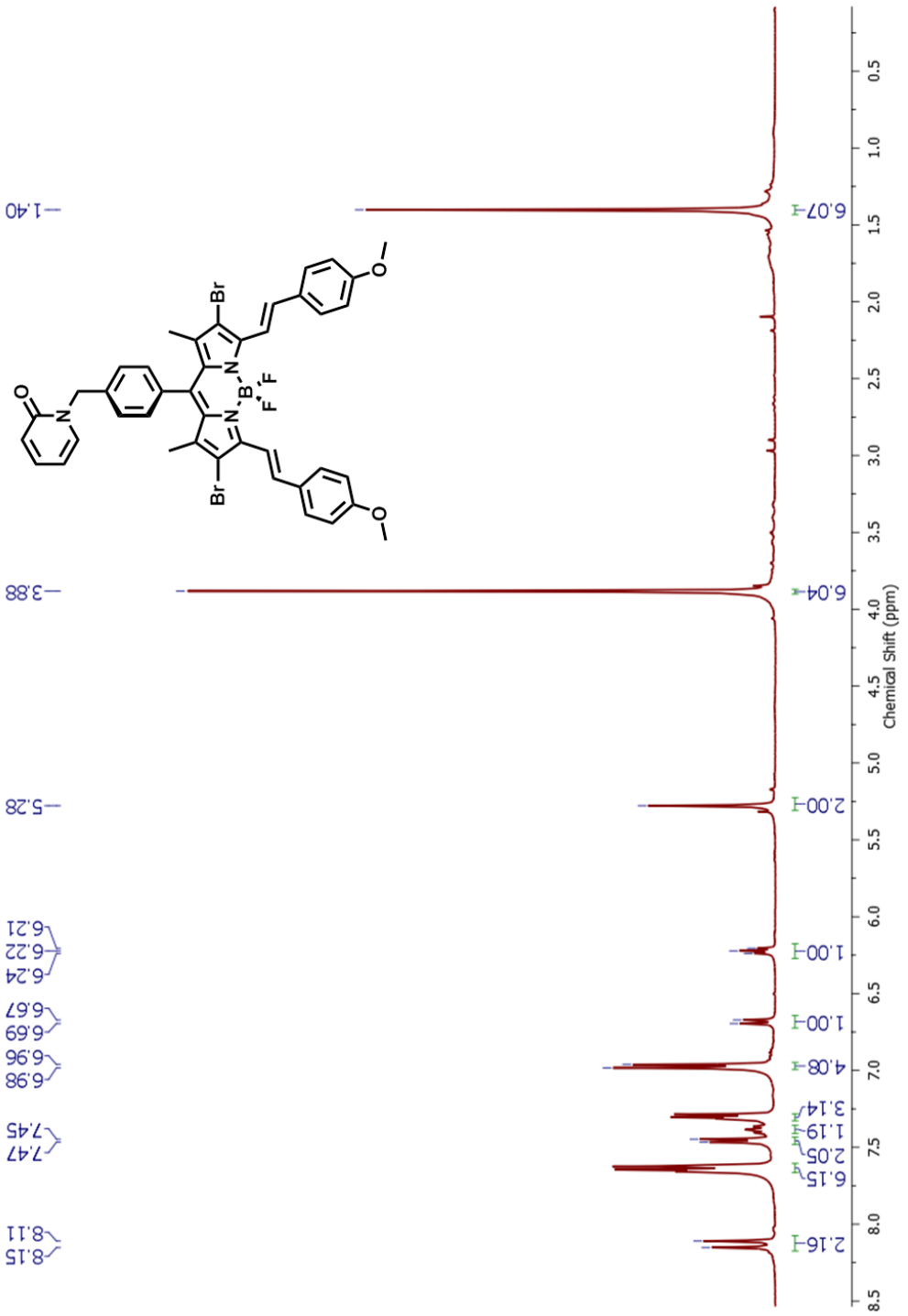

Figure 46. ^{1}H NMR Spectrum of Compound **17** in $CDCl_3$

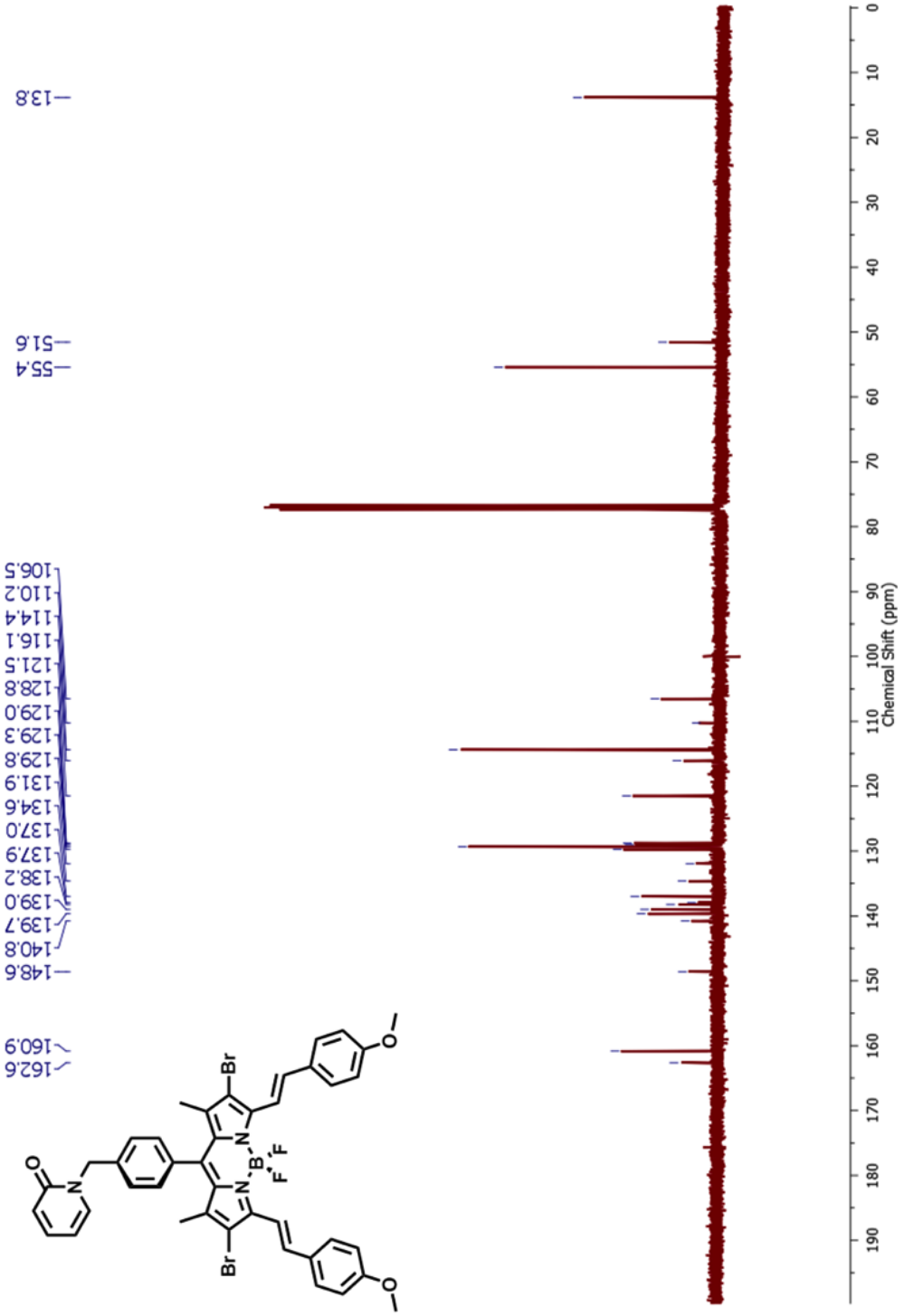

Figure 47. ^{13}C NMR Spectrum of Compound **17** in $CDCl_3$

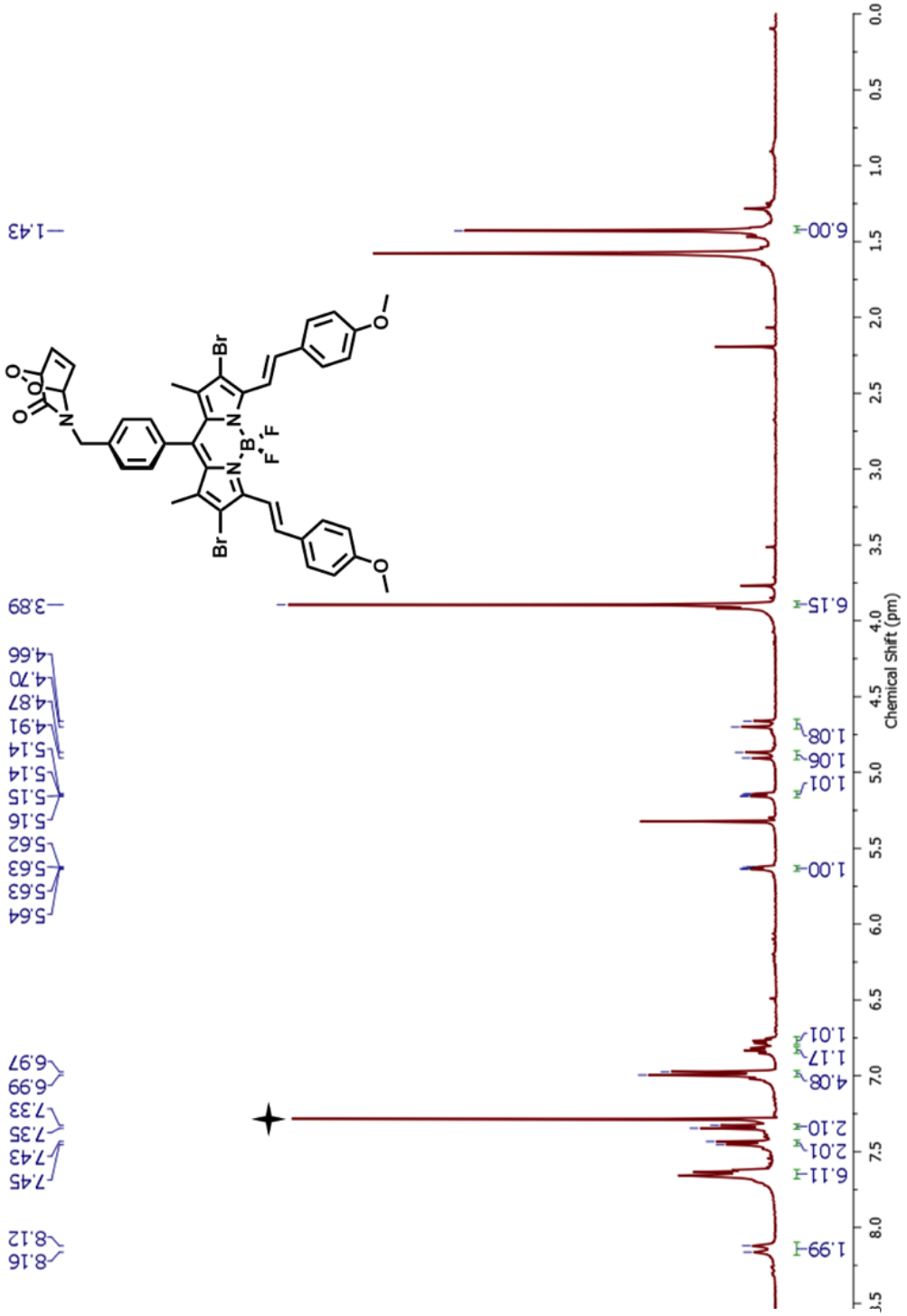

Figure 48. ^{1}H NMR Spectrum of Compound **18** in $CDCl_3$

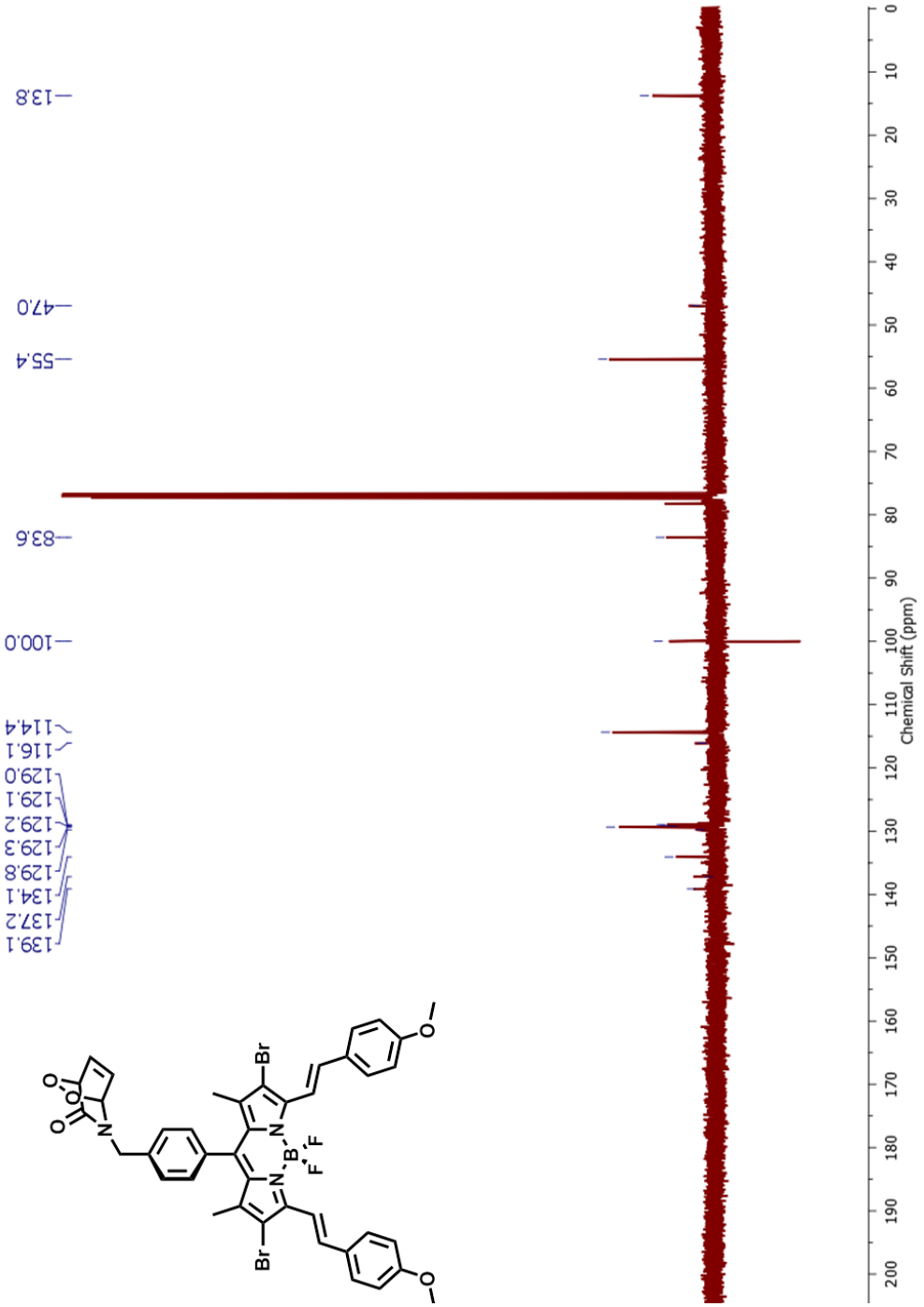

Figure 49. ^{13}C NMR Spectrum of Compound **18** in $CDCl_3$

Appendix-B

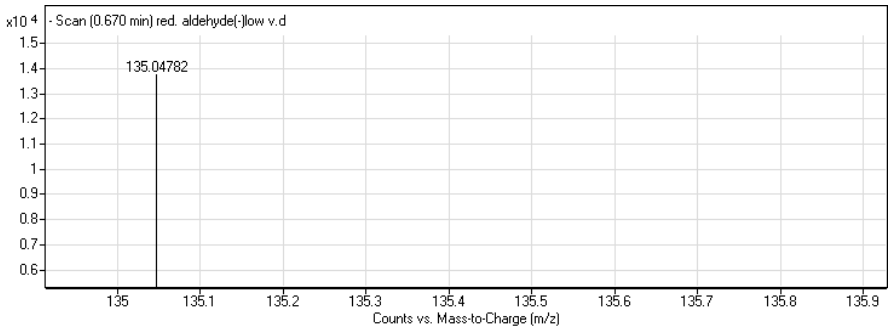

Figure 50. HRMS Spectrum of **12**

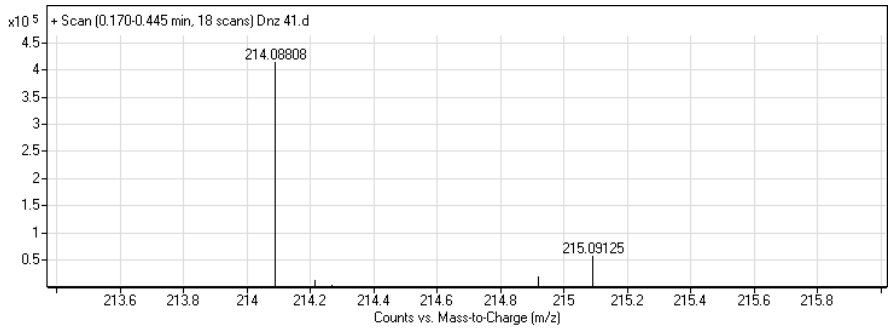

Figure 51. HRMS Spectrum of **14**

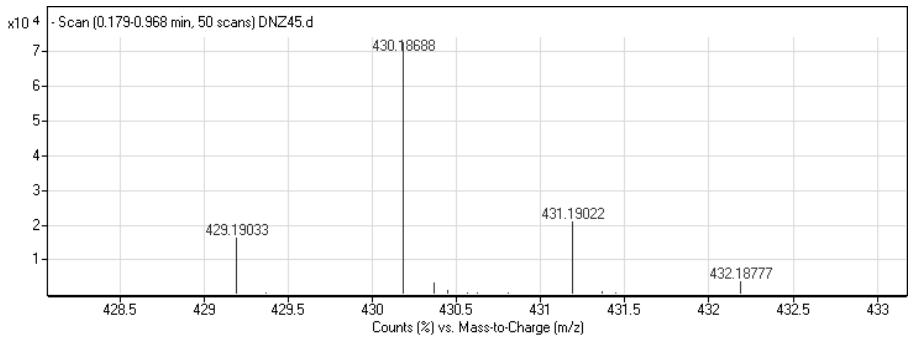

Figure 52. HRMS Spectrum of **15**

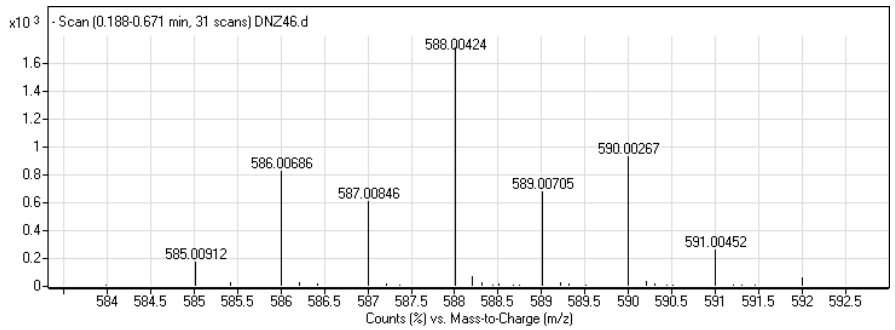

Figure 53. HRMS Spectrum of **16**

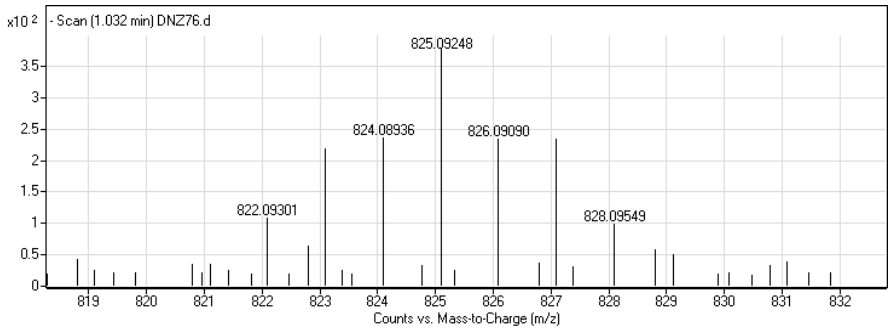

Figure 54. HRMS Spectrum of **17**

Appendix-C

			Diam. (nm)	% Number	Width (nm)
Z-Average (d.nm):	156,5	Peak 1:	49,87	100,0	19,73
PdI:	0,280	Peak 2:	0,000	0,0	0,000
Intercept:	0,373	Peak 3:	0,000	0,0	0,000
Result quality :	Good				

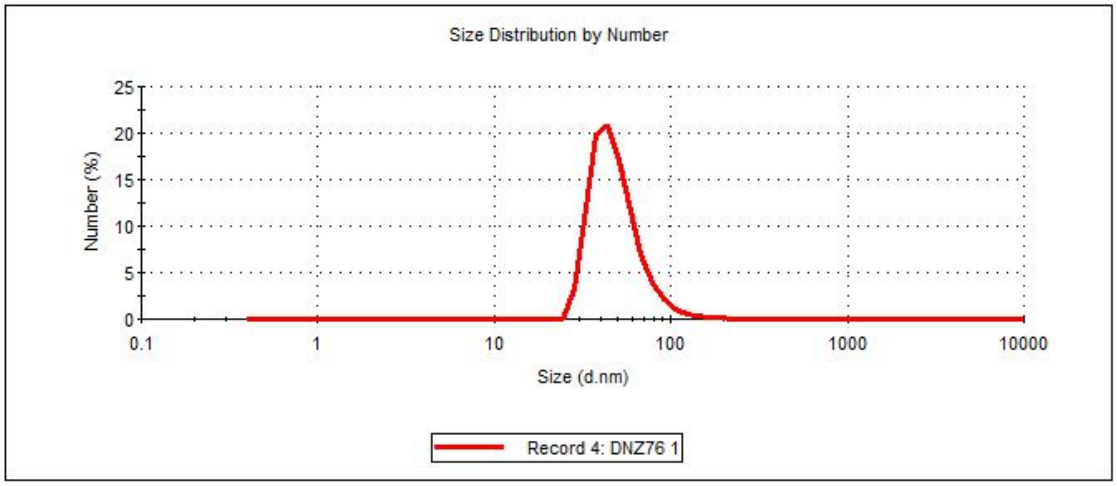

Figure 55. Size distribution of compound micellar compound **17**. Cremophor EL was used for micelle formation.